POLITECNICO DI TORINO

Master's Degree in Mechanical Engineering

Master's Degree Thesis

High resolution Godunov numerical methods for validation of new 1D compressible flows exact solutions

Academic Supervisors

Prof. Alessandro FERRARI

Dott. Oscar VENTO

Candidate

Alberto LUZIO

October 2021

Contents

Abstract

The aim of this thesis is to validate the new exact solution for a 1D compressible flow experiencing wall friction and heat exchange and to solve, numerically, a flow in which are present all the possible factors driving the flow properties changes: area variation, friction and heat exchange. The numerical scheme used for this purpose is an high resolution Godunov scheme: a finite volume upwind scheme which belongs to the class of the Riemann solvers.
The numerical code has been validated by comparing the numerical simulations with the analytical steady state solutions for the Fanno flow, the Rayleigh flow and the flow across a nozzle, with and without a straigh shock in the divergent part. The validated code has been used to assess the consistency of the new exact solution pertaining a flow with wall friction and heat exchange. Finally, the obtained numerical code has been used to solve a one-dimensional flow in which all the possible factors driving the flow properties changes are taken into account.

1 Introduction

The compressible fluid flow has a substantially different behavior with respect to the incompressible one, especially in supersonic cases. In fact, in a fluid flow, in presence of area variation, friction and heat exchange, a sudden alteration of properties can occur, causing shock waves. To properly characterize this phenomena, high resolution shock-capturing method are required. The mathematical model that will be used to analyze the compressible gas behaviour is the Euler's equations model in presence of perfect gas with a source term. It will be the starting point to develop our numerical scheme .
At the moment, for the one-dimensional compressible flow are available exact solutions for an isoentropic nozzle, for the Fanno flow and for the Rayleigh flow. Recently, also exact solutions for conic nozzle with wall friction and constant area duct with heat exchange and wall friction [1] have been found.
After a theoretical description of the physical model we will introduce the mathematical model of the Euler equations in presence of perfect gas with a source term and its properties. It will be the starting point to develop our high resolution Godunov scheme. These are very recent numerical solvers based on the resolution of a Riemann problem at each point of the computational domain. These numerical methods follow the physic of the problem and they are very suitable for the application on compressible fluid flows. Even if the theoretical approach to the subject was fully developed in the early 50' by Sergei Godunov, they found popularity and applications only in the last decades thanks to the exponential evolution of the computational power. Despite the great performances of these numerical methods, they are still used for very few academic application but they can gain popularity in the next years.
The practical implementation of a numerical code into a calculator will be introduced with all the steps to develop an algorithm. At the end the code will be validated through the comparison with simple models for which an analytical steady state solution is present. At the end of this document we will have a one dimensional high resolution numerical method . The great utility for the 1D models computed with an High resolution Godunov scheme as first design for thermofluid dynamics systems such as heat exchangers, refrigerator's systems and gas transport systems is underlined: the one-dimensional codes are much easier to be obtained with respect to the three dimensional ones but they give satisfying results in very short times.
Once that the numerical code will be validated, we will build an High Resolution Godunov scheme solving a De Laval nozzle with the presence of wall friction, heat exchange and area variation at the same time.

The exact solution for this model is not available at the time and so, the only way to analyze this problem is through a numerical solution.

2 The physical compressible flow field in 1D

As presented by Ferrari in [2] (chapter 11), the physical case that we're going to study in the further chapters can be inserted into the analytical one-dimensional models for a compressible fluid. In this field of study we can find three different main sub-models :

1. 1D compressible isentropic flow with area variation;
2. Fanno flow: 1D viscous adiabatic flow through a constant cross-section area pipe;
3. Rayleigh flow: 1D inviscid diabatic flow through a constant cross-section area pipe;

in which we will consider both the subsonic and supersonic flows. These three models are all steady-state and will be described in the following pages. The one-dimensional unsteady gas-dynamic models are the starting points for a simple modeling of 1D thermo-fluid machines. We must be aware of the fact that this model can only describe the variation of the properties along the longitudinal axis with a good description for the physic involved and a simply mathematical description until, 2D phenomena, such as oblique shocks, appear. The use of a one-dimensional model is a good choice when these hypothesis are observed:

- the change of the section must be little in respect with the axial length;
- we are looking for the mean flow properties for each section. The fluid properties don't vary along a single section but only from a longitudinal point to another;
- great curvature radius of the duct in respect with the diameter are required.

The cases in which our model cannot be used, will be analyzed in the following pages.
Our numerical model will include all these three cases simultaneously. To check the effectiveness of the numerical code in respect to the single physical sub-case, a validation must be performed using the analytical solutions. After this the general code will be considered able to work, at the same time, in presence of area variation, wall friction and heat

exchange with the external ambient.

2.1 Causes of variation of fluid properties inside a 1D conduct.

Considering a 1D fluid-dynamic model without diffusive effects and a fluid flow inside a constant area duct, the only way in which its properties can change, is because of the presence of a source term. The sources in the 1D model are of 3 types:

- Area variation inside the duct;
- friction between the fluid and the walls of the duct;
- heat exchange with the external environment.

If none of this source is present the fluid properties will remains the same inside the duct.
The study of the influence of each of these sources upon the fluid properties will be studied in the following pages

2.1.1 Area variation

If we consider an adiabatic flow without the presence of friction on the walls with an Area modeled as $A = A(x)$, where $A(x)$ is a continuous function with the second derivative continuous, we obtain, by applying the principle of the conservation of total energy, a constant total Temperature flow at steady state.

In our study case we will consider a De Laval nozzle with subsonic flow at inlet with, as boundary conditions, a fixed total pressure p_1^0 and total temperature T_1^0 at the inlet (Reservoir properties) and a varying outlet pressure p_2.
Fixing the inlet properties and varying the outlet pressure we can appreciate all the different working behaviour for our nozzle classified in function of the pressure ratio as reported in figure (1) :

- $p/p_1^0 = p_{ad}/p^0$.
  We are in *design working condition* and the outlet flow is supersonic. The flow becomes sonic at the throat where the critical pressure $p_c = p_1^0(\frac{2}{(\gamma+1)})^{\frac{\gamma}{\gamma-1}}$ is reached . It expands iso-entropically until the p_{ad} design pressure is reached.
- $p_s/p_1^0 < p/p_1^0 < p_1^0/p_1^0$.
  In this condition the outlet pressure is a slightly lower than the inlet total pressure and the flow is fully subsonic along the nozzle. This is called Venturi working condition.

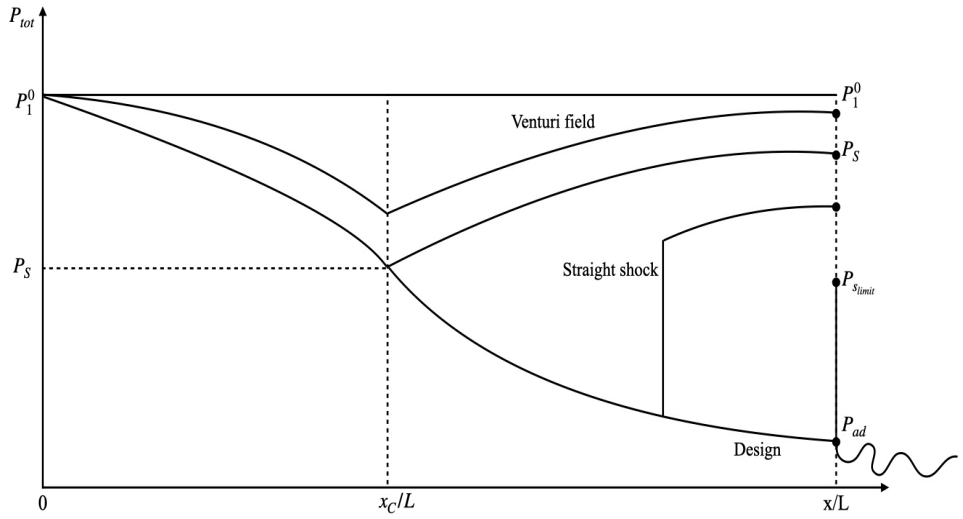

Figure 1: De Laval nozzle different working conditions depending on outlet pressure.

- $p/p_1^0 = p_s/p_1^0$.
  This is the limit condition for which the flow becomes sonic at the throat and subsonic at the outlet because the diverging part acts as a diffuser and it compresses the flow till the pressure p_s.

- $p_s/p_1^0 > p/p_1^0 > p_{s_{limit}}/p_1^0$.
  In this condition we reach the sonic state at the end of the converging part and, in the diverging one, the flow becomes supersonic until a straight shock occurs, making the flow subsonic and the evolution no more across the entire nozzle. The evolution continues with a compression in the last diverging part until the outlet pressure p_2 is reached. The straight shock travels to the exit section as we reduce the outlet pressure.

- $p_{ad}/p_1^0 < p/p_1^0 < p_{slimit}/p_1^0$.
  In this case we have no more straight shock inside our diverging part and we cannot use a 1D model to analyze the flow properties variation. In fact from experimental evidences, in this working condition there is the presence of oblique shocks in the diverging part that can continue also outside the nozzle with the post-expansion phenomena. The flow is not isoentropic and we need at least a 2D model to evaluate the property variation inside our nozzle.

- $p/p_1^0 < p_{ad}/p_1^0$.

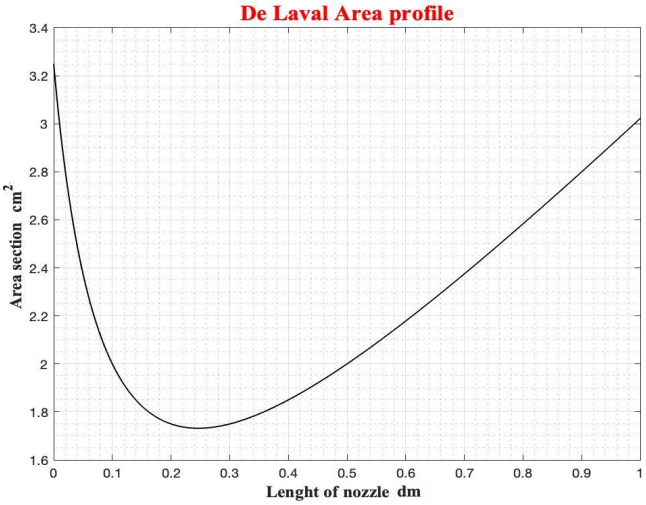

Figure 2: De Laval nozzle area profile

In this condition the profile of pressure is the same in the case of design working condition but we have outside expansion waves that occurs with the post-expansion dynamic.

The shape considered in our model is :

$$A(x) = 2.5(x + 0.1) + \frac{0.3}{x + 0.1} \quad , \tag{1}$$

and it is represented in figure (2). If no shock is present inside the divergent part, we will have an isotropic flow (no friction and no heat exchanges). The steady state analytical solutions for the flow properties will be found in the section (7.2).

2.1.2 The Fanno Flow

As described in [5], the Fanno flow is a stationary uni-dimensional compressible flow along a duct with constant-cross section area without exchange of energy with the ambient and with the presence of viscous effect on the walls. Since the total enthalpy and the mass flow in this model are constant, we have a total temperature constant flow as in case of area variation.
The frictional effect, in this model, induces the changes in the properties of the flow and is the only source of entropy. It will increase in any case when friction is present until a maximum Entropy state is reached. It will correspond to the sonic outlet condition. If a flow has an initial subsonic state, the friction effect will increase the velocity

and the Mach number and decrease the enthalpy and the pressure of the flow.
We can have two different main cases for our flow:

- *Subsonic flow.* If the flow at the inlet of our duct is subsonic the friction will transform the total pressure into internal energy with an increase of temperature and a decrease in density. This effect will cause an increase in speed to keep the mass flow constant. The friction in this case produces an acceleration of the flow until Mach = 1 is reached. This is the chocked condition and, once is reached, the flow cannot be more influenced by the inlet properties and so, changing the pressure ratio, the flow will still remain the same inside the duct. In this chocked condition the only parameter that can modify the flow properties is the length of duct. Increasing the length the Mach=1 condition will be the same whereas the mass flow will reduce. This effect is crucial in long pipes design.

- *Supersonic flow.* If the flow is initially supersonic the effect of friction will reduce Mach number and speed and will increase pressure and enthalpy. Since the flow is supersonic the only parameter that can affect the flow properties is the pipe length. If we increase it, the flow will reduce its Mach number, tending to a Mach=1 outlet condition as limit. This is also called star condition and depends on the inlet properties of the flow and it will correspond to a length of the duct and to a set of properties (star properties) at the outlet in which the Mach number will be equal to one. When the length is increased more than the star length, a steady state shock occurs. The shock appears in order to fulfill the second law of thermodynamic because no supersonic flow can became subsonic with a continuous evolution. After this shock the Mach number will be lower than one and the evolution will continue till the sonic state if the downstream pressure is lower than the star one.

In any case the overall effect of the friction will include a decrease in the total pressure for both supersonic or subsonic case and so, the wall friction, tends to reduce the effectiveness of all types of flow machinery. The evolution of the flow is deeply influenced by whether the flow is initially subsonic or supersonic. The effect of the friction is evident in particular in the supersonic case where, for the same variation in Mach number for a subsonic case, we have a loss in total pressure doubled. This is the reason why we use short ducts in case of supersonic flows.

2.1.3 The Rayleigh flow

From [2]: in Rayleigh flow, the change in the flow properties is induced only by an heat exchange with the external environment since frictional effects and area variations are absent. The changes in flow properties are linked to the variations of the total temperature induced by the heat flow. If we know the heat exchanged in every section we can understand all the changes in properties.
The heat exchange will be, for this model, the only source of Entropy and, as for the Fanno flow, also for Rayleigh flow we will have a state of maximum entropy, if the flow is heated up enough, that will correspond to Mach=1 for any case. The main situations for this model are two for the case of heating (positive heat flow) and two for the case of cooling (negative heat flow). For our purpose we will analyze only the heating cases:

- *Subsonic flow.*
  Starting from a subsonic inlet the presence of a positive heat flow increases the total temperature as $q_{in} = cp(T_2^0 - T_1^0)$ from the state one to the state two. This variation induces an increase in the Mach number proportional to the heat induced by the system. As for every subsonic flow we can reach at maximum the Mach= 1 state at the outlet. In this case the heat flow tends to reduce pressure, density and the total pressure.
  A peculiar situation is linked ,in this case, with the Temperature variation.
  The temperature increase until Mach= $\frac{1}{\sqrt{\gamma}}$ is reached and decreases in $1 >$ Mach $> \frac{1}{\sqrt{\gamma}}$ range, with $\gamma = c_p/c_v$. This phenomenon, apparently paradoxical, find explanation in a moving flow where, the speed in the $1 >$ Mach $> \frac{1}{\sqrt{\gamma}}$ part, increases with a rate higher than the Temperature.For this reason, the flow cool down to reduce the density and to keep the mass flow conserved . When the Mach = 1 is reached we have the chocking condition for the flow (star condition) to which we can link a q_{lim}. In this condition the flow cannot stand more inlet heat flow and further introduction of heat will cause the mass flow rate to reduce while the outlet conditions remain the same. Increasing the length of the duct, if we have a constant introduction of heat for every x section, we are indirectly introducing more heat in the system and so the length can cause a variation for the properties of the flow.

- *Supersonic flow.*
  When the inlet flow is supersonic, this is non-sensitive to the

upstream properties variation and, the only driving term for a change in properties becomes the length of the duct. The exchange of heat along this length induces an increase in speed and in pressure. Also the total pressure increases in this case whereas the Mach number decreases until limit of Mach=1. The length correspondent to this state will be the limit $L*$. In this state the flow cannot absorb more heat without lowering the mass flow rate and it is defined as chocked. Increasing further the length we are introducing more heat and when $q > q_{lim}$ there will be the creation of an adiabatic shock to respect the second law of Thermodynamic. Thanks to this shock the flow downstream is subsonic and will become sonic at the outlet. Nevertheless the location of the shock cannot be inside the duct because the shock will not cause any total temperature variation. For this reason the only acceptable location will be inside the De Laval nozzle feeding the duct. As the heat increases further, the shock will travel more and more upside to the nozzle. In this way the flow will be subsonic chocked along the duct.

In case of *cooling* the variation of properties and the different cases are just opposite respect to the heating case.

2.1.4 Analogy between The Fanno, the Rayleigh and the Area Variation flow.

The three models studied before, present some analogy between themeselves:

- In case of subsonic flow in a nozzle there is a limit Area section and a limit outlet pressure after which the flow become sonic and so, insensible to the upstream flow properties. For the Fanno and the Rayleigh flow we can observe the same phenomena but driven from different effects (friction and heat);
- another analogy is between Fanno and Rayleigh about the mass flow rate. In the Fanno subsonic flow, if we increase too much the work produced by the friction or if we reduces too much the outlet pressure, there will be a change in mass flow as well as in case of a Rayleigh subsonic flow if we increase too much the heat exchanged or reduce too much the outlet pressure;
- the supersonic Fanno and Rayleigh flows presents some similar features about the Entrophy generation. In Fanno the friction causes Entropy generation whereas in Rayleigh the heat exchange causes the same effect;

- All the three models in supersonic case present the creation of a shock in some condition. This shock is source of Entropy and its generation is the only way to respect the second law of thermodynamic;
- Both the area variation and the Fanno flow are models with a constant total temperature in steady state.
- The variation of pressure for all these models can also be source of instabilities in all the subsonic cases. If $L_< L_{max}$ or $0 < q < q_{lim}$ and diminishing the pressure at the outlet we arrive to the critic value, the mass flow cannot vary anymore. If we reduce again the outlet pressure there will be the creation of dissipative phenomena (post-expansion) outside the duct to reach the outlet environment pressure. A similar effect can be found in a supersonic flow with an outlet pressure higher than the critical one.

3 The one-dimensional Euler Equations

The homogeneous Euler equations constitute a system of non-linear hyperbolic conservation laws that describes the dynamic behaviour of a compressible material. This model comes directly from the Navier-Stokes-Fourier system of equations in which are neglected the diffusive mechanisms. Because of this, discontinuous solution as shock waves can born and so, the numerical scheme to solve them must be able to correctly reproduce them. For the validation of our numerical model the choice of The Euler equations, as analytical starting point, is motivated by the fact that the absence of the diffusive mechanisms makes this model the most unstable one for a compressible flow. If our numerical scheme will work fine with this model, it will work fine also for NSF. There are several set of variables used to describe the fluid properties under consideration. In our case we will use the primitive variables formulation at the boundaries (ρ, u, p) and the conserved variable formulation $(\rho, \rho u, E)$ into the inner domain. The latter set of variables derives directly from the fundamental laws of conservation of mass, Newton's Second Law and the law of conservation of total energy without any diffusive flux and with an ideal Equation of state. They will be analyzed in (3.1).
The primitive variables' formulation will be the starting point for the Method of Characteristics whereas the conservative variable formulation is the starting point for the application of the Godunov scheme (conservative Upwind scheme). In our case we will start from the unsteady 1D Euler equations' model with a perfect gas.

3.1 Definition of a conservation law

A formulation is considered a conservation law if the variation in time of the total amount of a quantity inside a given domain is equal to the balance between the amount of that quantity entering and leaving the domain plus the contribution from source terms generating that quantity. If we can mathematically lead back a general equation to this form:

$$\frac{\delta}{\delta t}\int_{\Gamma} y_{\Gamma}\, d\Gamma + \int_{A} \mathbf{F}\cdot\mathbf{n}\, dA = \int_{\Gamma} Q_{\Gamma}\, d\Gamma + \oint \mathbf{Q}_{A}\cdot\mathbf{n}\;\; dA \;\;, \qquad (2)$$

our equation is a conservation law. The terms in the equation 2 are :

- $\frac{\delta}{\delta t}\int_{\Gamma} y_{\Gamma}\, d\Gamma$: *the accumulation term.* It highlights how much our quantity changes in time.
- $\int_{A} \mathbf{F}\cdot\mathbf{n}\, dA$: *the inflow term.* It accounts for the rate of how much of our quantity enters across the domain boundaries and how much is leaving the domain's boundaries.
- $\int_{\Gamma} Q_{\Gamma} d\Gamma$ and $\oint \mathbf{Q}_{A}\cdot\mathbf{n}\;\; dA$: *volume and surface source terms.* They account for how much of our quantity is generated on the surface or into our domain.

The equations we will work with, are all conservation laws because they can be rendered to the (2) equation's form.

3.2 Integral form of the Euler's conservation laws

The integral formulation of the conservation laws involved in the Euler's model, is the starting point for any finite volume method and requires stringent hypothesis on the functions involved but it is the starting point for every numerical method able to solve correctly discontinuous phenomena. The differential formulation, instead, holds on less stringent smoothness hypothesis on the flow variables that are not verified in discontinuities cases and so it will give bad results in presence of shocks. For these reasons we will choose the integral form of the conservation laws for our Euler's equations. The following analysis is taken from [6].

3.2.1 Conservation of Mass

The conservation of mass law states that no mass can be generated or annihilated into a general V volume. It is written in this form:

$$\int\int\int_{V} \frac{\partial \rho}{\partial t}\, dV + \int\int_{A} \mathbf{n}\cdot(\rho\mathbf{V})\, dA \;= 0 \;\;, \qquad (3)$$

where the first integral is the variation in time of the mass inside the control volume whereas the second integral is mass inflow entering through the surfaces with a speed $\mathbf{V}$ less the mass outflow exiting the surfaces with a speed $\mathbf{V}$, per unit of time. Considering a V control volume independent on time we can have the final form:

$$\frac{d}{dt}\int\int\int_V \rho \, dV = -\int\int_A \mathbf{n}\cdot(\rho\mathbf{V}) \, dA \quad . \tag{4}$$

3.2.2 Conservation of Momentum

The conservation of momentum, in the Euler's equations, comes directly from the application of Newton's second law neglecting the diffusive phenomena and states that the rate of change of the momentum quantity in any control volume V is equal to the total force acting on the volume V. Considering the definition of momentum:

$$\mathbf{M}(t) = \int\int\int_V \rho\mathbf{V} \, dV \, , \tag{5}$$

with the definition of the forces acting on the surfaces of the control volume and of the volume forces:

$$f_S = \int\int_A \mathbf{S} \, dA, \; f_V = \int\int\int_V \rho \, \mathbf{g} \, dV \quad , \tag{6}$$

in which we can recognize the $\mathbf{S}$ vector of stresses, the total force acting on the control volume can be written as:

$$f_{tot} = f_S + f_V \quad . \tag{7}$$

Equaling the time derivative of $\mathbf{M}(t)$ and f_{tot} and elaborating the equation, we obtain:

$$\frac{d}{dt}\int\int\int_V (\rho\mathbf{V}) \, dV = -\int\int_A \mathbf{V}(\mathbf{n}\cdot\rho\mathbf{V}) \, dA + f_{tot} \, , \tag{8}$$

in which the general CV is time independent.
The rate of change in time of the momentum quantity, can be seen as due to the net of the entering and exiting momentum quantity across the surfaces and due to the sources of momentum located on the surfaces and in the CV.
Neglecting the viscous stresses and the volume sources we obtain the conservation of momentum in integral form for the Euler equations:

$$\frac{d}{dt}\int\int\int_V (\rho\mathbf{V}) \, dV = -\int\int_A \mathbf{V}(\mathbf{n}\cdot\rho\mathbf{V}) \, dA \quad . \tag{9}$$

3.2.3 Conservation of total Energy

The conservation of total Energy states that, in a control volume (CV), the rate of change of total Energy is equal to the work done, per unit of time, by all the forces acting in the CV and by the net between the total energy entering, minus the total energy leaving the CV across the surfaces.
The total energy quantity is defined as:

$$E_{tot} = \int\int\int_V E \, dV \ , \tag{10}$$

defined as $E = U + E_C + E_p$ sum of Internal energy, Kinetic energy and Potential energy.
The work produced by the surface and the volume forces if given by the dot product between the general force and the general speed ($\mathbf{f}\cdot\mathbf{V}$). Here we summarize the terms accounting for the surface forces' work and for the volume forces' work:

$$E_S = -\int\int_A p(\mathbf{V}\cdot\mathbf{n})dA + \int\int_A \mathbf{V}\cdot(\mathbf{n}\cdot\Pi)\, dA \tag{11}$$

$$E_V = \int\int\int_V \rho(\mathbf{V}\cdot\mathbf{g})\, dV \ . \tag{12}$$

Considering a single CV independent on time the conservation of energy is given by:

$$\frac{d}{dt}\int\int\int_V E \, dV = -\int\int_A (\mathbf{n}\cdot E\mathbf{V})\, dA + E_S + E_V + E_Q \ , \tag{13}$$

with E_Q is the heat flow into the CV per unit of time across a general surface element dA:

$$E_Q = -\int\int_A (\mathbf{n}\cdot\mathbf{Q}) \ . \tag{14}$$

Neglecting the viscous effects, the heat exchanges and the volume and surface work terms, we obtain the conservation of total energy for the homogeneous Euler's equations.

3.3 Conservative formulation

The conservative formulation of the Euler's equations in differential form using the conserved variable set, is the starting point for the application of Finite Volume methods. The system can be expressed as:

$$\mathbf{U}_t + \mathbf{F}(\mathbf{U})_x = \mathbf{0} \tag{15}$$

in which $\mathbf{U}$ is the vector of the conserved variables whereas $\mathbf{F(U)}$ is the vector of the fluxes. They are defined as

$$\mathbf{U} = \begin{bmatrix} u_1 \\ u_2 \\ u_3 \end{bmatrix} \equiv \begin{bmatrix} \rho \\ \rho u \\ E \end{bmatrix}, \quad \mathbf{F(U)} = \begin{bmatrix} f_1 \\ f_2 \\ f_3 \end{bmatrix} \equiv \begin{bmatrix} \rho u \\ \rho u^2 + p \\ u(E+p) \end{bmatrix}. \tag{16}$$

In this system ρ is the density, p is the pressure, u is the flow velocity and E is the total energy per unit volume:

$$E = \rho \left(\frac{1}{2}u^2 + e\right) \ . \tag{17}$$

To close our system of equations we need an equation of state to express the specific internal energy for our fluid. The fluid considered in our model is the dry air modeled as a perfect gas obeying to the ideal thermal equation of state:

$$pV = RT \ , \tag{18}$$

with R specific gas constant. In this model the specific heats at constant pressure and at constant volume can be expressed as:

$$c_p = \frac{\gamma R}{\gamma - 1} \ , c_v = \frac{R}{\gamma - 1} \ , \tag{19}$$

with $\gamma = c_p/c_v$ for an ideal gas. For our purpose we will use $\gamma = 1.4$, that is a very good approximation of the *dry air* as ideal gas in a temperature range from $0°\ C$ to $1000°C$ and it results experimentally accurate for the monatomic gasses. Thanks to the equation of state we can link the density and the pressure through the specific internal energy as :

$$e = e(p, \rho) = \frac{p}{(\gamma - 1)\rho}. \tag{20}$$

For these conditions the *speed of sound* can be expressed as

$$a = \sqrt{\frac{\gamma p}{\rho}}. \tag{21}$$

The system is now in a closed form and we can analyze its mathematical properties that allows us to solve numerically our problem.

3.4 Properties of the homogeneous Euler equations

In this part we'll discuss about the fundamental properties of the Euler equations in homogeneous form (15) as starting point to apply the Godunov numerical method in the further chapter. We will focus only on the properties useful to our scope.

3.4.1 Quasi-linear form, Eigenvalues and Eigenvectors

A system of PDE is called quasi-linear when the coefficients of the highest order derivatives of the dependent variables, don't depend on the highest order derivatives of the variable itself. Our Euler system of conservation laws can be written in a quasi-linear form applying the chain rule to the equation 15 :

$$\frac{\partial \mathbf{F}(\mathbf{U})}{\partial x} = \frac{\partial \mathbf{F}}{\partial \mathbf{U}} \frac{\partial \mathbf{U}}{\partial x} \ , \tag{22}$$

obtaining the expression:

$$\mathbf{U}_t + \mathbf{A}(\mathbf{U})\mathbf{U}_x = \mathbf{0} \tag{23}$$

where the $\mathbf{A(U)}$ matrix is called Jacobian matrix defined as

$$\mathbf{A}(\mathbf{U}) = \frac{\partial \mathbf{F}}{\partial \mathbf{U}} = \begin{bmatrix} \frac{\partial f_1}{\partial u_1} & \frac{\partial f_1}{\partial u_2} & \frac{\partial f_1}{\partial u_3} \\ \frac{\partial f_2}{\partial u_1} & \frac{\partial f_2}{\partial u_2} & \frac{\partial f_2}{\partial u_3} \\ \frac{\partial f_3}{\partial u_1} & \frac{\partial f_2}{\partial u_2} & \frac{\partial f_3}{\partial u_3} \end{bmatrix} \tag{24}$$

in which f_1, f_2, f_3 are the fluxes and u_1, u_2, u_3 the conserved variables. The Euler's equations (15) satisfy also the homogeneity properties which is the starting point for the Flux Vector Splitting methods. Thanks to this property the fluxes of the system can be written in this form:

$$\mathbf{F}(\mathbf{U}) = \mathbf{A}(\mathbf{U})\mathbf{U} \ . \tag{25}$$

Computing $\mathbf{A(U)}$ for the Euler equations we obtain :

$$\mathbf{A}(\mathbf{U}) = \begin{bmatrix} 0 & 1 & 0 \\ -\frac{1}{2}(\gamma-3)(\frac{u_2}{u_1})^2 & (3-\gamma)(\frac{u_2}{u_1}) & \gamma-1 \\ -\frac{\gamma u_2 u_3}{u_1^2} + (\gamma-1)(\frac{u_2}{u_3})^3 & \frac{\gamma u_3}{u_1} - \frac{3}{2}(\gamma-1)(\frac{u_2}{u_1})^2 & \gamma(\frac{u_2}{u_1}) \end{bmatrix}$$

The Eigenvalues of the Jacobian matrix $\mathbf{A}$ are :

$$\lambda_1 = u - a \ \ , \lambda_2 = u \ \ , \lambda_3 = u + a \tag{26}$$

and the Eigenvectors correspondent and composing the matrix $\mathbf{K}$ are:

$$\mathbf{K}_1 = \begin{bmatrix} 1 \\ u-a \\ H-ua \end{bmatrix} \ , \mathbf{K}_2 = \begin{bmatrix} 1 \\ u \\ \frac{1}{2}u^2 \end{bmatrix} \mathbf{K}_3 = \begin{bmatrix} 1 \\ u+a \\ H+ua \end{bmatrix} \ , \tag{27}$$

with total enthalpy $H = (E+p)/\rho \equiv \frac{1}{2}u^2 + h$.
The Eigenvectors are linearly independent and the Eigenvalues all real.

3.4.2 Hyperbolicity and Non-linearity for the Euler's equations.

A system of partial differential equation of m equations in m unknowns is said to be hyperbolic in a generic point (x,t) of a domain x-t if the Jacobian matrix associated, has m real Eigenvalues and a corresponding set of m linearly independent right Eigenvectors. If all the Eigevalues are distinct the system is strictly hyperbolic. The unsteady one-dimensional Euler's equations are a set of non-linear hyperbolic equations because the Eigenstructure (26) satisfies the property just described.
The main features of an hyperbolic homogeneous system of PDEs are based on the fact that , in this kind of problems, the information provided at time $t = 0$ propagates in time along characteristic curves. The slope of these curves in x-t plane is given by their Eigenvalues. In a linear hyperbolic PDE the initial information remains constant evolving in time whereas the information of a non-linear hyperbolic PDE are distorted because of the non-linearity.
The Euler equations are non-linear since the speed of propagation of the information of the system, are dependent on the system properties.

3.4.3 Characteristic lines and Well Posed Problem theory

A characteristic curve is defined as a curve in the x-t domain along which a PDE set of equations can be decomposed in ODE. The number of characteristic lines for an hyperbolic system is equal to the number of Eigenvalues. Thanks to the Method of Characteristics the Euler equations can be decoupled in a set of 3 wave equations along which the Riemann variables remains constant. Even if this method will not be used in the Godunov scheme, it reveals the physical meaning of the propagation of information mechanism inside the Euler's equations.
Following the characterization of Hadamard:

Definition 3.1 *"A mathematical model describing physical phenomena is a well-posed problem if:*

- *a solution exist*
- *the solution is unique*
- *the solution's behaviour changes continuously with the initial conditions and the boundary conditions."*

An hyperbolic system of PDEs composes a well-posed problem if :

- The domain is infinite and initial conditions are provided for every point of the domain and for every unknown property. The initial conditions must not be provided along characteristic lines.

- The domain is limited, boundary conditions are provided for each piece of boundary in the number foregone by the Theory of Characteristic and both initial conditions and boundary conditions must not be provided along characteristic lines.

In these cases a solution exist and it is unique.

Now that we have faced all the properties for the homogeneous Euler's equations we can introduce the complete model, including a source term, that will be used for the Godunov numerical method. The Eigenstructure will remain the same of the homogeneous analysis.

3.5 Generalized Euler equations with source term

To fully describe the behaviour of the physical model presented in the chapter (2) we have to add the uni-dimensional source terms to our homogeneous Euler equations.

3.5.1 Generalized Euler equations

Even if the diffusive mechanisms are not involved into the Euler equations, they can be modeled by uni-dimensional source terms accounting for the viscous effect induced by the friction in our duct walls and for the heat exchanged in any section. From [2] chapter 5.5.1, the model that includes the friction and the heat exchange with environment is:

$$\begin{cases} \frac{\partial \rho}{\partial t} + \frac{\partial(\rho u)}{\partial x} = 0 \\ \frac{\partial(\rho u)}{\partial t} + \frac{\partial(p+\rho u^2)}{\partial x} = -\frac{4\tau_w}{D} \\ \frac{\partial(\rho\, e_{tot})}{\partial t} + \frac{\partial(\rho u h^0)}{\partial x} = \frac{4\,\dot{q}_f}{D} \end{cases} \tag{28}$$

in which we have τ_w , $\dot{q_f}$ that are respectively the friction on the walls and the thermal power exchanged through the walls by convection.
All the right-side terms of the system (28) are treated , as volume terms, with a dependence only on the system's quantity and not dependent on the derivatives in time and space of them.
Considering the τ_w coefficient linked with the Moody diagram as $\tau_w = \lambda\rho\frac{u}{8}|u|$ and considering $f = \lambda/4$ we can write :

$$\tau_w = f\rho\frac{u}{2}|u|. \tag{29}$$

Considering an infinitesimal volume $Adx = \pi D^2 dx/4$ for a circular shape area (for other shapes an equivalent diameter can be chosen), we have:

$$\frac{\tau_w \pi D dx}{\pi/4 D^2 dx} = \frac{4\tau_w}{D} \quad , \tag{30}$$

the ratio between the work produced by the friction force on the infinitesimal duct length over the infinitesimal duct volume.

3.5.2 Evaluation of friction factor f

In the previous model we have used an f mean friction factor along the duct as starting point for our model. Following [2] for lengths higher than $50D$ and a subsonic compressible flow, the f friction factor isn't affected by the Mach number and we can evaluate $f = \lambda/4$ with a good approximation with:

$$\frac{1}{\sqrt{\lambda}} = -2\log_{10}\frac{2.51}{Re_D\sqrt{\lambda}}\ , \tag{31}$$

for smooth ducts and with the Colebrook-White formula:

$$\frac{1}{\sqrt{\lambda}} = -2\log_1 0\left(\frac{2.51}{Re_D\sqrt{\lambda}} + \frac{\epsilon}{3.71D}\right) \tag{32}$$

for non-smooth ducts with ϵ relative roughness. The value of $\lambda(Re, \epsilon)$ can be found with iterative methods for a material and a length, finding the Reynolds number and knowing the experimental relative roughness. In a length from 0 to $50D$ and a subsonic flow we cannot consider a flow one-dimensional because of the change in the speed profiles. In this case we can introduce an f_{app} mean apparent friction factor that will include a coefficient to take in account the speed change for each section. This will be similar to the Moody diagram one in case of turbulent flow whereas it will be higher than the Moody one in case of laminar flow.
In the supersonic flows, the length L_{max} is usually too much short to have a fixed profile of speed and so it is used always an f_{app} coefficient to take in account the speed variations in a single section. Experimental evidences in supersonic flows have outlined a value of $0.002 < f < 0.003$ in the supersonic field for 1.2 <Mach< 3 and $25 \cdot 10^3 < Re < 7 \cdot 10^5$. These values are doubled in respect to the incompressible ones for the same Reynolds range and they underlines the crucial difference between compressible and incompressible flows.
In our numerical model we will use the experimental value: $f = 0.003$.

3.5.3 Evaluation of the heat exchanged

The quantity considered in the Rayleigh model is an heat flow entering each diameter section from the external. For the purpose of this work we are considering a positive constant flow for each section . This

choice is motivated by the fact that the heat flow constant value allows to find the analytical solution in a much simple way whereas a variable heat flow should be analyzed with a more complex approach.
A variable heat flow should be defined by a convective heat transfer for each section proportional to the difference between the inner temperature and the environment's temperature multiplied by the convective heat transfer coefficients. Since the difficulty to correctly model the convective heat transfer coefficient, especially for a supersonic flow, this case has been not considered in what follows, where a constant heat flux has been considered.

3.5.4 The Euler's equation with Area variation

To take to account also the Area variation, in our Euler's equations, we can refer to the model presented by Toro in ([6]) chapter 1.6.2 :

$$\boldsymbol{U_t + F(U)_x = S} \ , \tag{33}$$

with:

$$\mathbf{U} = \begin{bmatrix} \rho \\ \rho u \\ E \end{bmatrix}, \ \mathbf{F(U)} = \begin{bmatrix} \rho u \\ \rho u^2 + p \\ u(E+p) \end{bmatrix} \ \mathbf{S} = -\frac{1}{A}\frac{dA}{dt} \begin{bmatrix} \rho \\ \rho u \\ (E+p) \end{bmatrix}$$

with $\frac{dA}{dt} = A_t + uA_x$.
In our case we will consider the variation of the area A only dependent on space and so $A_t = 0$. Thanks to this particular formulation we can avoid to rebuild the complete Eigenproblem of the Euler equation and we can use the same Eigenstructure of the homogeneous Euler's system. In this way, in our Godunov scheme, the area variation will be considered only into the source term. The goodness of this formulation will be proved in the Validation section.

3.5.5 Complete Euler model with source term

Merging the two previous models (3.5.4) and (3.5.1) we arrive, finally, to the complete model for the unsteady one-dimensional Euler's equation with wall friction, heat exchange with the environment and area variation.
The model can be written as:

$$\begin{cases} \frac{\partial \rho}{\partial t} + \frac{\partial(\rho u)}{\partial x} = -\frac{1}{A}\frac{dA}{dx}\rho u \\ \frac{\partial(\rho u)}{\partial t} + \frac{\partial(p+\rho u^2)}{\partial x} = -\frac{4\tau_w}{D} - \frac{1}{A}\frac{dA}{dx}\rho u^2 \\ \frac{\partial(\rho e_{tot})}{\partial t} + \frac{\partial(\rho u h^0)}{\partial x} = \frac{4\dot{q}_f}{D} - \frac{1}{A}\frac{dA}{dx}u(E+p) \end{cases} \tag{34}$$

or in compact form as eq.(33) with :

$$\mathbf{U} = \begin{bmatrix} \rho \\ \rho u \\ E \end{bmatrix}, \quad \mathbf{F(U)} = \begin{bmatrix} \rho u \\ \rho u^2 + p \\ u(E+p) \end{bmatrix} \mathbf{S} = \begin{bmatrix} -\frac{1}{A}\frac{dA}{dx}\rho u \\ -\frac{4\tau_w}{D} - \frac{1}{A}\frac{dA}{dx}\rho u^2 \\ \frac{4\dot{q}_f}{D} - \frac{1}{A}\frac{dA}{dx}u(E+p) \end{bmatrix} \tag{35}$$

4 The Riemann problem for the Euler's Equations

In agreement with [6]: the exact solution of the Riemann problem for the Euler's equations is the starting point for a Godunov scheme and it contains the fundamental physic behind the behaviour of compressible materials. There is no closed-form solution for Riemann problem

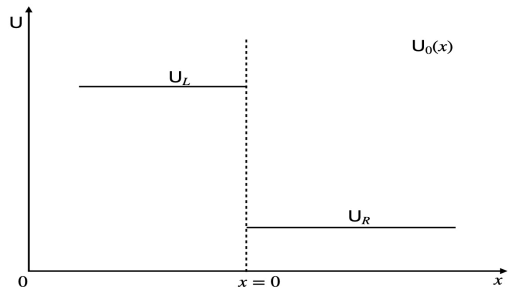

Figure 3: The Riemann problem

for Euler's equation with ideal gasses, neither substituting the energy equation with a more easy homoentropic or iso-thermal evolution but, it is possible to find a solution iteratively with any practical degree of accuracy.
The first exact Riemann solver for the Euler Equation is accredited to Godunov. There are two Riemann's solvers developed by Godunov but for our purpose we'll use the more efficient second Riemann solver. In this chapter we'll describe the solution of the Riemann problem as elementary waves which divide our domain in different parts with different properties depending on the wave considered and upon the initial conditions for the Riemann problem.

$$\begin{cases} \mathbf{U}_t + \mathbf{F(U)}_x = \mathbf{0} \\ \mathbf{U}(x,0) = \mathbf{U}^{(0)}(x) = \begin{cases} \mathbf{U}_L \ \text{if} x < 0 \\ \mathbf{U}_R \ \text{if} x > 0 \ . \end{cases} \end{cases} \tag{36}$$

The classical solution of the Riemann problem is graphically depicted in figure (4)

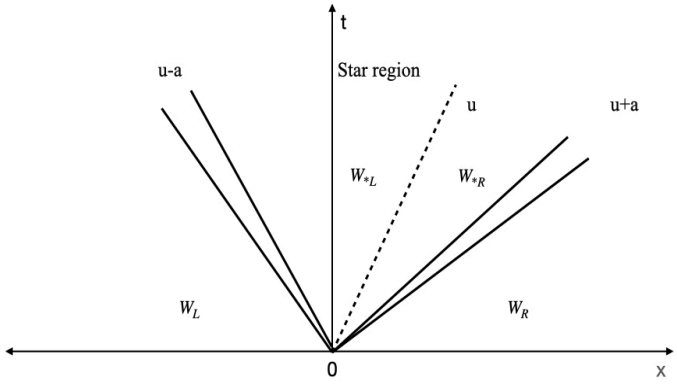

Figure 4: The Riemann problem's solution.

with three non-linear waves, each one associated with an eigenvalue, which seize three internal zones and which nature depends upon the right and left initial conditions.
The wave associated with the second eigenvalue λ_2 is a *contact discontinuity* whereas the waves associated to λ_1 and λ_3 can both be a *shock wave* or a *rarefaction fan* depending on the initial conditions and on the properties for the Riemann problem inside the different zones of the (x-t) domain. The property in the inner domain must be investigated through an iterative process which will be described in details in chapter (4.1), since no exact solution exists for this Riemann problem. In the figure (5) we have a shock wave for the first eigenvalue, a contact discontinuity and a rarefaction fan for the third eigenvalue. For the rarefaction wave we have that :

$$u_R - a_R \leq u_{R*} - a_{R*} \ . \tag{37}$$

For the shock wave related to the third eigenvalue:

$$u_{L*} + a_{L*} > S_3 > u_L + a_L \ \ , \tag{38}$$

with S_3 speed of the shock. For the contact discontinuity associated with the eigenvalue two we have :

$$u_{R*} = u_{L*} = S_2 \tag{39}$$

with S_2 speed of the discontinuity. We must characterize now each discontinuity and how the properties change across them.

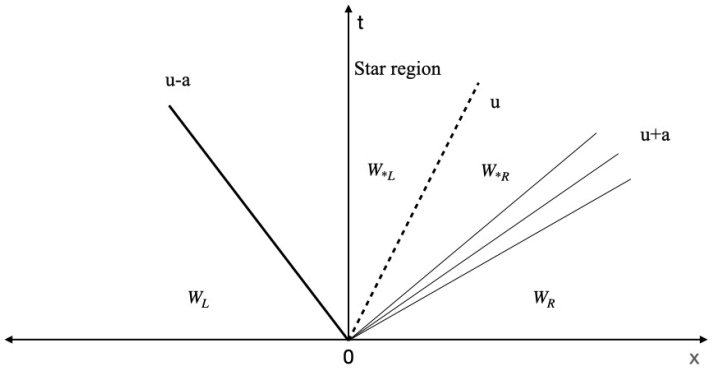

Figure 5: Example for a Riemann problem's solution.

4.0.1 The non-linear wave equation.

To correctly forecast the change of the properties across a general discontinuity we need the characterization of the non-linearities and shock formation.
The analysis is restricted to a single non linear wave equation. The Riemann problem for the Euler's equations will use the same reasoning.
In a non-linear case the characteristic speed $\lambda(u)$ of a discontinuity is function of the solution itself and so, the initial value is propagated with changes as shocks and distortions of the initial data. Mathematically, these phenomena, are linked to the convex nature of the flux function for which some values in the domain move faster than others. If in times after the initial instant the initial data transform into a flatter region we are in an expansive region and the $\lambda_x > 0$ while, if the data becomes narrower and steeper we have a compressive region and $\lambda_x < 0$. In the Euler's equations model there's an increasing compression effect that can end with the creation of a shock wave (in Euler's homogeneous equation we have an inviscid model and more predisposition in creating shocks.)
We will analyze the change of properties across each discontinuity present in the Riemann problem for the Euler's equations.

4.0.2 Contact discontinuity

A contact wave is a discontinuity across which the only properties that change are the density and all the properties related to it (internal energy, sound speed, temperature etc.). The pressure and speed, instead,

keep constant across it. These results came directly from the evaluation of the Eigenstructure of the Euler's equations. We can arrive to the relation:

$$d\rho = \frac{d(\rho u)}{u} = \frac{dE}{1/2u^2} \tag{40}$$

and rearranging it we can arrive to define that, across a contact discontinuity:

$$p = constant \;\; u = constant \; . \tag{41}$$

4.0.3 Rarefaction waves

Rarefaction waves are associated with the first and third eigenvalues. Recalling Riemann's invariant and the Entropy formulation we can state that the p, ρ and u vary as:

$$across \;\; \lambda_1 = u - a \begin{cases} I_L(u,a) = u + \frac{2a}{\gamma - 1} = constant \\ s = constant \end{cases} \tag{42}$$

$$across \;\; \lambda_3 = u + a \begin{cases} I_R(u,a) = u - \frac{2a}{\gamma - 1} = constant \\ s = constant \end{cases} \tag{43}$$

Across a rarefaction wave the Entropy keeps constant, the shape is a fan type enclosed between an head and a tail and the properties vary as prescribed by general Riemann's invariant. The variation of the properties will be discussed for the Euler equation in chapter (4.5.2).

4.0.4 Shock waves

The shock waves are discontinuities related to first and third Eigenvalues.
Across this discontinuity p, ρ and u changes. The relations across shock discontinuity are exposed by the Rankine-Hugoniot (RH) condition for a steady state shock. The general RH condition gives the general Shock speed as :

$$S = \frac{\Delta f}{\Delta u} \;\; , \tag{44}$$

with :

$$\Delta f = f(u(x_R,t)) - f(u(x_L,t)) \;\; , \;\; \Delta u = u(x_R,t) - (u(x_L,t) \; , \tag{45}$$

respectively the flux function and the speed around the discontinuity. When the frame is fixed the speed is null and so more easy relations

can be applied. To analyze our case we cannot work with a null speed but we can use the relative speeds in a transformed plane:

$$u_{rel_*} = u_* - S_3 \ , \ u_{rel_R} = u_R - S_3 \ , \tag{46}$$

with S_3 shock speed. Applying the Rankine-Hugoniot conditions we obtain:

$$\rho_* u_{rel_*} = \rho_R u_{rel_R} \ ; \tag{47}$$

$$\rho_* u_{rel_*}^2 + p_* = \rho_R u_{rel_R}^2 + p_R \ ; \tag{48}$$

$$u_{rel_*}(E_{rel_*} + p_*) = u_{rel_R}(E_{rel_R} + p_R) \ . \tag{49}$$

Developing our RH conditions we resort to the equations useful to understand how the flow properties changes across a shock. The relation on the density is:

$$\frac{\rho_*}{\rho_R} = \frac{(\gamma+1)(M_R - M_S)^2}{(\gamma-1)(M_R - M_S)^2 + 2} \ . \tag{50}$$

The relation for the pressure is:

$$\frac{p_*}{p_R} = \frac{2\gamma(M_R - M_S)^2 - (\gamma-1)}{(\gamma+1)} \ ; \tag{51}$$

with:

$$M_R = u_R/a_R \ \ M_S = S_3/a_R \ , \tag{52}$$

M_R Mach number in the flow at the right side in respect with the shock and M_S the shock Mach number. We can relate shock speed S_3 to density and pressure ratios using $M_R - M_S$. At the end we obtain an expression for shock speed as function of pressure ratio across the discontinuity:

$$S_3 = u_R + a_R \sqrt{(\frac{\gamma+1}{2\gamma})\frac{p_*}{p_R} + \frac{\gamma-1}{2\gamma}} \ . \tag{53}$$

4.1 Resolution of Riemann problem for 1D Euler equations

Following the passages proposed by E.Toro in [6] chapter 4 we can fully solve iteratively the Riemann problem for the equations (15). We're going to solve for a single point the Riemann problem for the Euler equations. In the Godunov scheme this solution will be extended to all the points inside the computational domain.

The Riemann problem for the Euler's equations is an initial value problem for the system:

$$\begin{cases} \mathbf{U}_t + \mathbf{F}(\mathbf{U})_x = \mathbf{0} \\ \mathbf{U}(x,0) = \mathbf{U}^{(0)}(x) = \begin{cases} \mathbf{U}_L \;\; if x < 0 \\ \mathbf{U}_R \;\; if x > 0 \; . \end{cases} \end{cases} \tag{54}$$

We're interested to find a value for each conserved variable $(\rho, \rho u, E)$ in all the points (x,t) in the x-t plane for $-\infty < x < \infty$ with $t > 0$. In case of infinite domain, the solution will depend only on the initial condition (IVP).
If we consider a discontinuity as figure (3) pointed at x = 0 that separates two constant states, during the propagation in time, a sudden variation of the properties of the flow can occur. Depending on the initial condition and on the property values of the x-t domain the discontinuity can lead to different property variations as shown in figure (6). To fully define these properties we have to solve the Riemann problem. For simplicity we will use the primitive variables' formulation to find the solution to the Riemann problem and after we'll return to conservative variables to apply the upwind part of the Godunov scheme.
The initial constant properties at left and right of the $x = 0$ point are $\mathbf{W}_L = (\rho_L, u_L, p_L)$ and $\mathbf{W}_R = (\rho_R, u_R, p_R)$. If no vacuum is present (vacuum condition will be explained later) the complete solution of the Riemann problem is given by the subdivision of the x-t plane in in four constant regions subdivided by the waves generated for each property. The eigenvalues of the Euler equations $\lambda_1 = u - a$, $\lambda_2 = u$ and $\lambda_3 = u + a$ subdivide the domain into the constant regions. The first and the third Eigenvalues, depending on the properties in the domain, can became both a shock discontinuity or a rarefaction fan; the second eigenvalue, instead, is always a contact discontinuity and defines the $\mathbf{W}_{L*}$ left star region and the $\mathbf{W}_{R*}$ right star region.
All the possible cases are four as depicted in figure (7). To find the complete solution we start knowing the left and the right initial constant properties. After we proceed finding iteratively the p* and u* properties which are the same in the left and right star regions and, at the end the ρ_{*L} and ρ_{*R} values which are different between them. The only properties that change across the contact discontinuity are the density and all the properties related to it.
Once we've done this we can characterize the first and the third characteristic lines' nature and we find all the properties in the whole domain. The problem would be closed and all the zones in x-t plane are defined if the star properties are known. To clarify we show in figure(8) a classical pattern solution for a Riemann problem once the star properties

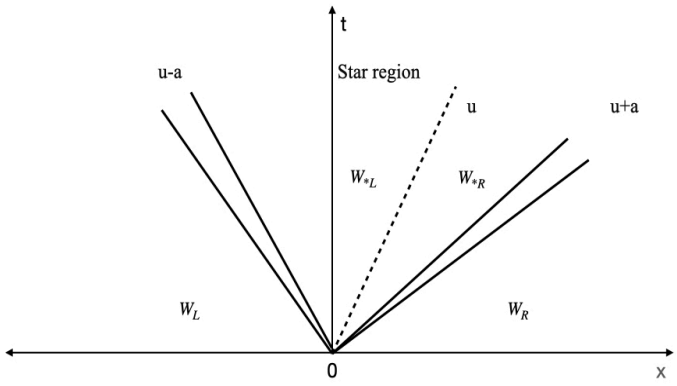

Figure 6: The Riemann problem's solution.

are known. In the next section we will fully define the star zones.

4.2 Finding p* and u*

To find the star region properties we must use an iterative method. Following Toro in [6] : the solution for pressure p* of the Riemann problem with the ideal gas equation of State is given by the root of the equation:

$$f(p, \mathbf{W}_R, \mathbf{W}_L) \equiv f_L(p, \mathbf{W}_L) + f_R(p, \mathbf{W}_R) + \Delta u = 0 \tag{55}$$

with

$$\Delta u \equiv u_R - u_L \ , \tag{56}$$

and with f_L and f_R defined as:

$$f_L(p, \mathbf{W}_L) = \begin{cases} (p - p_L)\left[\frac{A_L}{p+B_L}\right]^{\frac{1}{2}} & \text{if} p > p_L(shock) \\ \frac{2a_L}{(\gamma-1)}\left[\left(\frac{p}{p_L}\right)^{\frac{\gamma-1}{2\gamma}} - 1\right] & \text{if} p < p_L(rarefaction) \end{cases} \tag{57}$$

$$f_R(p, \mathbf{W}_R) = \begin{cases} (p - p_R)\left[\frac{A_R}{p+B_R}\right]^{\frac{1}{2}} & \text{if} p > p_R(shock) \\ \frac{2a_R}{(\gamma-1)}\left[\left(\frac{p}{p_R}\right)^{\frac{\gamma-1}{2\gamma}} - 1\right] & \text{if} p < p_R(rarefaction) \end{cases} \tag{58}$$

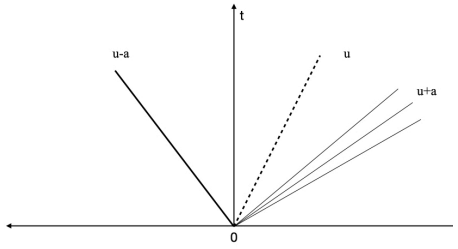

(a) Left shock wave and right rarefaction fan.

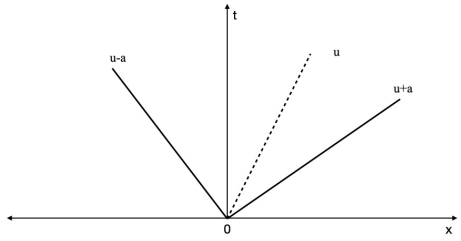

(b) Left shock wave and right shock wave.

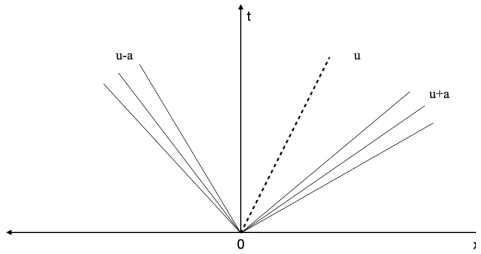

(c) Left rarefaction fan and right rarefaction fan.

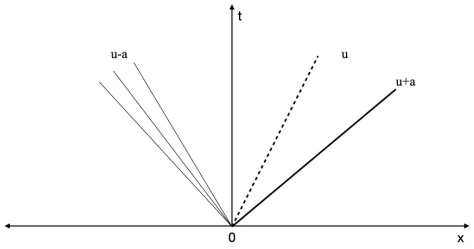

(d) Left rarefaction fan and right shock wave.

Figure 7: All the possible different wave patterns in the solution of the Riemann problem.

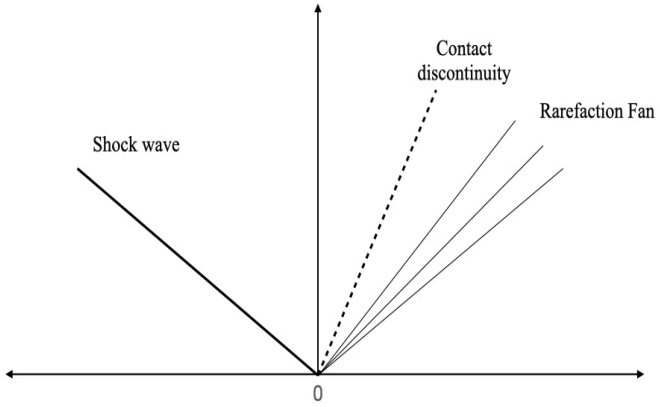

Figure 8: A Riemann problem 's solution example.

and with the constants A_L , B_L , A_R , B_R:

$$\begin{cases} A_L = \frac{2}{(\gamma+1)\rho_L} \ , \ B_L = \frac{(\gamma-1)}{(\gamma+1)} p_L \\ A_R = \frac{2}{(\gamma+1)\rho_R} \ , \ B_R = \frac{(\gamma-1)}{(\gamma+1)} p_R \end{cases} \tag{59}$$

with p a generic pressure in the zone after the discontinuity. If we have $f(p) = 0$ we have found our $p*$.
The iterative nature of the procedure is due to the fact that $f_L(p, \mathbf{W}_L)$ and $f_R(p, \mathbf{W}_R)$ are dependent on the $p*$ and so we have to impose a p_{try} and we have to find the f_R and f_L functions for this p_{try}. If $f(p_{try}) = 0$, the p_{try} is our p_* and we're done. If not, we have to use another p_{try} and check again if $f(p_{try}) = 0$.
The u* can be found once we know p* as

$$u_* = \frac{1}{2}(u_L + u_R) + \frac{1}{2}[f_R(p_*) + f_L(p_*)] \ . \tag{60}$$

4.3 f_L and f_R functions

Both the f_L and f_R functions depends on the nature of the left and right waves and both the functions can be a shock or a rarefaction wave depending on the primitive variables before and after the wave. We will analyze the left function but all the consideration below can be applied, considering the right parameters, also for the right function.

4.3.1 f_L function in shock case

The left wave is linked to the first eigenvalue λ_1 and its nature depends upon p* and $\mathbf{W}_L$ properties. If we assume that the left wave is a shock moving with the S_L speed ,the relation between left values (ρ_L, p_L, u_L) and the post-shock values $(\rho_{*L}, p_{*L}, u_{*L})$ is given by the Rankine-Hugoniot condition considering a relative speed. In order to work with the steady state shock formulas we have to introduce the relative speeds:

$$u_{Lrel} = u_L - S_L \ , \ u_{*rel} = u_* - S_L \tag{61}$$

that are equivalent to consider our frame moving with the shock speed S_L. The Rankine-Hugoniot condition across the shock wave gives:

$$\rho_L u_{Lrel} = \rho_{*L} u_{*rel} \ , \tag{62}$$

$$\rho_L u_{Lrel}^2 + p_L = \rho_{*L} u_{*rel}^2 + p_* \ , \tag{63}$$

$$u_{Lrel}(E_{Lrel} + p_L) = u_{*rel}(E_{*rel} + p_*) \ , \tag{64}$$

With E_{Lrel} and E_{*rel} total energy per unit of volume evaluated using the relative speeds. After some passages we arrive to a relation for the ρ_{*L} in function of p_* :

$$\rho_{*L} = \rho_L \left[\frac{(\frac{\gamma-1}{\gamma+1}) + \frac{p_*}{p_L}}{(\frac{\gamma-1}{\gamma+1})\frac{p_*}{p_L} + 1} \right] . \tag{65}$$

For the flow velocity in star region we obtain:

$$u_* = u_L - f_L(p*, \mathbf{W}_L) . \tag{66}$$

For the f_L relation we obtain:

$$f_L(p_*, \mathbf{W}_L) = (p_* - p_L) \left[\frac{A_L}{p_* + B_L} \right]^{\frac{1}{2}} \tag{67}$$

with

$$A_L = \frac{2}{(\gamma+1)\rho_L} \ , \ B_L = \frac{(\gamma-1)}{(\gamma+1)} p_L . \tag{68}$$

4.3.2 f_L function for left rarefaction

In case of $p*$ conditions for which we have a rarefaction fan we can find the properties inside and after the rarefaction fan using the isoentropic relation and the generalized Riemann invariant linked to the first eigenvalue across the fan to link the properties of the star region with $\mathbf{W}_L$. After some calculation we obtain the f_L function in case of rarefaction fan:

$$f_L(p_*, \mathbf{W}_L) = \frac{2a_L}{(\gamma-1)} \left[\left(\frac{p_*}{p_L} \right)^{\frac{\gamma-1}{2\gamma}} - 1 \right] \ ; \tag{69}$$

here a_L is found from:

$$a_L = \sqrt{\gamma \frac{p_L}{\rho_L}} \tag{70}$$

The density in the left part of the star region is given by the isoentropic evolution across the fan:

$$\rho_{*L} = \rho_L \left(\frac{p_*}{p_L} \right)^{\frac{1}{\gamma}} \tag{71}$$

The flow speed in the star region is :

$$u_* = u_L - f_L(p*, \mathbf{W}_L) \tag{72}$$

4.3.3 f_R function for right shock case

The same considerations can be applied in the same way to found f_R in both the cases of shock and rarefaction as the previous procedure. The starting point in this case are the relative speeds:

$$u_{Rrel} = u_R - S_R \ , \ u_{*rel} = u_* - S_R \ . \tag{73}$$

All the other passages are the same of the left case. Here we report the formulas:

$$f_R(p_*, \mathbf{W}_R) = (p_* - p_R)\left[\frac{A_R}{p_* + B_R}\right]^{\frac{1}{2}} \tag{74}$$

with

$$A_R = \frac{2}{(\gamma+1)\rho_R} \ , \ B_R = \frac{(\gamma-1)}{(\gamma+1)} p_R \ . \tag{75}$$

The particle velocity in the right star region is:

$$u_* = u_R + f_R(p, \mathbf{W}_R) \ . \tag{76}$$

4.3.4 f_R function for right rarefaction fan

Also for the right rarefaction case there's the same reasoning as the left one. Here we report the formulas. After some calculation we obtain the f_R function in case of rarefaction fan:

$$f_R(p_*, \mathbf{W}_R) = \frac{2a_R}{(\gamma-1)}\left[\left(\frac{p_*}{p_R}\right)^{\frac{\gamma-1}{2\gamma}} - 1\right] \tag{77}$$

Where a_L is found from

$$a_R = \sqrt{\gamma \frac{p_R}{\rho_R}} \tag{78}$$

The particle velocity in the right star region is:

$$u_* = u_R + f_R(p, \mathbf{W}_R) \ . \tag{79}$$

Now we are able to compose our $f(p, \mathbf{W}_R, \mathbf{W}_L)$ function by equaling the left and right u_*. In fact we know that across the contact discontinuity the pressure and the speed are constant. The result will be the function

$$f(p, \mathbf{W}_R, \mathbf{W}_L) \equiv f_L(p, \mathbf{W}_L) + f_R(p, \mathbf{W}_R) + \Delta u = 0 \tag{80}$$

The solution of $f(p) = 0$ numerically defines the left and right case completely:

- if $p_* > p_L$ and $p_* > p_R$ we have a left and a right shock;
- if $p_L > p_*$ and $p_R > p_*$ we have a left and a right rarefaction.
- if $p_L > p_*$ and $p_* > p_R$ we have a left rarefaction and a right shock.
- if $p_* > p_L$ and $p_R > p_*$ we have a left shock and a right rarefaction.

Once the right and left conditions are defined we can define the u_* speed from one of the two formulas of u_* (left and right case) or from a mean value :

$$u_* = \frac{1}{2}(u_R + u_R) + \frac{1}{2}(f_R(p, \mathbf{W}_R) - f_L(p, \mathbf{W}_L)) \ . \tag{81}$$

4.4 p* Iterative algorithm

To solve the non-linear $f(p) = 0$ function we can apply any numerical method. The function $f(p) = 0$ is monotone and concave and Δu , p_L and p_R are the fundamental parameters to find the numerical root. The main condition to find a unique solution is to respect the non-vacuum condition. For too much low Δu the non-linear waves cannot create in vacuum and the solution of Riemann problem and gives a negative $p*$. To avoid this condition we must verify the *pressure positive condition* for which:

$$(\Delta u)_{critic} \equiv \frac{2a_L}{\gamma - 1} + \frac{2a_R}{\gamma - 1} > u_R - u_L \ . \tag{82}$$

In the resolutive algorithm, if this condition is violated we cannot find a $p*$ and we have to apply a different numerical method from the following one. If this condition of non-vacuum is respected given the initial data $\mathbf{W}_L, \mathbf{W}_L$ a unique positive solution p_* exists. The algorithm used is Newton-Raphson with a p_{guess} initial value. The choice of the initial guess can only affect the time to reach the convergence in the method but it's not a critical parameter for the success in find the root. The choice in the algorithm is:

$$p_{TR} = \left[\frac{a_L + a_R - \frac{1}{2}(\gamma - 1)(u_R - u_L)}{a_L / p_L^{\frac{\gamma-1}{2\gamma}} + a_R / p_R^{\frac{\gamma-1}{2\gamma}}} \right]^{\frac{2\gamma}{\gamma-1}} , \tag{83}$$

this is called two rarefaction approximation because, if applied in searching of Riemann solution, it would give a rarefaction discontinuity both

for the left and right waves. Since the equation (55) is non-linear we have to guess an initial value and, if it is not correct, to try with another value. To find the correct iteration till the $p*$ value we use the Newton-Raphson procedure. It is based on the Taylor expansion since the smooth condition for $f(p)$ is satisfied.

$$f(p_0 + \delta) = f(p_0) + \delta f'(p_0) + O(\delta^2) \tag{84}$$

If the p_0 is a solution for f(p) then

$$f(p_0) + \delta f'(p_0) = 0\,, \tag{85}$$

so the value corrected $p_1 = p_0 + \delta$ is

$$p_1 = p_0 - \frac{f(p_0)}{f'(p_0)}\,. \tag{86}$$

We can iterate this procedure until the relative pressure change (RPC) between the k^{th} iteration and the $k^{th} - 1$ iteration is less than a prescribed tolerance , usually $\epsilon = 10^{-6}$.

$$RPC = \frac{|p_{(k)} - p_{(k-1)}|}{\frac{1}{2}|p_{(k)} + p_{(k-1)}|} \tag{87}$$

The first derivative of the $f(p, \mathbf{W}_R, \mathbf{W}_L)$ to be insert in the numerical method is:

$$f'_k = \begin{cases} \left(\frac{A_k}{B_k+p}\right)^{\frac{1}{2}} \left[1 - \frac{p-p_k}{2(B_k+p)}\right] & if p > p_K(shock) \\ \frac{1}{\rho_K a_K}\left(\frac{p}{p_K}\right)^{-(\gamma+1)/2\gamma} & if p \leq p_K(rarefaction)\,, \end{cases} \tag{88}$$

with A_K and B_K as in (59), in which the $(K = L, R)$ letter generalize the fact that substituting the value of the left or right wave we can obtain, respectively, the left or right function first derivative.

4.5 Complete solution of Riemann problem

Thanks to the iterative scheme we've found the p_* pressure and consequently the u_*. These values are the same for the left and the right part in the star region because of the presence of the contact discontinuity. The last information to be determined are ρ_{L*} and ρ_{R*}. These values depend on the type of waves on the left and on the right. We will consider all the possible cases. For shock wave we'll need only the density before the wave and the shock speed whereas in the rarefaction case we'll need the density before the wave and the tail and head equations. In this case several cases are analyzed.

4.5.1 Left Shock Wave

If $p_* > p_L$ we have a left shock condition and we can workout the ρ_{L*} density. Now we know $p*$ and $u*$ and recalling the density across a shock:

$$\rho_{*L} = \rho_L \left[\frac{(\frac{\gamma-1}{\gamma+1}) + \frac{p_*}{p_L}}{(\frac{\gamma-1}{\gamma+1})\frac{p_*}{p_L} + 1} \right] . \tag{89}$$

To completely know the solution we lack of the S_L shock speed in order to identify the exact position in the x-t system of coordinates of the complete $\mathbf{W}_*$ zone. It will be included between the S_L and u* line.

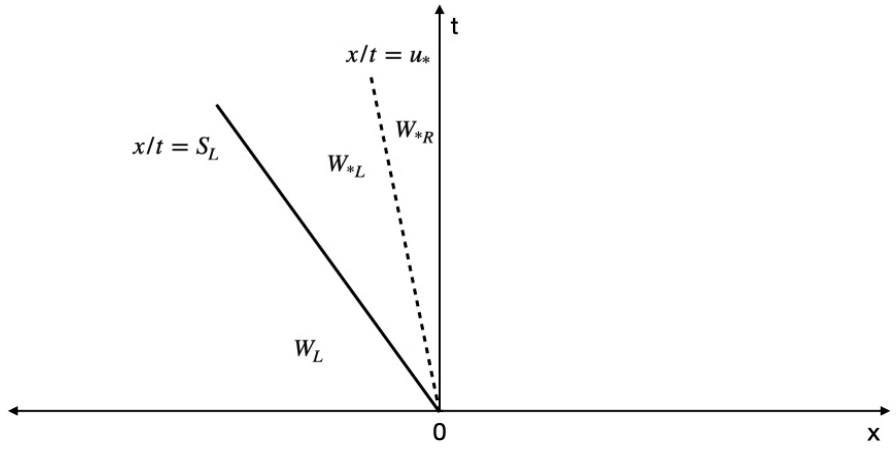

Figure 9: Left shock wave sampled solution.

from the Rankine-Hugoniot condition across a shock we can easy identify S_L as function of p_* , and $\mathbf{W}_*$ properties (now all known). In figure (9) is depicted the division of x-t plane for a left shock.

$$S_L = u_L - a_L \left[\frac{\gamma+1}{2\gamma}\frac{p_*}{p_L} + \frac{\gamma-1}{2\gamma} \right]^{\frac{1}{2}} . \tag{90}$$

We have determined all the properties of the left star region and its exact location in the x-t plane.

4.5.2 Left Rarefaction fan

If for the left wave we have $p_L > p_*$ we will have a rarefaction fan. In this case we will have a rarefaction fan enclosed between an head and a tail and the star region before the contact discontinuity will start from

the fan tail.
The ρ_{L*} can be easily found from the isentropic evolution between left and star left zone:

$$\rho_{*L} = \rho_L \left(\frac{p_*}{p_L} \right)^{\frac{1}{\gamma}} \quad . \tag{91}$$

To determine the speeds of the head and the tail of the rarefaction we also need the a_{L*} speed. This can be found with the isentropic evolution :

$$a_{*L} = a_L \left(\frac{p_*}{p_L} \right)^{\frac{\gamma-1}{2\gamma}} \quad . \tag{92}$$

The rarefaction fan is enclosed between an head and a tail as shown in figure, identified by S_{HL} and S_{TL} respectively:

$$S_{HL} = u_L - a_L \quad , \quad S_{TL} = u_* - a_{*L} \; . \tag{93}$$

To complete the discussion for the left star zone we have to identify

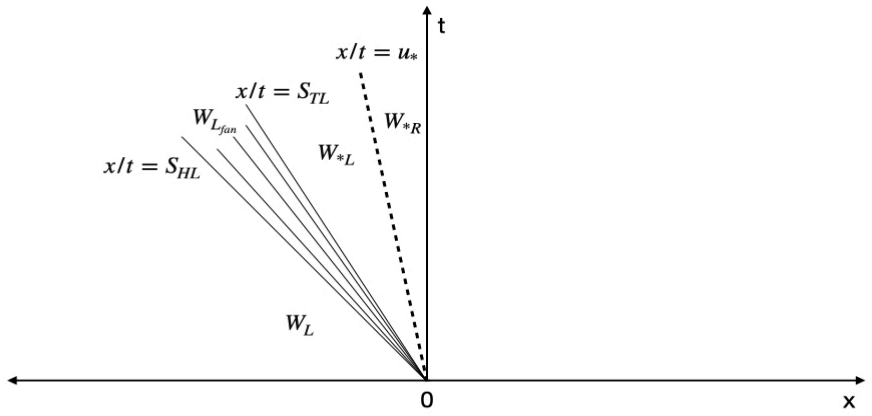

Figure 10: Left rarefaction fan sampled solution

the properties inside the fan $\mathbf{W}_{Lfan} = (\rho, u, p)^T$. The identification of a generic point (x,t) inside the fan is made through the characteristic ray as shown in figure (10). It starts in the zero point of our Riemann problem and has an inclination

$$\frac{dx}{dt} = \frac{x}{t} = u - a \quad , \tag{94}$$

where a and u are the sought particle sound speed and speed at (x,t). Using the generalized Riemann invariant $I_L(u,a)$ between the state before the fan and inside the fan, we're able to link the two states:

$$u_L + \frac{2a_L}{\gamma - 1} = u + \frac{2a}{\gamma - 1} \quad . \tag{95}$$

Using the two above equation the two sound speed and the isentropic evolution we arrive at :

$$\mathbf{W}_{Lfan} = \begin{cases} \rho = \rho_L \left[\frac{2}{(\gamma+1)} + \frac{(\gamma-1)}{(\gamma+1)a_L}(u_L - \frac{x}{t}) \right]^{\frac{2}{\gamma-1}} , \\ u = \frac{2}{(\gamma+1)} \left[a_L + \frac{(\gamma-1)}{2} a_L + \frac{x}{t} \right] , \\ p = p_L \left[\frac{2}{(\gamma+1)} + \frac{(\gamma-1)}{(\gamma+1)a_L}(u_L - \frac{x}{t}) \right]^{\frac{2\gamma}{\gamma-1}} \end{cases} . \tag{96}$$

4.5.3 Right Shock Wave

Similar considerations can be expressed for the right cases. As for the left part if $p_* > p_R$ we have a left shock condition and we can workout the ρ_{R*} density. Now we know p_* *and* u_* and recalling the density across a shock:

$$\rho_{*R} = \rho_R \left[\frac{(\frac{\gamma-1}{\gamma+1}) + \frac{p_*}{p_R}}{(\frac{\gamma-1}{\gamma+1})\frac{p_*}{p_R} + 1} \right] . \tag{97}$$

The S_R shock speed is given by

$$S_R = u_R + a_R \left[\frac{\gamma+1}{2\gamma} \frac{p_*}{p_R} + \frac{\gamma-1}{2\gamma} \right]^{\frac{1}{2}} \quad . \tag{98}$$

We have determined all the properties of the right star region and their exact location in the x-t plane.

4.5.4 Right Rarefaction Wave

As for the left zone if for the right wave we have $p_R > p_*$ we will have a rarefaction fan. The ρ_{L*} can be easily found from the isoentropic evolution between left and star left zone:

$$\rho_{*R} = \rho_R \left(\frac{p_*}{p_R} \right)^{\frac{1}{\gamma}} \quad . \tag{99}$$

The a_{*R} speed can be found with the isentropic evolution :

$$a_{*R} = a_L \left(\frac{p_*}{p_R} \right)^{\frac{\gamma-1}{2\gamma}} \quad . \tag{100}$$

The rarefaction fan is enclosed between an head and a tail as shown in figure, identified by S_{HR} and S_{TR} respectively:

$$S_{HR} = u_R + a_R \quad , \quad S_{TR} = u_* + a_{*R} \, . \tag{101}$$

To complete the discussion for the right star zone we have to identify the properties inside the fan $\mathbf{W}_{Rfan} = (\rho, u, p)^T$. The identification of a generic point (x,t) inside the fan is made through the characteristic ray. It starts in the zero point of our Riemann problem and has an inclination

$$\frac{dx}{dt} = \frac{x}{t} = u - a \quad , \tag{102}$$

where a and u are the sought particle sound speed and speed at (x,t). The properties inside the fan are

$$\mathbf{W}_{Rfan} = \begin{cases} \rho = \rho_R \left[\frac{2}{(\gamma+1)} + \frac{(\gamma-1)}{(\gamma+1)a_R}(u_R - \frac{x}{t}) \right]^{\frac{2}{\gamma-1}} \, , \\ u = \frac{2}{(\gamma+1)} \left[a_R + \frac{(\gamma-1)}{2} a_R + \frac{x}{t} \right] \, , \\ p = p_R \left[\frac{2}{(\gamma+1)} + \frac{(\gamma-1)}{(\gamma+1)a_R}(u_R - \frac{x}{t}) \right]^{\frac{2\gamma}{\gamma-1}} \quad . \end{cases} \tag{103}$$

We have now fully solved the Riemann problem for the Euler equations in a single point. The utility of this resolution will be seen in the resolution of the Godunov scheme.

5 Godunov scheme for Non-linear Euler equations

The solution for the Riemann problem for the Euler equations, found in the previous section, is the starting point for the application of a Godunov scheme for non-linear system.
The Godunov scheme is an upwind conservative method. As well as all the conservative numerical methods, the main computational issue for the Godunov scheme is represented by the research of the numerical fluxes. In the following passages we'll find the solution to this problem.

5.1 Conservative Numerical methods

Numerical methods are mathematical tools used to replace the the continuous problem represented by the PDEs by a finite set of discrete values.
For a physical problem in which are present discontinuities such as shocks, we need stringent requirements on the mathematical formulation of the governing equations and on the numerical schemes. For these reasons we have chosen in chapter (3.2) the integral formulation of the Euler's equation with a set of conserved variable as starting point for our numerical scheme. The numerical method we're going to use is in *conservative form*. From [3]:

Definition 5.1 *"A numerical method is said to be in conservative form if it can be written as:*

$$u_i^{n+1} = u_i^n - \frac{\Delta t}{\Delta x}\left[\Phi_{i+\frac{1}{2}}(u_{i_p}^n, u_{i_{p+1}}^n ...) - \Phi_{i-\frac{1}{2}}(u_{i_p}^n, u_{i_{p+1}}^n ...)\right] \text{ "} , \quad (104)$$

where Φ is called numerical flux and depends upon the p arguments.
The main property of a conservative scheme is that it maintains the discretized version of the conservative statement *exactly*, except for round-off error for any mesh size over an arbitrary limited region containing the conservative property. Since in our Euler's equations we are dealing with PDEs describing conservation law, a conservative scheme is the most accurate numerical approximation of our problem, especially in the cases of discontinuities in the solution. The main issue of the conservative methods is the evaluation of the inter-cell fluxes for the calculation of the conserved variables at the next time step. The Godunov scheme is an upwind method because we are evolving in time the flow properties following the flow direction.

5.2 Convergence, consistency and stability for conservative schemes

The convergence, for a general numerical scheme guarantees a relation between the exact solution of a PDE and the numerical solution of the scheme. In linear case for non-conservative schemes we usually pass first from the stability and consistency properties through the Von Neumann analysis. For the non-linear cases the analysis is much more complicated. In conservative schemes we can use another approach. From [3] it can be shown that a conservative numerical scheme is *consistent* with the original conservation law if the numerical fluxes reduce to the physical flux for a constant flow. When we check consistency

we refine the mesh of our numerical scheme in time and space domain. Considering the expression:

$$u_i^{n+1} = u_i^n - \frac{\Delta t}{\Delta x}\left[\Phi_{i+\frac{1}{2}}(u_{i_p}^n, u_{i_{p+1}}^n ...) - \Phi_{i-\frac{1}{2}}(u_{i_p}^n, u_{i_{p+1}}^n ...)\right] \text{ "} \qquad (105)$$

As we refine the mesh all the U_i values tend to U physical values:

$$Numerical flux \equiv \Phi(u_{i_p}^n, u_{i_{p+1}}^n ...) \qquad (106)$$

$$Physical flux \equiv (u)$$

$$if \;\; \Delta x \, , \Delta t \;\; \to 0 \;\; \Phi(u,u,u,u) = f(u) \; .$$

When we check the form (106), we have a consistent conservative numerical scheme. As long as a numerical flux is equal to the physical flux, we have a constant flow.
The *convergence* for a non-linear conservative scheme is derived from the Lax-Wendroff theorem :

Theorem 1 *" If the solution U_i^n of the discretized equation in conservative form converges boundarly almost everywhere to some function $U(x,t)$ when Δx and Δt tends to 0, then $U(x,t)$ is a weak solution of our non-linear PDE"*

The solutions of a conservation law can be :

- *Genuine solution*: the solution is continuous and the first derivative of the solution can admit a bounded discontinuity (jump discontinuity);
- *Weak solution*:the solution is continuous everywhere but we can have a line in which we can have a discontinuity.

As our physical model forecasts the presence of shock, the convergence of our conservative scheme to a weak solution will give the correct numerical solution.
Unfortunately the theorem (1) does not guarantee the convergence because we need to converge *boundly* to some function. For this reason we need *stability*. In linear case we can apply the Von Neumann analysis to check this property but, in case of conservative schemes, thanks to Lax-Wendroff theorem, we can avoid to check stability if, applying directly our conservative scheme, we resort to some function as solution. This function will be, for sure a weak solution that satisfies the Rankine-Hugoniot condition and so it is physical consistent. The convergence to a weak solution, allowing discontinuities is another peculiar feature of the conservative schemes because it allows us to work with discontinuity. A non-conservative scheme could not include a discontinuity in its solution and so it could give wrong results.
The Godunov scheme is a conservative scheme.

5.3 The Godunov scheme

The conservative schemes, thanks to their telescopic property, allow to correctly report any discontinuity speed without the presence of error linked to the derivatives.
The Godunov schemes are shock-capturing method alternative to Flux vector splitting schemes. They start from the idea to apply a Riemann problem at each border point of the grid in order to evaluate the numerical flux. We are fully exploiting the telescopic property for all the possible shocks creating in all the domain. The most important point of the Godunov schemes is that they follow the physic of the problem since, for every point of the domain, we are applying the Rankine-Hugoniot condition (analytical evaluation of change in physical properties across a shock).
Considering a grid of discretized constant volumes, for which we have a constant value related to each point as shown in figure (11), the Godunov idea is based on the fact that at the cell border we have a Riemann problem between two consecutive cells. If the physical con-

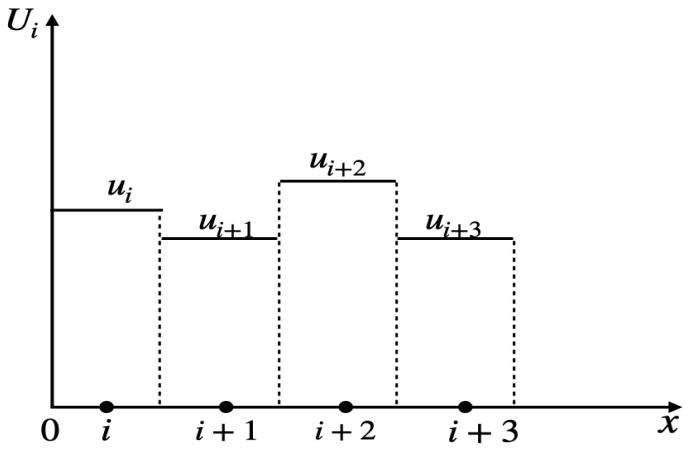

Figure 11: Piece-wise constant distribution of a property in the $x-t$ plane.

ditions between the properties impose the presence of a shock, we are capturing the physical phenomenon while, if there's no a physical shock, the numerical difference between the two volumes creates a vanishing shock.

5.4 Bases of Godunov's first order method

The starting point for our study case is represented by the Initial-Boundary value problem (IBVP) for non linear-system hyperbolic conservation laws. Differently from the ideal case, in real cases we have a limited domain and so we must add so he boundary conditions to well pose our problem (3.4.3).
The initial boundary value problem is here represented:

$$IBVP \begin{cases} \mathbf{U}_t + \mathbf{F(U)}_x = 0 \ , \quad PDEs \\ \mathbf{U}(x,0) = \mathbf{U}^{(0)}(x) \ , \quad ICs \\ \mathbf{U}(0,t) = \mathbf{U}_1(t) \ , \mathbf{U}(L,t) = \mathbf{U}_r(t) \quad BCs \end{cases} \tag{107}$$

Where the vector $\mathbf{U}(x,t)$and $\mathbf{F(U)}$ are the vectors of the conserved variables and of the fluxes found in the chapter (3.3),
$\mathbf{U}^{(0)}(x)$ is the set of initial data for every point of the domain and for every conserved variable at time t = 0.
$\mathbf{U}_L(t)$ and $\mathbf{U}_R(t)$ are the functions expressing the evolution in time of the boundary conditions in the space domain considered. We suppose the existence of a solution for this problem and the existence of an integral form in order to admit discontinuities.

5.4.1 Spatial and time discretization

The spatial one-dimensional domain considered is the $[0, L]$ range, subdivided into N+1 total points and N internal finite volumes $I_i = [x_{i-\frac{1}{2}}, x_{i+\frac{1}{2}}]$ each one centered in the i point of the domain. Each finite volume has the same length $dx = L/N$.
The geometric discretization is now completed so we can easily know any position of any finite volume inside the domain and the respective boundaries.
The last discretization must be made in the time domain $[0, T]$ to which we are referring. To guarantee the stability of our model we must impose the dt advancing time interval at any time step following the CFL condition. This issue is linked to the non-linearity of the Euler's equations. The stability condition for dt interval will be explained later in (5.6)

5.4.2 Inter-cell fluxes solving strategy

The Riemann problem will be used in Godunov method to evaluate the inter-cell flux looking for the properties in the $x/t = 0$ position. The set of variables used to solve the Riemann problem can be different from the conservative one. In fact, after the resolution of Riemann

problem we can easily reconstruct the conservative variable inside the finite volume and the conservative fluxes at the boundaries. We choose the primitive variable set inside each cell $\mathbf{W} = (\rho, u, p)^T$. At time $t = 0$ we are provided of the initial data
$\mathbf{U}^{(0)}(x)$ at each point of the spacial domain with the exception of the boundary points. In the first order Godunov scheme, the properties inside each finite volume are considered constant inside each finite volume. Since the initial data are written in terms of conserved variables we must algebrically find the respective primitive variables to impose the Riemann problems. To define all the properties inside the domain, we must evaluate the $\mathbf{W}$ variables at the boundaries through the boundary condition problem. Independently on the boundary properties we are provided, we must end the calculation on the BC with the primitive variables in order to start the Riemann problems.
Now we have a full set of constant values inside our domain at the time $t = 0$. We can now solve the Riemann problem at each $x_{i+\frac{1}{2}}$ cell boundary considering the $(\mathbf{U}_i^n, \mathbf{U}_{i+1}^n)$ data centered respectively inside the i and i+1 volumes. The solution of the Riemann problem defines fully all the properties in all the (x,t) points around the point in which is located the discontinuity. Any of these points is identified by the slope x/t but for the purpose of the Godunov scheme *we are interested only in the properties at the borders and so for x/t = 0*. This concept will be fundamental when we'll consider the possible position of our inter-cell flux inside the eventual rarefaction fan.
At the first time step $t = dt$ we can now identify the numerical fluxes for:

$$u_i^{n+1} = u_i^n - \frac{\Delta t}{\Delta x}\left[\Phi_{i+\frac{1}{2}}(u_{i_p}^n, u_{i_{p+1}}^n ...) - \Phi_{i-\frac{1}{2}}(u_{i_p}^n, u_{i_{p+1}}^n ...)\right], \tag{108}$$

as :

$$\Phi_{i+\frac{1}{2}}(u_{i_p}^n, u_{i_{p+1}}^n ...) . \tag{109}$$

We can now apply the same procedure for every point and advancing with the time steps but we must take care of the conditions imposed to dt and we must impose the boundary conditions.

5.4.3 Boundary conditions with the Method of characteristics

The first step to solve our code with a Godunov scheme is to provide the boundary conditions for the left and right boundary. The procedure that we will follow is taken from [3]. The numerical method applied to have a time evolution of the BC starting form initial data is the Method of the Characteristics. This is a non-conservative method (we

are starting from the non-conservative form for the Euler equation) based on the decoupling of the Euler equations through the matrix of the Eigenvectors (27) in wave equations. Once that the Euler's equations are decoupled we can apply any numerical scheme to each wave equation to evaluate the next time step. In the particular case of the application of the MOC only at the boundary we must supply also boundary conditions values to correctly define the time evolution scheme. The number of Boundary conditions that we must provide will depend deeply on the initial state of our properties whereas the equations for the time evolution of each BC will depend on the structure of the problem. In our study case we will include area variation , friction at the walls and heat exchange.
Since we're basing our BC evaluation on the primitive variable formulation, we must start from the conservative form of the Euler's equations with source term and differentiate them.

$$\begin{cases} \frac{\partial(\rho A)}{\partial t} + \frac{\partial(\rho u A)}{\partial x} = 0 \\ \frac{\partial(\rho u A)}{\partial t} + \frac{\partial(\rho u^2 + p)A}{\partial x} = p\frac{\partial A}{\partial x} - \tau\pi D \\ \frac{\partial(E A)}{\partial t} + \frac{\partial u(E+p)A}{\partial x} = \pi D q \end{cases} \tag{110}$$

The first step is passing to the primitive formulation developing the partial derivatives and to explicit all the source terms.
For the *continuity equation* we obtain:

$$\frac{\partial \rho}{\partial t} + u\frac{\partial \rho}{\partial x} + \rho\frac{\partial u}{\partial x} = -\frac{\rho u}{A}\frac{\partial A}{\partial x} \quad . \tag{111}$$

Developing in the same way the partial derivatives in *the momentum conservation equation* we obtain:

$$uA\left(\frac{\partial \rho}{\partial t} + u\frac{\partial \rho}{\partial x} + \rho\frac{\partial u}{\partial x}\right) + \rho A\left(\frac{\partial u}{\partial t} + u\frac{\partial u}{\partial x} + \frac{1}{\rho}\frac{\partial p}{\partial x}\right) = -u^2\rho\frac{\partial A}{\partial x} - \tau\pi D \tag{112}$$

and by substituting (111) into (112) we obtain

$$\left(\frac{\partial u}{\partial t} + u\frac{\partial u}{\partial x} + \frac{1}{\rho}\frac{\partial p}{\partial x}\right) = -\frac{\tau\pi D}{\rho A} \quad . \tag{113}$$

The *total Energy conservation equation* differentiation is:

$$\frac{\partial\left(\frac{1}{2}\rho u^2 + \frac{p}{(\gamma-1)}\right)A}{\partial t} + \frac{\partial\{uA[\left(\frac{1}{2}\rho u^2 + \frac{p}{(\gamma-1)}\right) + p]\}}{\partial x} + = -\pi D q \quad . \tag{114}$$

Expliciting and rearranging derivatives we arrive to:

$$\frac{u^2A}{2}\left(\frac{\partial u}{\partial t}+u\frac{\partial \rho}{\partial x}+\rho\frac{\partial u}{\partial x}\right)+\rho uA\left(\frac{\partial u}{\partial t}+u\frac{\partial u}{\partial x}+\frac{1}{\rho}\frac{\partial p}{\partial x}\right)+\frac{A}{(\gamma-1)}\frac{\partial p}{\partial t}+ \tag{115}$$
$$+\frac{1}{2}\rho u^3\frac{\partial A}{\partial x}+\frac{uA}{(\gamma-1)}\frac{\partial p}{\partial x}+\frac{pA}{(\gamma-1)}\frac{\partial u}{\partial x}+\frac{\rho u}{(\gamma-1)}\frac{\partial A}{\partial x}+$$
$$+\frac{up}{(\gamma-1)}\frac{\partial A}{\partial x}+\frac{pA}{(\gamma-1)}\frac{\partial u}{\partial x}=\pi Dq \ .$$

Substituting (112) and (111) and knowing that $p\gamma = a^2\rho$ we finally obtain:

$$\frac{\partial \rho}{\partial t}+u\frac{\partial p}{\partial x}+a\rho^2\frac{\partial u}{\partial x}=\frac{\pi Dq}{A}(\gamma-1)+\frac{\pi\tau Du}{A}(\gamma-1)-\frac{a^2\rho u}{A}\frac{\partial A}{\partial x} \ .$$

In this form the primitive Euler equations have the same Eigenstructure of the homogeneous one. The eigenvalues that decouple the equations are:

$$\lambda_1 = u-a \ , \ \lambda_2 = u \ , \ \lambda_3 = u+a \ . \tag{116}$$

and the associated matrix of the Eigenvectors $\mathbf{K}$ is :

$$\mathbf{K}=\begin{bmatrix}1 & 1 & 1\\ -a/\rho & 0 & a/\rho\\ a^2 & 0 & a^2\end{bmatrix} \tag{117}$$

The system of Euler with the primitive variables, thanks to the homogeneity propert, can be written as:

$$\mathbf{W}_t+\mathbf{A(W)}\mathbf{W}_x=\mathbf{B} \ , \tag{118}$$

With $\mathbf{A}$ Jacobian matrix and $\mathbf{W}=(\rho,u,p)^T$. set of primitive variables. We can express all in matrix form with:

$$\mathbf{W}=\begin{bmatrix}\rho\\ u\\ p\end{bmatrix} \quad \mathbf{A(U)}\begin{bmatrix}u & \rho & 0\\ 0 & u & 1/\rho\\ 0 & \rho a^2 & u\end{bmatrix} \quad \mathbf{B}=\begin{bmatrix}-\frac{\rho u}{A}\frac{\partial A}{\partial x}\\ -\frac{\tau\pi D}{\rho A}\\ \frac{\pi Dq}{A}(\gamma-1)+\frac{\pi\tau Du}{A}(\gamma-1)-\frac{a^2\rho u}{A}\frac{\partial A}{\partial x}\end{bmatrix}.$$

Using the eigenvalues (118) we can diagonalize our system using the matrix of the Eigenvector $\mathbf{K}$ and $\mathbf{K}^{-1}$:

$$\mathbf{K}^{-1}=\begin{bmatrix}0 & -\rho/2a & 1/2a^2\\ -1 & 0 & -1/a^2\\ 0 & \rho/2a & 1/2a^2\end{bmatrix} \tag{119}$$

After the pre-multiplication by $\mathbf{K}^{-1}$: we arrive to:

$$\boldsymbol{K^{-1}W_t + K^{-1}AKK^{-1}W_x = K^{-1}B} \quad , \tag{120}$$

in which we can recognize the $\mathbf{Q} = \mathbf{K}^{-}1\mathbf{B}$ matrix.

$$\mathbf{Q} = \begin{bmatrix} \frac{4\tau}{2aD} + \frac{1}{2a^2}\left[\frac{4q}{D} + \frac{4\tau u}{D}\right](\gamma - 1) - \frac{\rho u}{2A} \\ -\frac{1}{a^2}\left[\frac{4q}{D} + \frac{4\tau u}{D}\right](\gamma - 1) \\ -\frac{4\tau}{2aD} + \frac{1}{2a^2}\left[\frac{4q}{D} + \frac{4\tau u}{D}\right](\gamma - 1) - \frac{\rho u}{2A} \end{bmatrix} \tag{121}$$

Now we are able to express our system of PDEs as a system of ODEs along the characteristics line. This is made through the Riemann's variables as follow:

$$\begin{cases} R_1 = -\frac{\rho}{2a}u + \frac{1}{2a^2}p \quad \frac{dR_1}{dt} = Q_1 \;\; if \;\; \frac{dx}{dt} = \lambda_1 \\ R_2 = \rho + \frac{1}{a^2}p \quad \frac{dR_2}{dt} = Q_2 \;\; if \;\; \frac{dx}{dt} = \lambda_2 \\ R_3 = \frac{\rho}{2a}u + \frac{1}{2a^2}p \quad \frac{dR_3}{dt} = Q_3 \;\; if \;\; \frac{dx}{dt} = \lambda_3 \end{cases} \tag{122}$$

5.4.4 Practical development of physical left boundary conditions

For a De Laval nozzle we need to give a different number of boundary conditions, at left and right part, depending on the physical situation. In the case of subsonic inlet and subsonic outlet we need two fixed BC at the inlet and 1 BC at the outlet. The reason is linked with the theory of the characteristics, for which, the number of BC to be given is the same number of the characteristic lines entering the domain in this exact boundary as shown in figure (12). The other cases will be fully analyzed in the following pages.

For the boundary conditions at the inlet we provide the total pressure

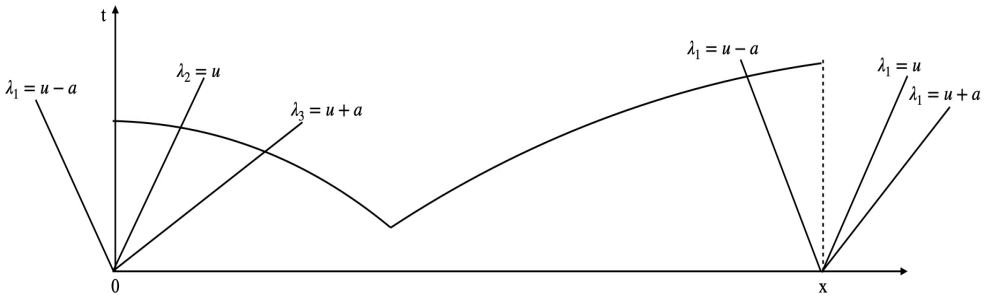

Figure 12: De Laval nozzle number of left and right boundary condition's number for a subsonic inlet and a subsonic outlet.

P_1^0 and the total temperature T_{1^0}. This choice is physically motivated

by the fact that usually, in the experimental field, the flow properties are the ones measured through sensor. The total pressure quantities are the theoretical properties more near to the measured quantities. The system to find the primitive variables in the Left Boundary condition is:

$$\begin{cases} P_1^{0\ n+1} = p_1^{n+1}\left(1+\frac{(\gamma-1)}{2}\frac{(u_1^{n+1})^2}{(a_1^{n+1})^2}\right)^{\frac{\gamma}{\gamma-1}} \\ T_1^{0\ n+1} = T_1^{n+1} + \frac{1}{2}\frac{(u_1^{n+1})^2}{cp} \\ R_1^{n+1} = -\frac{\rho^{n+1}}{2a}u^{n+1} + \frac{1}{2a^2}p^{n+1} \qquad \frac{dR_1}{dt} = Q_1 \ \ if \ \ \frac{dx}{dt} = \lambda_1 \end{cases} . \tag{123}$$

To know the Riemann variable value at the time n+1, we have to discretize our wave equation $\frac{dR_1}{dt} = Q_1$ knowing all the properties at the time $t = 0$ state . We can use a downwind scheme since the speed propagation of the Riemann variable $\lambda_1 = u - a$ is always negative for a subsonic inlet flow. The discretized equation is :

$$R_{1_1}^{n+1} = R_{1_1}^{n} + \frac{\Delta x}{\Delta t}\left[\lambda_{1_1}^{n} R_{1_1}^{n+1} - \lambda_{1_2}^{n} R_{1_2}^{n+1}\right] + \Delta t \ \ Q_{1_1}^{n} \ \ , \tag{124}$$

in which the first subscript refers to the Riemann's variable we are considering whereas, the second subscript, refers to the point of the grid in which the variable is calculated. Solving the first equation of (122) for all the points of the grid at time t, we can have the $R_{1_1}^{n}$ and the $R_{1_2}^{n+1}$ values. Thanks to the initial conditions for all the points of the domain we know all the values at time t and so we have all to solve (124). Knowing that $a = \sqrt{\gamma p/\rho}$ with $\gamma = c_p/c_v$ we have now a fully defined non-linear problem (123) with three equations in three variables $(\rho^{n+1}, u^{n+1}, p^{n+1})$. Because of the non-linearity of the system we must use a numerical method to solve the system (123). We can use Newton-Rhapson, already used in (84). We start from F:

$$\mathbf{F} = \begin{cases} F_1 : P_1^{0\ n+1} - p_1^{n+1}\left(1+\frac{(\gamma-1)}{2}\frac{(u_1^{n+1})^2}{(a_1^{n+1})^2}\right)^{\frac{\gamma}{\gamma-1}} \\ F2 : T_1^{0\ n+1} - T_1^{n+1} - \frac{1}{2}\frac{(u_1^{n+1})^2}{cp} \\ F3 : R_{1_1}^{n+1} - R_{1_1}^{n} - \frac{\Delta x}{\Delta t}\left[\lambda_{1_1}^{n} R_{1_1}^{n+1} - \lambda_{1_2}^{n} R_{1_2}^{n+1}\right] - \Delta t Q_{1_1}^{n} \ \ , \end{cases} \tag{125}$$

by evaluating the Jacobian $\mathbf{J}$ of $\mathbf{F}$ system, we can find the $\mathbf{X}_{new}$ value after the first iteration. The first value considered is $\mathbf{X}_{old}$ vector, evaluated as $\mathbf{X}_{old} = \mathbf{F(0)}$ with $\mathbf{F(0)}$ evaluated through the properties at

time t = 0, already known thanks to the ICs.

$$\mathbf{X}_{new} = \mathbf{X}_{old} - \frac{\mathbf{F}}{\mathbf{J}} \tag{126}$$

After some iteration we arrive at convergence and the $(\rho^{n+1}, u^{n+1}, p^{n+1})$ variables are found. This is the procedure to find time by time the values at the left boundary.

5.4.5 Practical development of physical right boundary conditions

The same reasoning can be applied to the right boundary to find the number of Boundary conditions useful to have a completely define the right boundary problem.
From the theory of characteristics in case of subsonic outlet we need only one fixed boundary condition at the outlet since the only line entering the domain is the one associate to the first eigenvalue $\lambda_1 = u - a$. We can impose the outlet ambient pressure p_2.
The system to solve in order to determine the right boundary conditions at the time n+1 is:

$$\begin{cases} {P_N}^{n+1} = p_2 \\ R_2^{n+1} = \rho^{n+1} + \frac{1}{{a^{n+1}}^2} p^{n+1} \qquad \frac{dR_2}{dt} = Q_2 \;\; if \;\; \frac{dx}{dt} = \lambda_2 \\ R_3^{n+1} = \frac{\rho^{n+1}}{2a^{n+1}} uv + \frac{1}{2{a^{n+1}}^2} p^{n+1} \qquad \frac{dR_3}{dt} = Q_3 \;\; if \;\; \frac{dx}{dt} = \lambda_1. \end{cases} \tag{127}$$

To evaluate the R_2^{n+1} and R_3^{n+1} we need to discretize the wave equation associated. In case of subsonic outlet we can use an upwind scheme since both $\lambda_2 = u$ and $\lambda_3 = u + a$ are positive . the equations are:

$${R_2}_1^{n+1} = {R_2}_1^n + \frac{\Delta x}{\Delta t}\left[{\lambda_2}_1^n {R_2}_1^{n+1} - {\lambda_2}_2^n {R_2}_2^{n+1}\right] + \Delta t {Q_2}_1^n \;\; , \tag{128}$$

and

$${R_3}_1^{n+1} = {R_3}_1^n + \frac{\Delta x}{\Delta t}\left[{\lambda_3}_1^n {R_3}_1^{n+1} - {\lambda_3}_2^n {R_3}_2^{n+1}\right] + \Delta t {Q_3}_1^n \;\; . \tag{129}$$

Recalling the speed of sound formula $a = \sqrt{\gamma p/\rho}$ we have a linear system of equations fully defined. We can solve it by substitution. Finding the $(\rho^{n+1}, u^{n+1}, p^{n+1})$ variables at right boundary we have found the properties at time step one. The next time step we can apply the same reasoning for advancing in time our scheme.

5.5 Application of first order Godunov to the inner domain

As presented by Toro in [6] we have different versions of the Godunov scheme. In our numerical method we present the second version of the Godunov scheme in conservative form:

$$\mathbf{U}_i^{n+1} = \mathbf{U}_i^n + \frac{\Delta x}{\Delta t}\left[\mathbf{F}_{i-\frac{1}{2}} - \mathbf{F}_{i+\frac{1}{2}}\right] \ , \tag{130}$$

where $\mathbf{U}_i^n$ is the finite volume constant value at time n for the i cell. The inter-cell numerical flux is found as explained in (5.3) finding the primitive variables at each border of the domain solving the Riemann problem at each boundary. The generic flux can be written as $\mathbf{F}_{i+\frac{1}{2}} = \mathbf{F}(\mathbf{U}_{i+\frac{1}{2}}(0))$ evaluated at the right border of the i point using the initial conditions and solving the Riemann problem at point $i + \frac{1}{2}$.

5.6 CFL condition

The finite volume formulation (130) is valid if the CFL stability condition on time step Δt is respected .
This is called the *not interference flux condition* and it is based on the hypothesis that, in a Riemann problem at the point i, the waves adjacent to i propagated by the other Riemann problems, don't influence the i Riemann problem itself. This condition is satisfied if a single wave can travel at most half cell for each time step. From this condition we obtain a Δt interval for which our numerical scheme will be stable:

$$\Delta t \leq \frac{\Delta x}{2S_{max}^n} \ . \tag{131}$$

S_{max} is the maximum speed, for each time step, calculated in all the space domain. This stability condition belong to the first formulation of Godunov scheme but we apply it in our numerical scheme since the second one CFL condition is less restrictive.

5.7 Practical evaluation of inter-cell fluxes

The evaluation of the inter-cell fluxes is the most important and difficult task for a conservative scheme.
Once we know the initial value $\mathbf{U}(0)$ in each internal point and the boundary values we can evaluate the inter-cell flux at each border of each point of the domain.
The evaluation of the properties is made up solving the Riemann problem at the generic interface $x_{i+\frac{1}{2}}$, $RP(\mathbf{U}_i, \mathbf{U}_{i+1})$. The exact point(x,t) chosen inside the domain of the Riemann problem will be *the one with*

the inclination $S = x/t = 0$. Since the resolution of the Riemann problem in (4.1) was solved for primitive variables $\mathbf{W} = (\rho, u, p)^T$ we have to evaluate the inter-cell fluxes as:

$$\mathbf{F(U)} = \begin{bmatrix} f_1 \\ f_2 \\ f_3 \end{bmatrix} \equiv \begin{bmatrix} \rho u \\ \rho u^2 + p \\ u(E+p) \end{bmatrix}. \tag{132}$$

The cases are multiple. We have two main cases for which we can find five other cases each. In figure (13) are summarized the cases for positive star flow speed and in figure (14) the cases for negative star

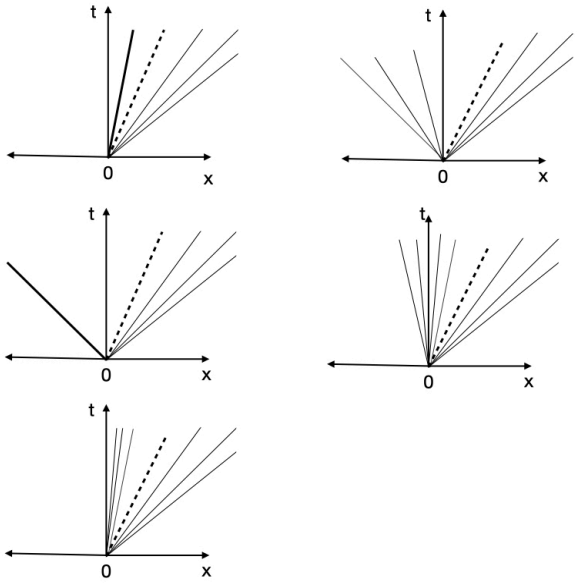

Figure 13: cases for the inter cell flux evaluation in case of positive u*.

flow speed :
Summarizing, we have to fully solve the Riemann problem between two consecutive cells and after this we have to choose the primitive value correspondent to the $S = x/t = 0$ slope. Once we've done it we have to insert these values inside the flux formulation and evaluate all the numerical fluxes for all the inter-cell borders. After this we can evaluate the $\mathbf{U}^{n+1}$ variables from the system (130). In the table (15) are practically reported all the possible conditions to evaluate the inter-cell fluxes.

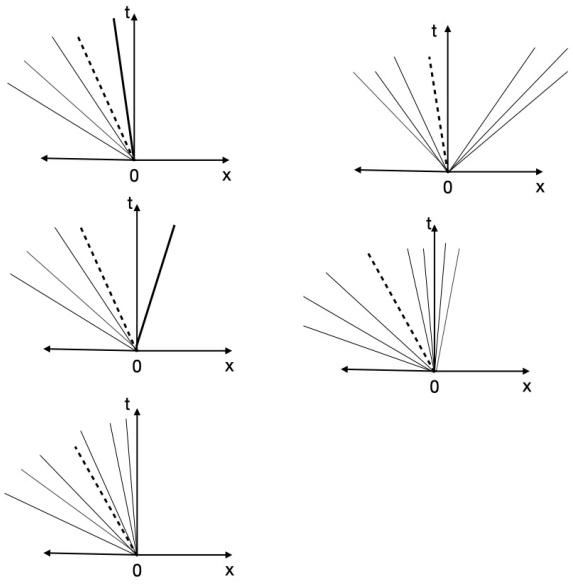

Figure 14: cases for the inter cell flux evaluation in case of negative u*.

Riemann problem for x/t = 0 All possible subcases			
$u_* < 0$		$u_* > 0$	
Left shock	**Left rarefaction**	**Right shock**	**Right rarefaction**
if $S_L > 0$, $\mathbf{W}_L$	if $S_{HL} > 0$, $\mathbf{W}_L$	$S_R < 0$, $\mathbf{W}_R$	$S_{HR} < 0$, $\mathbf{W}_R$
if $S_L < 0$, $\mathbf{W}_{*L}$	$if S_{TL} < 0$, $\mathbf{W}_{*L}$	$S_R > 0$, $\mathbf{W}_{*R}$	$if S_{TR} > 0$, $\mathbf{W}_{*R}$
	if $S_{TL} > 0$ *and* $S_{HL} < 0$, $\mathbf{W}_{L_{fan}}$		$S_{TR} < 0$ *and* $S_{HR} > 0$, $\mathbf{W}_{R_{fan}}$

Figure 15: Table of all the possible cases for intercell flux evaluation.

5.8 Application of complete Godunov scheme with the presence of source term

All the passages applied before are true for the resolution for a Godunov scheme without the presence of a source term. Since our physical model requires the presence of source terms driving the variation of the property studied as explained in part 3.5.5, we have to take in account the source in our numerical model. Recalling the complete model:

$$\begin{cases} \frac{\partial \rho}{\partial t} + \frac{\partial(\rho u)}{\partial x} = -\frac{1}{A}\frac{dA}{dx}\rho u \\ \frac{\partial(\rho u)}{\partial t} + \frac{\partial(p+\rho u^2)}{\partial x} = -\frac{4\tau_w}{D} - \frac{1}{A}\frac{dA}{dx}\rho u^2 \\ \frac{\partial(\rho e_{tot})}{\partial t} + \frac{\partial(\rho u h^0)}{\partial x} = \frac{4\dot{q}_f}{D} - \frac{1}{A}\frac{dA}{dx}u(E+p) \ , \end{cases} \tag{133}$$

and the numerical scheme to be applied to find the conserved variables for each point i at time n+1 to consider the presence of a source term every time, we have to add a numerical source term S_i^n evaluated at every point i and at every time step:

$$\mathbf{U}_i^{n+1} = \mathbf{U}_i^n + \frac{\Delta x}{\Delta t}\left[\mathbf{F}_{i-\frac{1}{2}} - \mathbf{F}_{i+\frac{1}{2}}\right] + \Delta t\ \mathbf{S}_i^n \ , \tag{134}$$

with:

$$\mathbf{S}_i^n = \begin{bmatrix} -\frac{1}{A_i^n}\ dA_i^n\ \rho_i^n\ u_i^n \\ -\frac{4{\tau_w}_i^n}{D_i^n} - \frac{1}{A_i^n}\ dA_i^n \rho_i^n\ u_i^{2\ n} \\ \frac{4{\dot{q}_f}_i^n}{D_i^n} - \frac{1}{A_i^n}\ dA_i^n\ u_i^n\ (E_i^n + p_i^n) \end{bmatrix} \ , \tag{135}$$

where all the quantities marked with i must be recomputed for each time step and at every cell.

6 High-resolution Godunov scheme

To achieve higher results in our numerical model, we'll improve our first order Godunov scheme to an high resolution Godunov scheme. The procedure is developed following [3] and [6].
The high resolution methods are very recent developed concept used for conservative schemes in order to reduce the oscillations around the discontinuity and to avoid the dissipation of information.
The dissipation error is a typical loss of information linked to all the first order schemes. To avoid this, in our Godunov scheme, we have to level up our scheme to the second order; in this way we are able to improve the resolution of our numerical solution.
The dispersion error, instead, is a problem linked with the second order schemes and it consists in numerical oscillations near to the discontinuity that can cause instabilities. To avoid this error we must be able to switch our scheme from the second to the first order near the discontinuities.
The high resolution methods are second order accuracy schemes in the smooth solution to avoid the dissipation error and switch to the first order around the discontinuity, in order to avoid the numerical oscillations of the dispersion error. Once reached this type of numerical method we will have the best possible numerical solution from our Godunov scheme.
The high resolution methods are divided into flux limiter methods, used in flux vector splitting methods and slope limiter methods, used for the Godunov schemes. The choice of this slope limiter will be crucial for switching from the second order of accuracy to the first order.

The first step to build an high-resolution Godunov scheme is the achievement of a Second order Godunov scheme.

6.1 Second order Godunov scheme

To transform a first order numerical scheme into a second order one we must change the order of our constant data inside each computational grid both in time and space. For the time domain we follow the linear reconstruction idea that the properties at each cell are no longer constant but inclined of a certain slope inside the cell as showns in figure(16).
The second order in the time domain, instead, is reached by evolving the boundary values of each cell from time t to time $t + \frac{1}{2}$. If we recall the finite volume evolution to the time step n+1 :

$$u_i^{n+1} = u_i^n - \frac{\Delta t}{\Delta x}\left[flux_{i+\frac{1}{2}}^{n+\frac{1}{2}} - flux_{i-\frac{1}{2}}^{n+\frac{1}{2}}\right], \tag{136}$$

we are considering the flux at the cell boundaries as averaged time values. To switch to the second order also in time we must develop a linear time variation different from the constant one. It will be implemented after the liner space reconstruction. The linear reconstruction in space

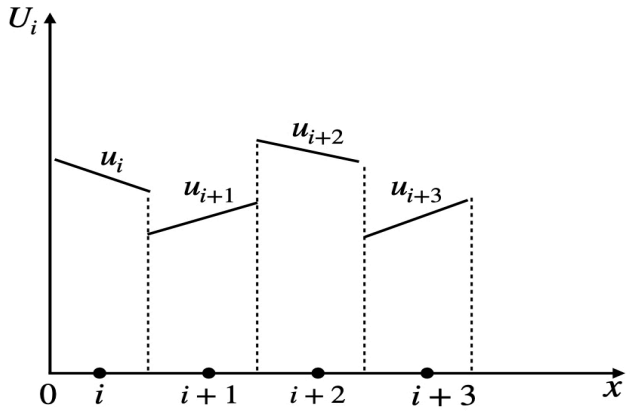

Figure 16: Linear reconstruction of piece-wise constant properties.

is based on this formula:

$$u_i(x) = u_i^n + \frac{\Delta i}{\Delta x}(x - x_i) \ . \tag{137}$$

In which u_i^n is the average value at the center of the cell i, Δx is the cell size and Δi is the slope of the line we are building. It will be chosen in

the following passages. This linear reconstruction must me performed at each I_i finite volume of our cell.
The Δi slope can be chosen from an upwind approximation of the first derivative as :

$$\begin{cases} \frac{\Delta i}{\Delta x} = \frac{u_i^n - u_{i-1}^n}{\Delta x} & Upwind\ formula \\ \frac{\Delta i}{\Delta x} = \frac{u_{i+1}^n - u_i^n}{\Delta x} & Downwind\ formula \\ \frac{\Delta i}{\Delta x} = \frac{u_{i+1}^n - u_{i-1}^n}{2\Delta x} & Centered\ formula \end{cases} . \tag{138}$$

The time reconstruction is performed considering the Boundary values at each cell, for each conserved variable fro time t to time $t + \frac{1}{2}$.

$$\bar{\mathbf{U}}_i^L = \mathbf{U}_i^L + \frac{1}{2}\frac{\Delta t}{\Delta x}\left[f(u_i^L) - f(u_i^R) \right] , \tag{139}$$

$$\bar{\mathbf{U}}_i^R = \mathbf{U}_i^R + \frac{1}{2}\frac{\Delta t}{\Delta x}\left[f(u_i^L) - f(u_i^R) \right] . \tag{140}$$

After the linear reconstruction in time and space we have a second order Godunov scheme.

6.2 Slope limiter choice and high resolution Godunov scheme

In the previous chapter we have reached the second order for our scheme. If we stop now the implementation, we will have an high resolution numerical results in the smooth regions, but we will be subjected to numerical oscillation near the discontinuities. Since our numerical scheme must deal with solutions including shocks we must apply a slope limiter to avoid the instability of our code.
The practical implementation of a slope limiter inside our code will put the Δi of the space linear reconstruction (137) at zero when a steep variation will be recognized and our Godunov scheme will return to the first order.
In our code we will use a Popular slope limiter from [3]:

$$\frac{\Delta i}{\Delta x} = min\ mod\ \left[\frac{u_i^n - u_{i-1}^n}{\Delta x} , \frac{u_{i+1}^n - u_i^n}{\Delta x} \right] , \tag{141}$$

where the *minmod* function states that:

$$min\ mod(a,b) = \begin{cases} a \ \ if|a| < |b| \ \ and \ \ ab > 0 \\ b \ \ if|b| < |a| \ \ and \ \ ab > 0 \\ 0 \ \ if \ \ ab < 0 \ \ . \end{cases} \tag{142}$$

These formulas recognize if an oscillation inside our grid is present and put the slope to zero in this case.
This slope limiter must be applied for each cell and for each term of **U** conserved variables. At the end we'll obtain three slope limiters, for each conserved variable, for each point at each time step.
Thanks to the slope limiter we have now an High Resolution Godunov scheme. The practical development of an HR Godunov scheme can be performed practically through the REA algorithm [3].

6.3 REA Algorithm (Reconstruction Evolution Average)

The practical implementation inside our code will be practically subdivided into three steps once we've chosen our slope limiter.

- **Step 1**:*Data reconstruction with the linear pattern inside cell at time n.*
  With this passage we are passing practically to the second order Godunov scheme. We can define the Boundary extrapolated values at time n as :

$$\begin{cases} \mathbf{U}_i^L = \mathbf{U}_i^n - \frac{1}{2}\Delta i \\ \mathbf{U}_i^R = \mathbf{U}_i^n + \frac{1}{2}\Delta i \ . \end{cases} \tag{143}$$

  We must perform this evolution for each boundary of each i point, and for the whole vector **U** of the conserved variables. We will obtain a left and a right value for each conserved variable at every boundary and we will use these value to perform a time evolution.

- **Step 2**: *time evolution of* $\boldsymbol{U}_i^L$ *and* $\boldsymbol{U}_i^R$.
  We are evolving our values at the boundaries from time t to time $t + \frac{1}{2}$. This step is made to make our code of the second order also in time.

$$\bar{\mathbf{U}}_i^L = \mathbf{U}_i^L + \frac{1}{2}\frac{\Delta t}{\Delta x}\left[f(u_i^L) - f(u_i^R) \right] \ , \tag{144}$$

$$\bar{\mathbf{U}}_i^R = \mathbf{U}_i^R + \frac{1}{2}\frac{\Delta t}{\Delta x}\left[f(u_i^L) - f(u_i^R) \right] \ . \tag{145}$$

  We must perform this evolution for each boundary point and for the whole vector U of the conserved variables at each boundary. The values obtained here will be the initial value of our Riemann problem for each cell.

- **Step 3**:*solution of the Riemann problem with values* $\bar{\boldsymbol{U}}_{\boldsymbol{i}}^{\boldsymbol{R}}$ *and* $\bar{\boldsymbol{U}}_{\boldsymbol{i+1}}^{\boldsymbol{L}}$ *at the* $\boldsymbol{x}_{\boldsymbol{i+\frac{1}{2}}}$ *boundary.*
  This step is based on the implementation of the Riemann problem to find the fluxes at each boundary of the cell starting from the values calculated in the Step 2. For our $\boldsymbol{x_{i+1/2}}$ cell boundary the left initial values will be $\bar{\mathbf{U}}_{\boldsymbol{i}}^{\boldsymbol{R}}$ and the right initial values will be $\bar{\mathbf{U}}_{\boldsymbol{i+1}}^{\boldsymbol{L}}$.
  Since our code base the resolution of Riemann problem on the vector of the primitive variables , we must find, as last step, the vector $\mathbf{W}_{\boldsymbol{i}}^{\boldsymbol{L}} = \boldsymbol{\rho_L, u_L, p_L}$ of the primitive variables from $\bar{\mathbf{U}}_{\boldsymbol{i}}^{\boldsymbol{R}}$ and the vector $\mathbf{W}_{\boldsymbol{i}}^{\boldsymbol{R}} = \boldsymbol{\rho_R, u_R, p_R}$ of the primitive variables from $\bar{\mathbf{U}}_{\boldsymbol{i+1}}^{\boldsymbol{L}}$. It can be performed algebrically.

After all this passages we have all the data to evaluate the $\mathbf{U}_i^{n+1}$ conserved variables at time $n+1$ for each cell i with an high resolution Godunov scheme:

$$\mathbf{U}_i^{n+1} = \mathbf{U}_i^n + \frac{\Delta x}{\Delta t}\left[\mathbf{F}_{i-\frac{1}{2}} - \mathbf{F}_{i+\frac{1}{2}}\right] \quad . \tag{146}$$

7 Numerical code and exact solutions

In this section we're going to analyze the numerical code used to reproduce the numerical model introduced before. After this we'll create the analytical solutions of the models introduced in chapter (2) and we will validate our numerical code matching it with the analytical solutions. The program used to compile the code is Matlab, and the version of the numerical scheme considered here is the High resolution Godunov scheme. The procedure to test a numerical code is based on evaluating all the different cases for which an analytical solution is disposable. Once we've done this we can suppose that the code can work with all the different cases at the same time.

7.1 Numerical code

The main architecture of the code is based into three main parts:

- *Case parameters, boundary and initial conditions.*
  In this part we define the full geometry that we're going to use in our study case (De Laval nozzle, convergent nozzle, constant section duct,etc.), the fluid chosen as perfect gas and the mesh

size for our numerical grid as well as the time used for our unsteady evolution. The f and q coefficients can be selected in this part of the code. In this section we also define the inlet and outlet boundary conditions and the initial conditions for our grid following section (3.4.3) and section (5.4.3).

- *Left and Right Boundary conditions.*
  The second part of our code is devoted to the development of the boundary conditions using the systems developed in section (5.4.4) and section (5.4.5). This part is crucial for every numerical code because changing the type of the boundary conditions we can spot different physical situations.

- *High Resolution Godunov for the inner domain.*
  The last part is the core of the numerical code and it is the computation inside the inner domain of the properties through the HR Godunov numerical scheme. At first we have to impose a slope limiter and we must make the inner grid initial conditions of second order in time and space as explained in section (6.1) and then we must use these properties as IC for the general Godunov scheme as explained in section (6.3). In this part of the code is also included the CFL stability condition (5.6) changed time by time and the reiteration of the properties at everytime step

Other parts added are the comments, crucial to clarify every passage and the plot part which is useful to make more user-friendly the evolution of the results time by time.

7.2 Exact solution for an Area Variation steady-state conduct

The analytical solution of a steady state flow inside a duct with area variation can be found considering the governing equation of the case. The solution for a *De Laval Nozzle* is the most general case and recalling the fig.(1) we have to find the pressure ratios that defines the limits for which the one-dimensional model is valid. The case for a simply convergent nozzle will be also treated.

7.2.1 Convergent nozzle and Design supersonic De Laval

Considering a simply convergent nozzle with a subsonic inlet the analytical solution can be found with the subsonic iterations method [2]

because the equation we are going to use are non linear. We can remember our Area profile chosen in (2.1.1) :

$$A(x) = 2.5(x + 0.1) + \frac{0.3}{x + 0.1} \quad , \tag{147}$$

The fist equation to consider is obtained equaling the mass flow rat equations when the critical section A_c is coincident with the outlet area A_u:

$$A_u^2 \, \frac{2}{\gamma - 1} \left[\left(\frac{p_2}{p_1^0} \right)^{\frac{2}{\gamma}} - \left(\frac{p_2}{p_1^0} \right)^{\frac{\gamma+1}{\gamma}} \right] = A_c^2 \left(\frac{2}{\gamma + 1} \right)^{\frac{\gamma+1}{\gamma-1}} \tag{148}$$

where we can use the K_c coefficient is only dependent on the fluid we are using:

$$K_c = \left(\frac{2}{\gamma + 1} \right)^{\frac{\gamma+1}{\gamma-1}} \frac{\gamma - 1}{2} \quad . \tag{149}$$

Rewriting all in the correct way we obtain the subsonic iteration ($p_{2D}/p^0 > p_c/p^0$) formula with $p_c = (2/(\gamma + 1))^{(\gamma/(\gamma-1))}$:

$$1 - \left(\frac{p_2}{p_1^0} \right)^{\frac{\gamma-1}{\gamma}} = \frac{A_c^2}{A_u^2} K_c \left(\frac{p_2}{p_1^0} \right)^{-\frac{2}{\gamma}} \quad , \tag{150}$$

and

$$\frac{p_2}{p_1^0} = \left[1 - \frac{A_c^2}{A_u^2} K_c \left(\frac{p_2}{p_1^0} \right)^{\frac{-2}{\gamma}} \right]^{\frac{\gamma}{\gamma-1}} \quad . \tag{151}$$

In case of supersonic flow ($p_{2D}/p^0 < p_C/p^0$) instead we can use the formula:

$$\left(\frac{p_2}{p_1^0} \right)^{\frac{2}{\gamma}} = \frac{A_c^2}{A_u^2} K_c \left[1 - \left(\frac{p_2}{p_1^0} \right)^{\frac{\gamma-1}{\gamma}} \right]^{-1} \tag{152}$$

which can be rewritten as:

$$\left(\frac{p_2}{p_1^0} \right) = \left[\frac{A_c^2}{A_u^2} K_c \left[1 - \left(\frac{p_2}{p_1^0} \right)^{\frac{\gamma-1}{\gamma}} \right]^{-1} \right]^{\frac{\gamma}{2}} \quad . \tag{153}$$

The iterative method target is to find the pressure ratio exact solution and it starts imposing a p_{try} ratio which value must be similar to p_2/p_1^0 to avoid the divergence of the algorithm. Starting from this value we solve the right part of the eq. (150). This value will be used in the

right part of the eq. (151) to find the final value for the first iteration. When several iterations are done we converge to the exact pressure ratio value.
For a *chocked convergent nozzle* with a subsonic inlet fix the total pressure and total temperature at the inlet, the outlet pressure and the geometry of our nozzle. From theory is known that if the working ratio $p_2/p_1^0 < p_c/p_1^0 = (2/(\gamma+1))^{\frac{\gamma}{\gamma-1}}$ is lower than the critical one, the exit is sonic and so the outlet Area is the critical one and we are in chocking conditions. Using only the (150) with A_c found from the minimum section in our geometry, we can find the theoretical solution for pressure ratio making the Area variyng as a function along our x axis.
For a *convergent nozzle* in non-chocked condition, the theoretical solution is found as the previous passages but substituting the critical area A_c with the formula:

$$A_c = \frac{\dot{m}}{\sqrt{\gamma \left[\frac{2}{\gamma+1}\right]^{\frac{\gamma+1}{\gamma-1}} p_1^0 \rho_1^0}} , \tag{154}$$

where the ρ_1^0 can be found from the initial conditions as $\rho_1^0 = \frac{p_1^0}{RT^0}$ and the mass flow rate $\dot{m}$ must be taken at the end of the numerical situation. For a *De Laval nozzle* in design conditions we must use both the (150) and the (152). The first iteration must be performed in the same way of the *chocked convergent* case. For the supersonic iteration we must use the (152) considering A_c the minimum section in the nozzle.
The temperature can be found in the same way for the subsonic case using the iteration:

$$1 - \frac{T_u}{T^0} = \frac{A_c^2}{A_u^2} K_c \left(\frac{T_u}{T^0}\right)^{-\frac{2}{\gamma-1}} \tag{155}$$

in function if the Area A_u with the A_c as the minimum area with the same iteration method used for the pressure part. The supersonic part of the temperature can be found from the supersonic iteration:

$$\frac{T_u}{T^0} = \left[\frac{A_c^2}{A_u^2} K_c \left[1 - \left(\frac{T_u}{T^0}\right)\right]^{-1}\right]^{\frac{\gamma-1}{2}} . \tag{156}$$

The other properties can be found in function of the analytical pressure function with density as :

$$\rho = \rho_1^0 \left(\frac{p}{p_1^0} \right)^{\frac{1}{\gamma}} , \tag{157}$$

speed as:

$$u = \sqrt{\frac{2\gamma}{\gamma - 1} \frac{p_1^0}{\rho_1^0} \left[1 - \left(\frac{p}{p_1^0} \right)^{\frac{\gamma-1}{\gamma}} \right]} , \tag{158}$$

Mach number as:

$$Ma = \sqrt{\frac{2}{\gamma - 1} \left[\left(\frac{p}{p_1^0} \right)^{\frac{\gamma-1}{\gamma}} - 1 \right]} \tag{159}$$

7.2.2 De Laval nozzle with straight shocks

This is the last case, for a De Laval nozzle in which the one dimensional model is valid and it is the case of straight shock. This condition is present when $p_s/p^0 > p/p^0 > p_{slimit}/p^0$. To find the analytical solution we must use the eq.(150) until the sonic state is reached (throat section) and after we must find with another iteration the position of the shock. The evolution from the inlet to the shock can be considered isoentropic whereas we must apply the Rankine-Hugoniot conditions to find the properties downstream the shock. We can use the temperature iteration for the converging part (155). For the location of the shock we must hypotize an x location and a correspondent try area A_{try} to insert into :

$$\frac{T_{sh,1}}{T^0} = \left[K_c \frac{A_c^2}{A_{try}} \left(1 - \frac{T_{sh,1}}{T^0} \right)^{-1} \right]^{\frac{\gamma-1}{2}} , \tag{160}$$

with the same iteration on the left and right part to find the the $T_{sh,1}$. The properties just before the shock can be found from:

$$\begin{cases} u_{sh,1} = \sqrt{2c_p(T^0 - T_{sh,1})} \\ p_{sh,1} = p_1^0 \left(\frac{T_{sh,1}}{T^0} \right)^{\frac{\gamma}{\gamma-1}} \\ Ma_{sh,1} = \frac{u_{sh,1}}{\sqrt{\gamma R T_{sh,1}}} , \end{cases} \tag{161}$$

with $u_{sh,1}$ flow velocity, $p_{sh,1}$ pressure and $Ma_{sh,1}$ Mach number upstream the shock .
The relations after the shock can be found with the Rankine-Huguniot condition:

$$\frac{p_{sh,2}}{p_{sh,1}} = \frac{2\gamma}{\gamma+1} Ma_{sh,1}^2 - \frac{\gamma-1}{\gamma+1} \tag{162}$$

$$Ma_{sh,2}^2 = \frac{Ma_{sh,1}^2 + \frac{2}{\gamma-1}}{\frac{2}{\gamma-1} Ma_{sh,1}^2 - 1} \, , \tag{163}$$

with a variation of total pressure expressed by:

$$p_{sh,2}^0 = p_{sh,2} \left(1 + \frac{\gamma-1}{2} Ma_{sh,2}^2 \right)^{\frac{\gamma}{\gamma-1}} \, . \tag{164}$$

The last part is the subsonic evolution of temperature till the outlet pressure modified with the change of total pressure:

$$1 - \frac{T_u}{T^0} = \left(\frac{p_1^0}{p_{sh,2}^0} \right)^2 \frac{A_c^2}{A_u^2} K_c \left(\frac{T_u}{T^0} \right)^{-\frac{2}{\gamma-1}} \, . \tag{165}$$

To verify that the guessed shock position is correct, we must check that the outlet pressure p_u is coincident with the p_2 theoretical one. So we can find our p_u with the isoentropic evolution from the downstream-shock case:

$$p_u = p_{sh,2}^0 \left(\frac{T_u}{T^0} \right)^{\frac{\gamma}{\gamma-1}} \, . \tag{166}$$

If the difference between the p_u and the p_2 is below a tolerance impose we have reached the convergence. If not we can change the try position for shock and the A_{try} correspondent and make the whole process again.

7.3 Analytical solution for the Fanno flow

We're going to validate our numerical code for the Fanno flow. The first step is finding the flow properties trends by means of the analytical Fanno flow solution. Following Ferrari in [2], for initial conditions of the flow we can find an analytical solution for every condition of the flow (subsonic or supersonic) in function of $4fdx/D$. Starting from :

$$4f\frac{dx}{D} = \frac{1-Ma^2}{\gamma Ma^4} \frac{1}{1+\frac{\gamma-1}{2}Ma^2} dMa^2 \, , \tag{167}$$

and integrating it between $[0, L_{max}]$ we obtain:

$$4\bar{f}\frac{L_{max}}{D} = \frac{1-Ma^2}{\gamma Ma^2} + \frac{1+\gamma}{2\gamma}\ln\frac{(1+\gamma)Ma^2}{2\left(1+\frac{\gamma-1}{2}Ma^2\right)} \tag{168}$$

with $\bar{f}$ mean value in $[0, L_{max}]$ section of duct. We know that the Fanno flow presents a length for both subsonic or supersonic flow for which we have no discontinuities, maximum entropy and sonic outlet. Exploiting these properties we can integrate the (167) between two generic section of the duct and find the properties in every position of the duct. We can start finding the Mach number and after all the other properties. We can write :

$$\int_0^L 4f\frac{dx}{D} = 4\bar{f}\frac{dx}{D} = \int_{Ma_1^2}^{Ma_2^2}\frac{1-Ma^2}{\gamma Ma^4}\frac{1}{1+\frac{\gamma-1}{2}Ma^2}dMa^2 - \tag{169}$$

$$\int_{Ma_1^2}^{Ma_2^2}\frac{1-Ma^2}{\gamma Ma^4}\frac{1}{1+\frac{\gamma-1}{2}Ma^2}dMa^2 = \left(4\bar{f}\frac{dx}{D}\right)_{Ma_1} - \left(4\bar{f}\frac{dx}{D}\right)_{Ma_2}.$$

In our algorithm to find the exact solution we must use the Mach at the inlet taken from the numerical code and insert it into the (168) equation and the $\left(4\bar{f}\frac{dx}{D}\right)_{Ma_1}$ value found, subtracted to the $4\bar{f}\frac{x}{D}$ value in the x position will be equal to $\left(4\bar{f}\frac{dx}{D}\right)_{Ma_2}$ in the position x. Applying the (168) we can find the Ma_2 Mach number at section 2. The equation must be solved with an iterative method because it is non linear. It can be used for subsonic and supersonic and , for this reason, we will find two solutions for each x abscissa. To find the subsonic one we must impose and iteration on the Mach number from 0 to 1 as maximum value. For the supersonic solutions we must impose iterations staring form Mach= 1 as try value. The other quantities can be found using the differential relation in Mach number function exploiting the star properties at Mach=1 (properties in the critic section). These can be found simplyifing the differential equations for Mach=1:

$$\frac{p}{p*} = \frac{1}{Ma}\sqrt{\frac{\gamma+1}{2\left(1+\frac{\gamma-1}{2}Ma^2\right)}}. \tag{170}$$

The star property for our flux can be found knowing the pressure at the inlet for the steady state condition for our numerical solution and using the inlet Mach number. The same procedure can be applied to find all the other star properties:

$$\begin{cases} \frac{u}{u*} = Ma \sqrt{\frac{\gamma+1}{2\left(1+\frac{\gamma-1}{2}Ma^2\right)}} \\ \frac{T}{T*} = \frac{\gamma+1}{2\left(1+\frac{\gamma-1}{2}Ma^2\right)} \\ \frac{\rho}{\rho*} = \frac{1}{Ma}\sqrt{\frac{2\left(1+\frac{\gamma-1}{2}Ma^2\right)}{\gamma+1}} \end{cases} . \tag{171}$$

Now that the star properties are all found from the inlet properties and the inlet Mach, we can find every property we want using the ratios found before. We take as an example the formula to find the pressure at the zone 2 knowing all the inlet properties and having found the Mach evolution along the nozzle:

$$\frac{p_2}{p_1} = \frac{(p/p*)_{Ma_2}}{(p/p*)_{Ma_1}} \tag{172}$$

.

The particular case in which the supersonic Fanno flow creates a straight shock in the duct can be found using both the previous evolutions and using another iterative method. To find the right theoretical condition we must end with a Mach=1 at outlet because this is the lower limit for a subsonic Fanno flow. To find it, we make an initial hypothesis on the position of the shock and we solve the supersonic evolution till this position, we apply the Rankine-Hugoniot condition to find the Mach downstream the shock:

$$Ma^2_{sh,2} = \frac{Ma^2_{sh,1} + \frac{2}{\gamma-1}}{\frac{2}{\gamma-1}Ma^2_{sh,1} - 1} , \tag{173}$$

and we continue with a subsonic evolution till the end. If the exit Mach is equal to one we have finished, otherwise we must make other iterations on the position of the shock.

7.4 Exact solution for the Rayleigh flow

For the validation for the Rayleigh flow we must find the analytical solution. We know that the change in properties is linked with the

change in total temperature induced in each section by the heat introduced or expelled from the system. As study case we will consider the case in which the heat is introduced into the system. The chocking condition is determined by the maximum heat that can be absorbed by the system, after this condition the system outlet Mach number will be fixed whereas the system will react diminishing the mass flow rate as long as we increase the length further.
The exact outlet total temperature can be determined with the first principle of the Thermodynamic for our system in differential form :

$$Q = c_p \frac{dT^0}{dx} \ . \tag{174}$$

Integrating the right part in Temperature and the left part in time we obtain:

$$Q(x - x_0) = c_p(T_2^0 - T_1^0) \ . \tag{175}$$

To link the Qgeneral heat flow J/(Kg m) to the q heat flow to be introduced in our code, we can use the quantity $\dot{m}/Area = \rho u$ which is constant in this flow. The total temperature in section two can be easily found if the heat introduced is constant for every section. Making a dimensional analysis we resort to:

$$T_2^0 = \frac{qD\pi A}{\dot{m}Ac_p}(x - x_0) + T_1^0 \ , \tag{176}$$

with A area of the duct:

$$Q = \frac{qD\pi A}{\dot{m}A}; \tag{177}$$

The q in our numerical model is J/(sm^2).
The conditions linked with the sonic state at the outlet can be found using the relations in function of the star conditions:

$$\begin{cases} \frac{p}{p*} = \frac{\gamma+1}{1+\gamma Ma^2} \\ \frac{T}{T*} = \frac{(\gamma+1)^2 Ma^2}{(1+\gamma Ma^2)^2} \\ \frac{u}{u*} = \frac{(\gamma+1)Ma^2}{(1+\gamma Ma^2)^2} \\ \frac{\rho}{\rho*} = 1/\frac{u}{u*} \ . \end{cases} \tag{178}$$

Knowing T_2^0 and T_1^0 and having found the $T*$ from the formulas upside we can find the variation of Mach number along all the duct. Knowing the Mach evolution the other properties can be found in a generic section 2 using the ratio:

$$\frac{p_2}{p_1} = \frac{p_2/p*}{p_1/p*} \ , \tag{179}$$

and knowing the inlet Mach number and initial numerical values for the properties we want to evaluate. Even in this case we must use an iteration considering a right initial choice and a limit of research in order to find the subsonic values in the subsonic flow.

7.5 Analytical solutions for one-dimensional diabatic flows with wall friction

As explained by Ferrari in [1] is possible to find the exact solution of a diabatic viscous flow inside a constant section duct with a constant heat flow.
We start form the conservation of mass:

$$\rho u = \dot{m}/A = const \tag{180}$$

and the momentum balance and total energy equation rearranged together:

$$\frac{\dot{m}}{A}\frac{dh}{dx} + \frac{\dot{m}}{A}\frac{d}{dx}\left(\frac{u^2}{2}\right) = \frac{4\dot{q}_f}{D} \ . \tag{181}$$

After some manipulation we can find the solution to this system of equation explicitly as:

$$x = -\frac{\dot{m}h_1^0}{q_f\dot{\pi}D} + \left\{ C - \frac{\gamma+1}{\gamma}\frac{D}{4f}\ln\left[\frac{\sqrt{\frac{u^2}{2}} + \sqrt{\frac{u^2}{2} + \frac{\gamma-1}{\gamma}\frac{\dot{q}_f\pi D^2}{4f\dot{m}}}}{\sqrt{\frac{\gamma-1}{\gamma}\frac{|\dot{q_f}|\pi D^2}{4f\dot{m}}}}\right]\right\}\frac{\sqrt{\frac{u^2}{2}}}{\sqrt{\frac{u^2}{2} + \frac{\gamma-1}{\gamma}\frac{\dot{q}_f\pi D^2}{4f\dot{m}}}} \tag{182}$$

where the abscissa x can be evaluated as a function of the kinetic energy and C represents a constant of integration.
If a subsonic flow is considered, using a tentative value of Ma_1 (Mach number at the pipe inlet) we can obtain $u_1^2/2$ and $\dot{m}$ from the equations :

$$\begin{cases} \frac{u_1^2}{2} = cpT_1^0 Ma_1^2\left(\frac{2}{\gamma-1} + Ma_1^2\right)^{-1} \\ \dot{m} = \frac{p_1^0}{\sqrt{RT_1^0}}A\sqrt{\gamma}Ma_1\left(1 + \frac{\gamma-1}{2}Ma_1^2\right)^{-(\gamma+1)/(2(\gamma-1))} \end{cases} . \tag{183}$$

which refers to an isoentropic evolution from the stagnation conditions to state 1. The constant C can be determined as:

$$C = \frac{\dot{m}h_1^0}{\dot{q}_f\pi D}\frac{\sqrt{\frac{u_1^2}{2} + \frac{\gamma-1}{\gamma}\frac{\dot{q}_f\pi D}{4f\dot{m}}}}{\sqrt{\frac{u_1^2}{2}}} + \frac{\gamma+1}{\gamma}\frac{D}{4f}\ln\left[\frac{\sqrt{\frac{u_1^2}{2}} + \sqrt{\frac{u_1^2}{2} + \frac{\gamma-1}{\gamma}\frac{q_f\dot{\pi}D^2}{4f\dot{m}}}}{\sqrt{\frac{\gamma-1}{\gamma}\frac{|\dot{q_f}|\pi D^2}{4f\dot{m}}}}\right] . \tag{184}$$

The equation (182) and the C value found from (184) can be used to find $u_2^2/2$ in correspondence of the pipe outlet $x_2 = L$. The density ρ_2 can be found from (180) applied for $x_2 = L$ and we can use:

$$h = h_1^0 + \frac{\dot{q_f}\pi D}{\dot{m}}x - \frac{u^2}{2} \tag{185}$$

At the end we can find the p_2 using ρ_2 and h_2 in:

$$p = \frac{\gamma - 1}{\gamma}\rho h\,. \tag{186}$$

If the p_2 value found is equal to a provided datum the guessed Ma_1 is correct, otherwise we must repeat the iteration with other values. Concerning a supersonic flow, the constant C can be evaluated by knowing the flow properties at the pipe inlet by means of equation (184) and the solution can be directly obtained.

8 Validation

In this section we show the validation for our High resolution Godunov scheme. All the different cases will be considered and the geometrical and model features, the mesh and the boundary conditions will be described for every case. Before the comparison between the numerical model and the analytical solutions, we must perform a convergence analysis to choose the mesh size and to avoid the possible numerical errors. We will perform, as an example case a convergence study on a the De Laval nozzle case. For all the other cases we consider a general mesh of $N = 1000$ elements because the results obtained with this refinement are enough accurate to fulfill the validations.

8.1 Convergence analysis

To complete the discussion upon our numerical code we have to make a convergence analysis on the mesh size to check, for which mesh size our solution will be the more near to the numerical one. Our analysis is based on a convergent divergent nozzle with an area section of :

$$A(x) = 2.5(x + 0.1) + \frac{0.3}{x + 0.1}\quad , \tag{187}$$

an inlet total pressure $p^0 = 100000$ Pa an inlet total temperature $T^0 = 500$ K and an outlet pressure $p_2 = 70000$ Pa. The length is $L = 1$ dm. For different mesh size we will measure the maximum error between the numerical and the analytical solution.

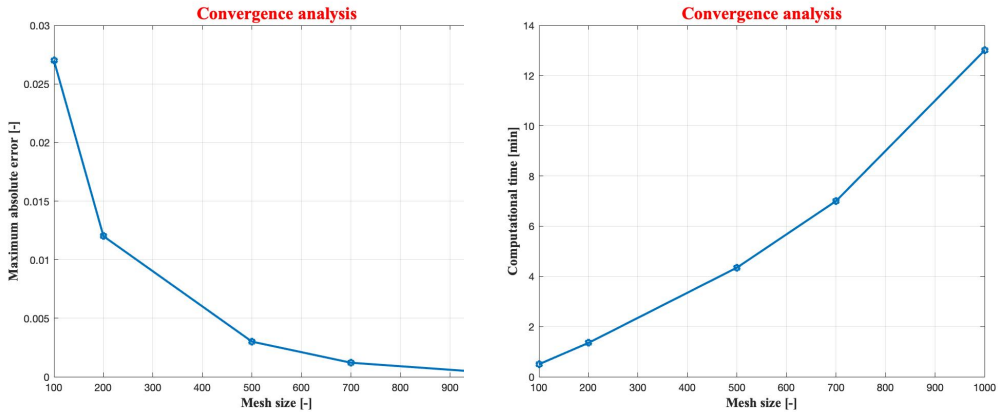

(a) Convergence analysis for minimum error.

(b) Computational time for different mesh sizes

Figure 17: Convergence analysis for a De Laval nozzle.

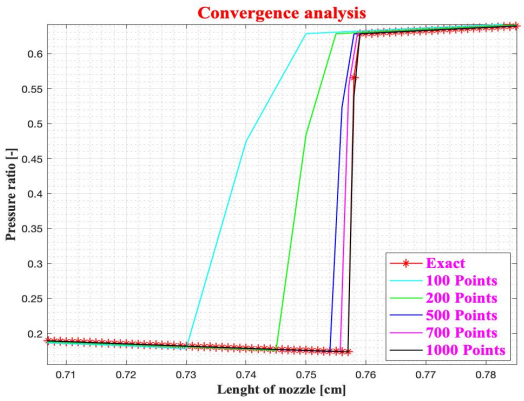

Figure 18: Shock detail for different mesh sizes.

The maximum error is measure as the maximum distance between the exact solution and the numerical solution in the shock position as shown in fig.(18). From the convergence analysis on a De Laval nozzle results that, for a mesh of $N = 1000$ elements, the error is close to 0 as shown in figure (17a). This will be the selected mesh size to be chosen, for every unit of length, to reach the best results from our code.
The computational time increases linearly as we increase the mesh size (fig.17b) and this must be taken into account for the more complex application of an HR Godunov scheme.

8.2 Area Variation validation

8.2.1 Convergent chocked nozzle

The results presented in figure (19) are obtained for a convergent chocked nozzle with an area section of :

$$A(x) = 2.5(x + 0.1) + \frac{0.3}{x + 0.1} \quad , \; x = [0, 0.246] \tag{188}$$

in the x interval $[0, 0.246]$ with an inlet total pressure $p0 = 100000$ Pa an inlet total temperature $T0 = 500$ K and an outlet pressure $p_2 = 50000$ Pa. The grid is composed by $N = 1000$ elements. The length is $L = 0.246$ dm. The f and q coefficients are null.

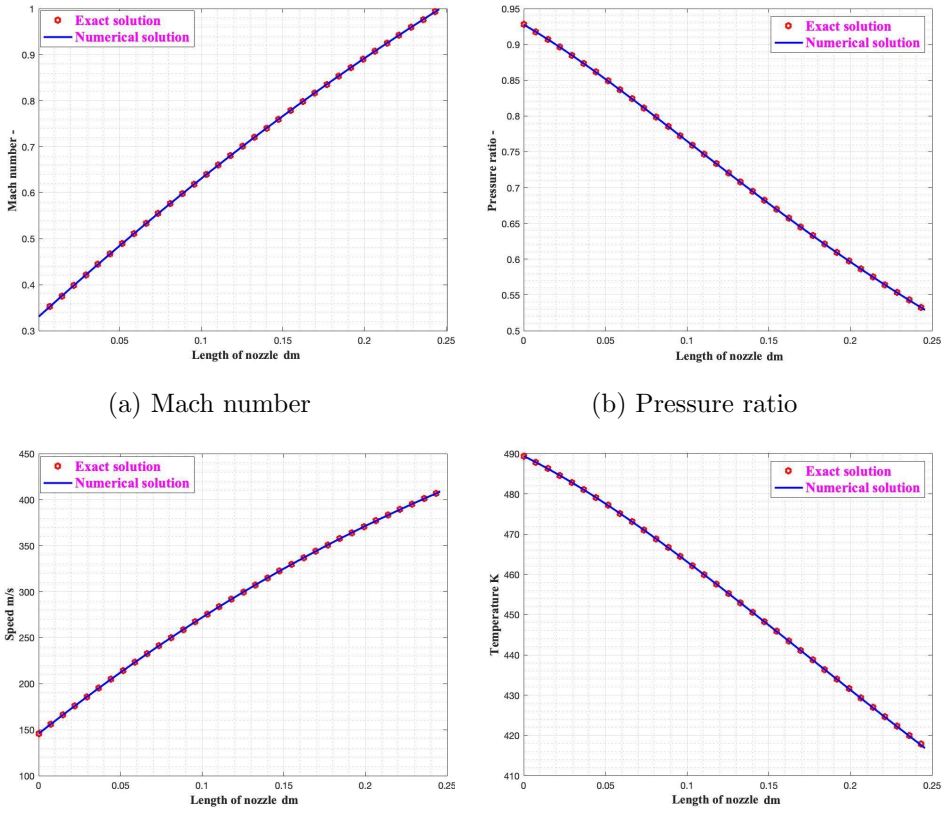

(a) Mach number

(b) Pressure ratio

(c) Speed

(d) Temperature

Figure 19: Convergent chocked nozzle validation with an HR Godunov scheme.

8.2.2 De Laval full subsonic nozzle

The results shown in figure (20) are obtained for a convergent divergent nozzle with an area section of :

$$A(x) = 2.5(x + 0.1) + \frac{0.3}{x + 0.1} \quad , \tag{189}$$

with an inlet total pressure $p^0 = 100000$ Pa an inlet total temperature $T^0 = 500$ K and an outlet pressure $p_2 = 93000$ Pa. The grid is composed by $N = 1000$ elements. The length is $L = 1$ dm. The f and q coefficients are null.

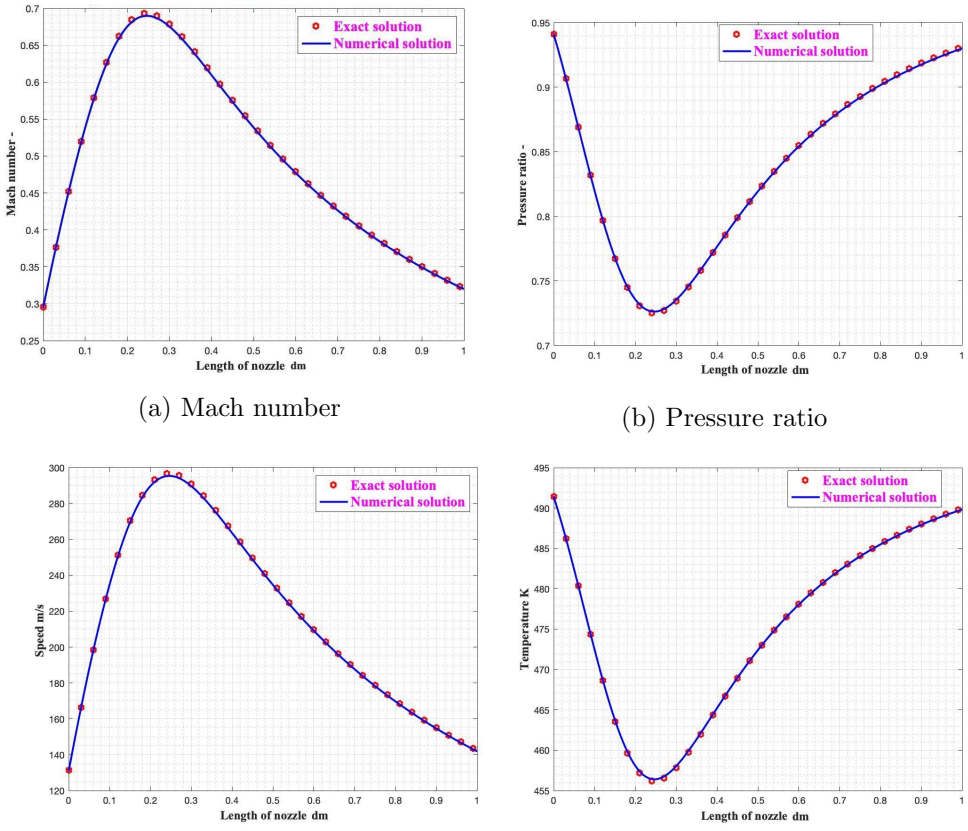

(a) Mach number

(b) Pressure ratio

(c) Speed

(d) Temperature

Figure 20: Subsonic De Laval nozzle validation with an HR Godunov scheme.

8.2.3 De Laval nozzle in design condition

The results shown in figure (21) are obtained for a convergent divergent nozzle with an area section of :

$$A(x) = 2.5(x + 0.1) + \frac{0.3}{x + 0.1} \quad , \tag{190}$$

with an inlet total pressure $p^0 = 100000$ Pa an inlet total temperature $T^0 = 500$ K and an outlet pressure $p_2 = 12000$ Pa. The grid is composed by $N = 1000$ elements. The length is $L = 1$ dm. The f and q coefficients are null.

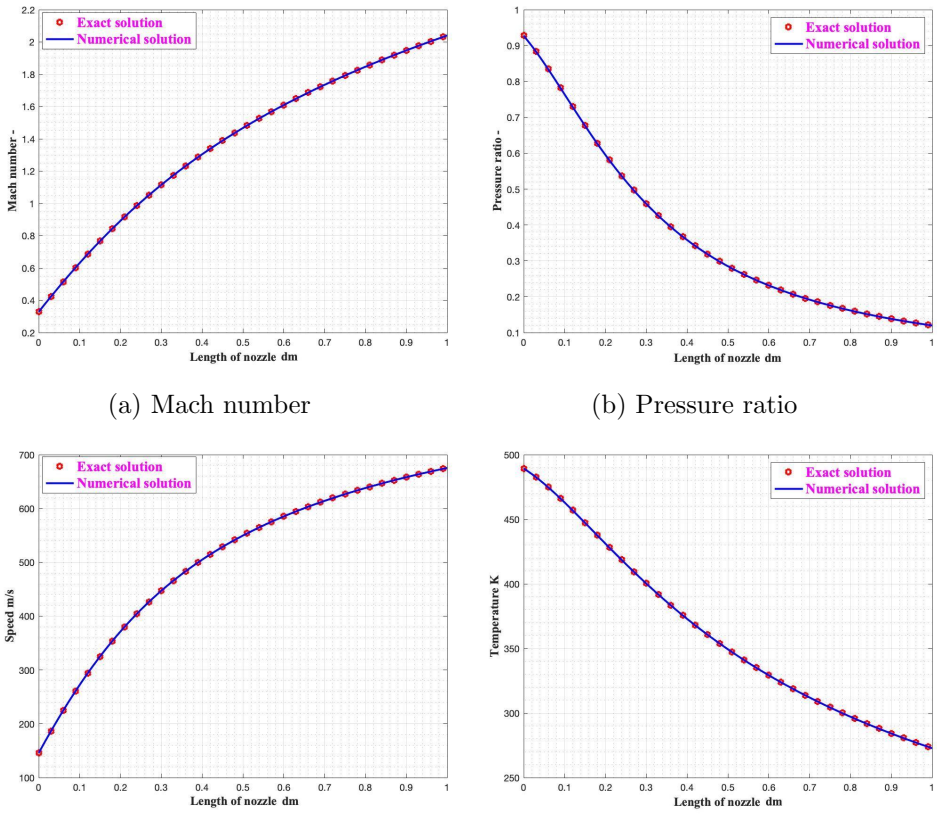

(a) Mach number

(b) Pressure ratio

(c) Speed

(d) Temperature

Figure 21: De Laval nozzle in design condition validation with an HR Godunov scheme.

8.2.4 De Laval nozzle with a straight shock

The results shown in figure (22) are obtained for a convergent divergent nozzle with an area section of :

$$A(x) = 2.5(x + 0.1) + \frac{0.3}{x + 0.1} \quad , \tag{191}$$

with an inlet total pressure $p^0 = 100000$ Pa an inlet total temperature $T^0 = 500$ K and an outlet pressure $p_2 = 70000$ Pa. The length is $L = 1$ dm. The grid is composed by $N = 1000$ elements. The f and q coefficients are null.

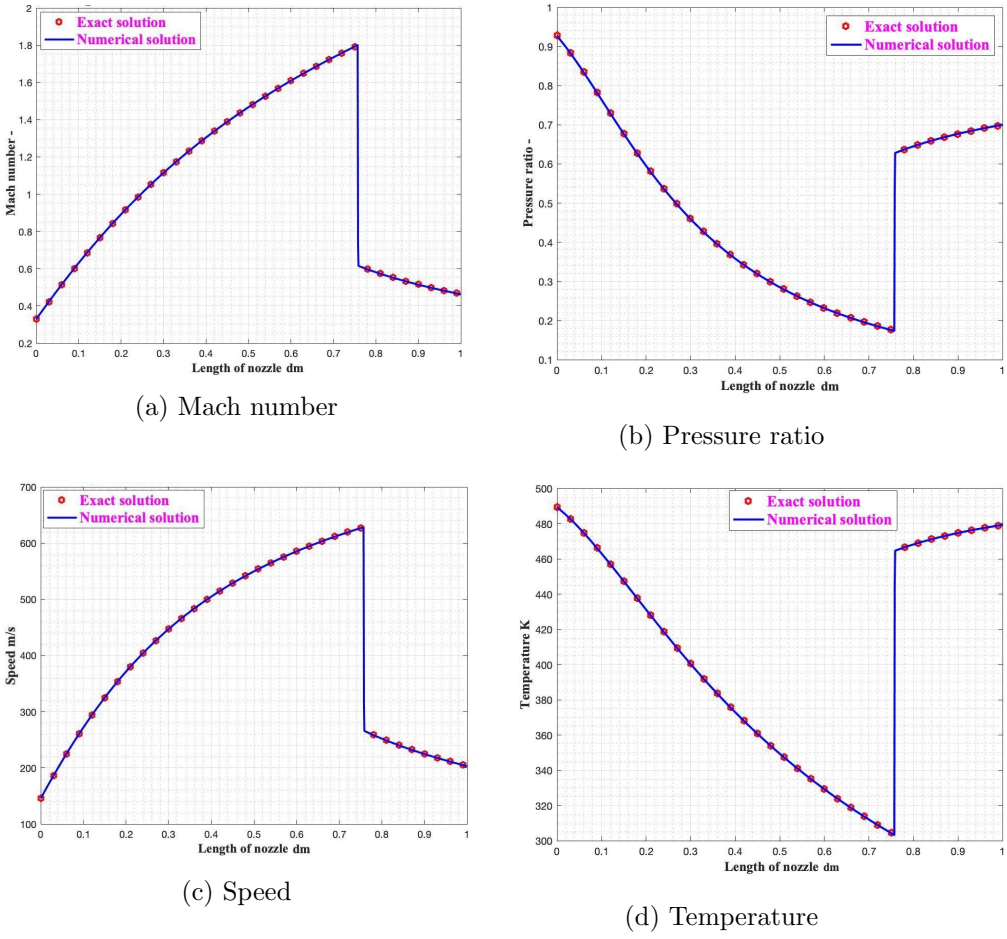

(a) Mach number

(b) Pressure ratio

(c) Speed

(d) Temperature

Figure 22: De Laval nozzle with a straight shock validation with an HR Godunov scheme.

8.2.5 Remarks

The numerical results converge all to the exact solution for a grid of $N = 1000$ points. For the *De Laval nozzle* we must be careful about the pressure ratio chosen. In absence of friction and heat exchange we have seen that there are theoretical limits for the application of the one-dimensional model. This limit is $0.12 < p/p_1^0 < 0.55$ for the selected geometry. In this range the solution is deeply influenced by oblique shocks and so, at least a 2D model is required. In the chocked *convergent* case the condition of Mach=1 represent a singularity. In general, the passage from a subsonic flow to a supersonic one, represent a change in the approach to the problem. This difference in behaviour can be easily manipulated when we are in well separated condition of supersonic or subsonic case, giving for each case different boundary conditions. The single outlet point in Mach=1 instead, represent the limit case for which the code tends to oscillate because, in Mach=1, the nature of the flow changes. This oscillation is also motivated by the fact that our boundary conditions are built with a non-conservative formulation (MOC) and so they give very poor results in the particular cases of shock formations in the BC. This argument is supported by the fact that, the condition of transition in case of the De Laval nozzle in which we have Mach=1 in the throat section, doesn't give any type of oscillation because it is solved with the internal Godunov scheme. Another issue for the convergent nozzle can be represented by the shape of the nozzle. Not all the convergent shapes allow to reach a sonic condition and we must be careful about the exit section for which a null variation of Area is needed to reach the sonic state.
The *subsonic De Laval Nozzle* is a very peculiar case since the pressure ratio that drives the flow is very low whereas the change in properties in the throat is very steep. Unless these difficulties satisfactory results are obtained in our numerical code. The *Design De Laval Nozzle* case is reached building transmissive BC at the right Boundary. From [6], the transmissive boundaries represents the correspondent physical condition for which the waves of the flow can pass the section without any effect on them. We can so write, for the last boundary:

$$\begin{cases} \rho(end) = \rho(end-1) \;\; Density \\ u(end) = u(end-1) \;\; Speed \\ P(end) = P(end-1) \;\; Pressure \; . \end{cases} \tag{192}$$

We are practically applying the Godunov resolution also to the right boundary to overcome the transition zone ($0.12 < p/p_1^0 < 0.55$), until the pressure of design is reached. The theoretical results prove this

approach.

8.3 The Fanno Flow Validation

8.3.1 Subsonic Fanno's Flow

The results in figure (23) are obtained for a constant section circular duct with a constant diameter $D = 0.7$ cm, with an inlet total pressure $p^0 = 100000$ Pa, inlet total temperature $T^0 = 500$ K and an outlet pressure $p_2 = 70000$ Pa. The length is $L = 10$ cm. The grid is composed by $N = 1000$ elements. The f coefficient is equal to 0.003 and the q coefficient is null.

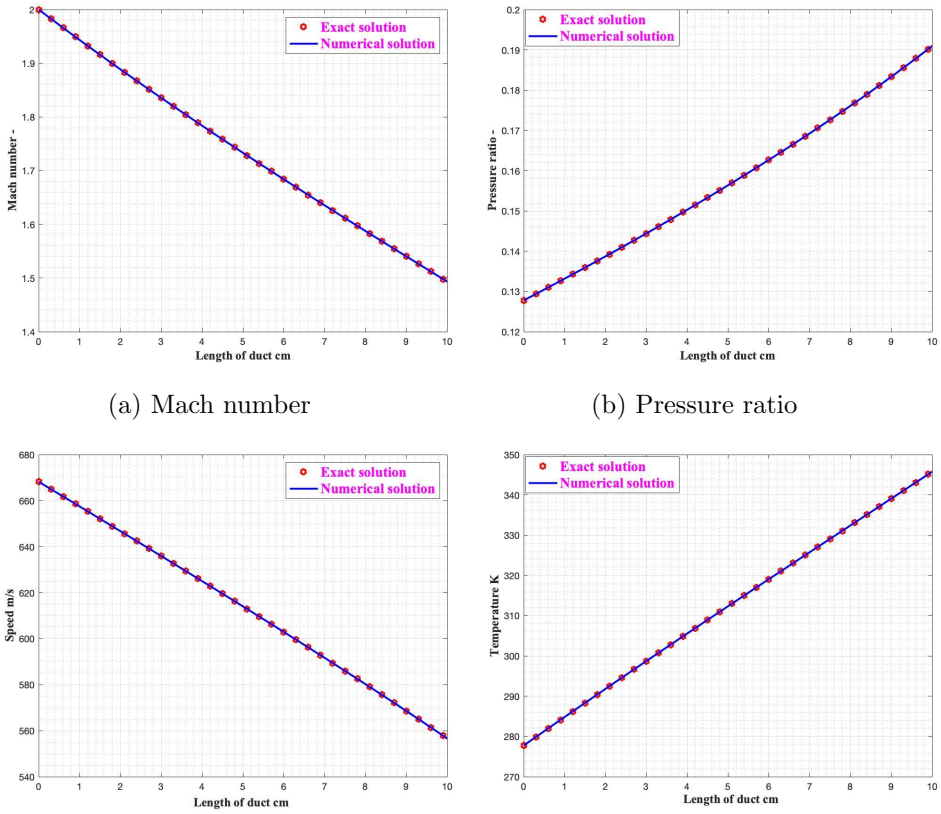

(a) Mach number

(b) Pressure ratio

(c) Speed

(d) Temperature

Figure 23: Subsonic Fanno's flow validation with an HR Godunov scheme.

8.3.2 Supersonic Fanno's Flow

The results in figure (24 are obtained for a constant section circular duct with a constant diameter $D = 0.7$ cm, an inlet total pressure $p^0 = 100000$ Pa, an inlet total temperature $T^0 = 500$ K, an inlet Mach=2 and an outlet pressure $p_2 = 70000$ Pa. The length is $L = 20$ cm. The grid is composed by $N = 1000$ elements. The f = coefficient is equal to 0.003 and the q coefficient is null.

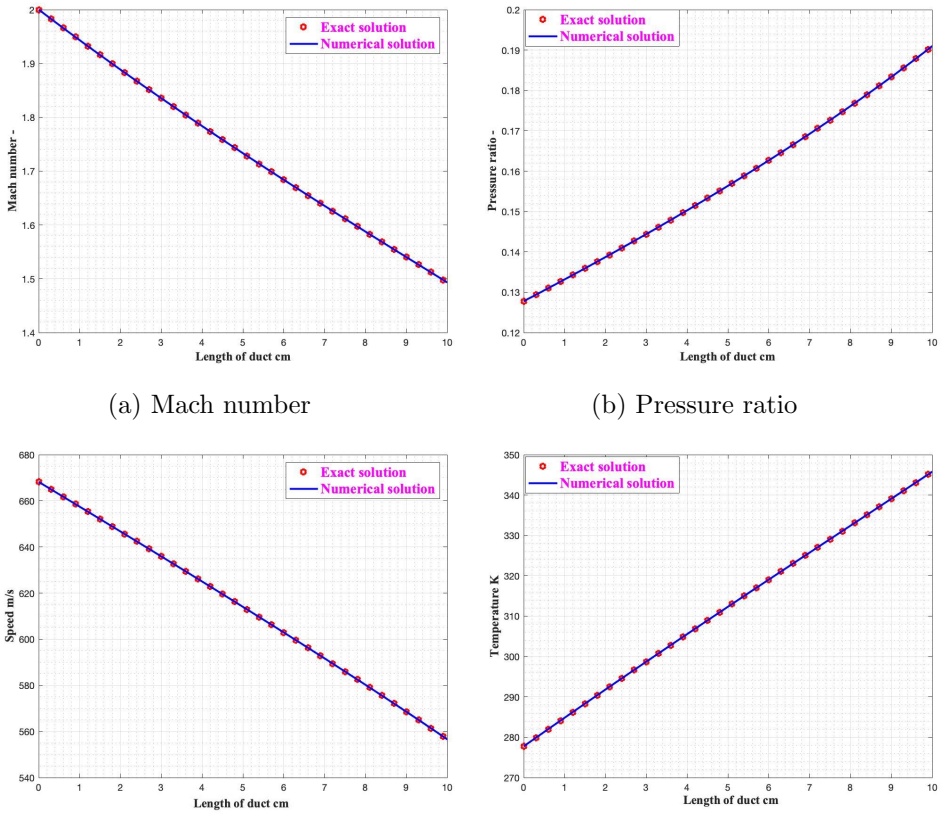

(a) Mach number

(b) Pressure ratio

(c) Speed

(d) Temperature

Figure 24: Supersonic Fanno flow's validation with an HR Godunov scheme.

8.3.3 Subsonic chocked Fanno's Flow

The results in figure (25) are obtained for a constant section circular duct with a diameter $D = 0.7$ cm, an inlet total pressure $p^0 = 100000$ Pa, an inlet total temperature $T^0 = 500$ K and an outlet pressure $p_2 = 50000$ Pa. The length is $L = 40$ cm. The grid is composed by $N = 1000$ elements. The f coefficient is equal to 0.003 and the q

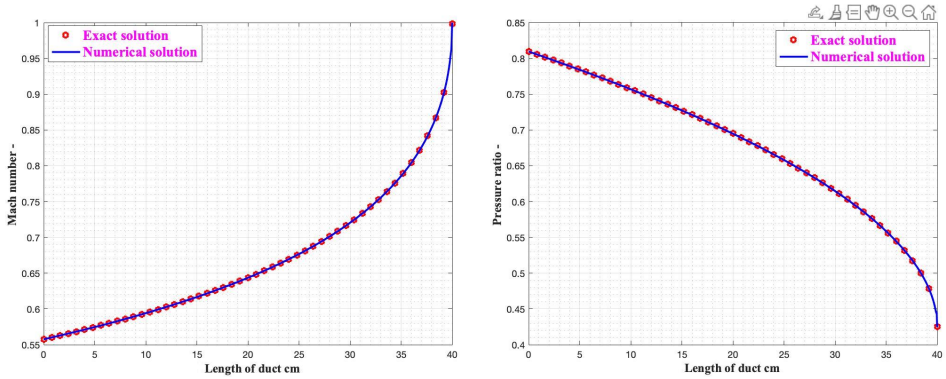

(a) Mach number

(b) Pressure ratio

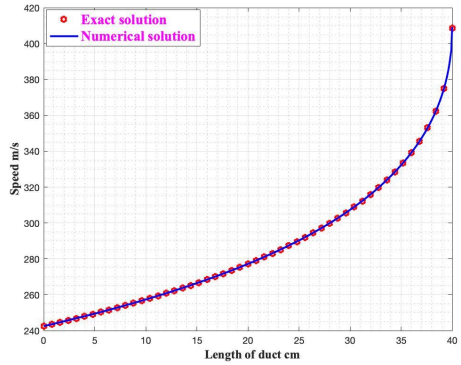

(c) Speed

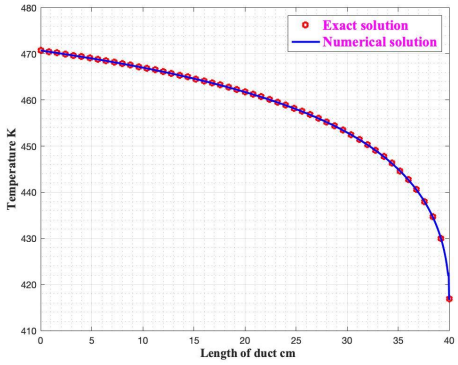

(d) Temperature

Figure 25: Subsonic chocked Fanno flow's validation with an HR Godunov scheme.

coefficient is null.

8.3.4 Supersonic Fanno's flow with a shock

The results in figure (26) are obtained for a constant section circular duct with a diameter $D = 0.7$ cm, an inlet total pressure $p^0 = 100000$ Pa, an inlet total temperature $T^0 = 500$ K , an inlet $Mach = 2$ and an outlet pressure $p_2 = 30000$ Pa. The length is $L = 20$ cm. The grid is composed by $N = 1000$ elements. The $f = 0.003$ and the q coefficient is null.

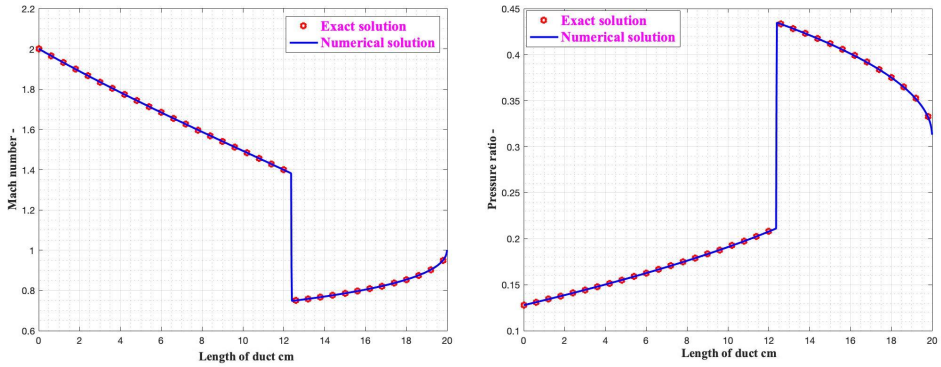

(a) Mach number

(b) Pressure ratio

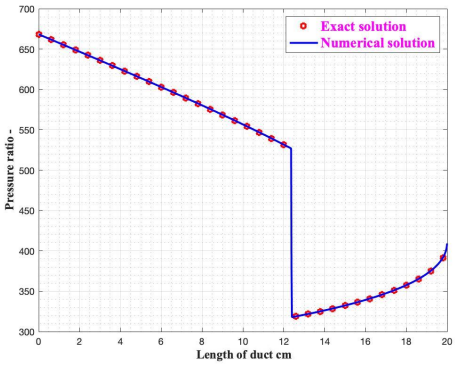

(c) Speed

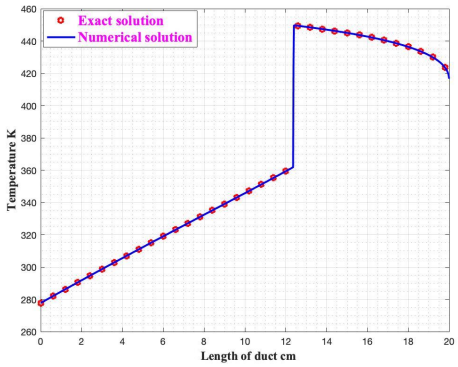

(d) Temperature

Figure 26: Supersonic shock Fanno flow's validation with an HR Godunov scheme.

8.3.5 Remarks

The numerical results obtained converges all to the exact solutions. The *subsonic case* is reached with a very good precision as well as the supersonic one. For the latter one we have formulated the left boundary conditions for a supersonic inlet. In this case, for the theory of characteristics we must provide three properties for our boundary to have a well defined problem. We've chosen the Mach number, the total pressure and the total temperature; the other properties can be evaluated staring from them. Since the Mach at the inlet is fixed, it will be more easy to evaluate the exact solution in the supersonic cases.
For the subsonic case the right boundary condition was the same of a generic subsonic outlet whereas, for the supersonic outlet case, we have applied a *Transmissive* boundary condition to avoid computational shocks at the exict of the duct.

The *chocked subsonic* case and the straight shock in supersonic case are the most particular cases. In the supersonic straight shock the length of duct is the only parameter that can influence the flow properties for a constant friction factor. When the length of a duct is longer than the star length we have overcame the limit condition of Mach=1 at the outlet. The flow will keep the sonic state at the outlet but a straight shock will create inside the nozzle as near to the inlet as we increase the length over the star length if the downstream pressure is lower than $p*$. We've already seen that the Mach=1 outlet condition is not easily developed in the code, especially when the mesh per unit of length diminish. To overcome this problem we can use an hybrid numerical-analytical boundary condition at the right boundary. Since the Mach=1 properties at the outlet are well known from the analytical solution (7.3) (Star properties), we can evaluate them at every time step and we can fix these condition at the outlet without influence the final solution.
For the *supersonic* case the evaluation of the star properties is quite simple since the properties at the inlet are fixed and depends only on the Mach number and so, before evolving in time our code, we can already know if our flow will develop a shock, depending on the inlet conditions and on the length. Once the length is higher than the star one, we can fix the outlet conditions as the star one.
For the *subsonic case*, since the inlet condition changes, at every time step we have to evaluate the star conditions and to update them. The parameter that will us when we can fix our outlet boundary conditions to the star one is the outlet pressure. If it is lower than the star pressure, from theory, we are sure that inside our duct the outlet pressure must be the star one. Outside the duct the post-expansion mechanism will make the pressure become equal to the environment one. Because of this mechanisms of dissipation, that occurs for subsonic flow in ducts with $L < L_*$ with an outlet pressure lower than the star pressure and because of the right boundary solved with a non conservative method, the code is unstable for length lower than $L = 15$ cm and pressure ratios much lower than the pressure star ratio p_*/p_1^0. The problem can be overcame building conservative BC or applying a convergent nozzle at the inlet. In this way we can let the flow inlet condition adapt properly to the fixed star properties.
To reach the chocking conditions very long ducts must be considered because, as we increase the length, we modify the inlet properties in iterative way. Another issue linked to the variation of the inlet condition for every time step is the evaluation of the exact solution for all the subsonic case. We must be sure to have reached the convergence for our

numerical code before giving the inlet Mach condition for evaluating the exact solution.

8.4 Rayleigh's flow validation

8.4.1 Subsonic Rayleigh flow

The results in figure (27), are obtained for a constant cross-section circular area duct with a diameter $D = 0.7$ cm, an inlet total pressure $p^0 = 100000$ Pa an inlet total temperature $T^0 = 500$ K and an outlet pressure $p_2 = 30000$ Pa. The length is $L = 10$ cm. The grid is

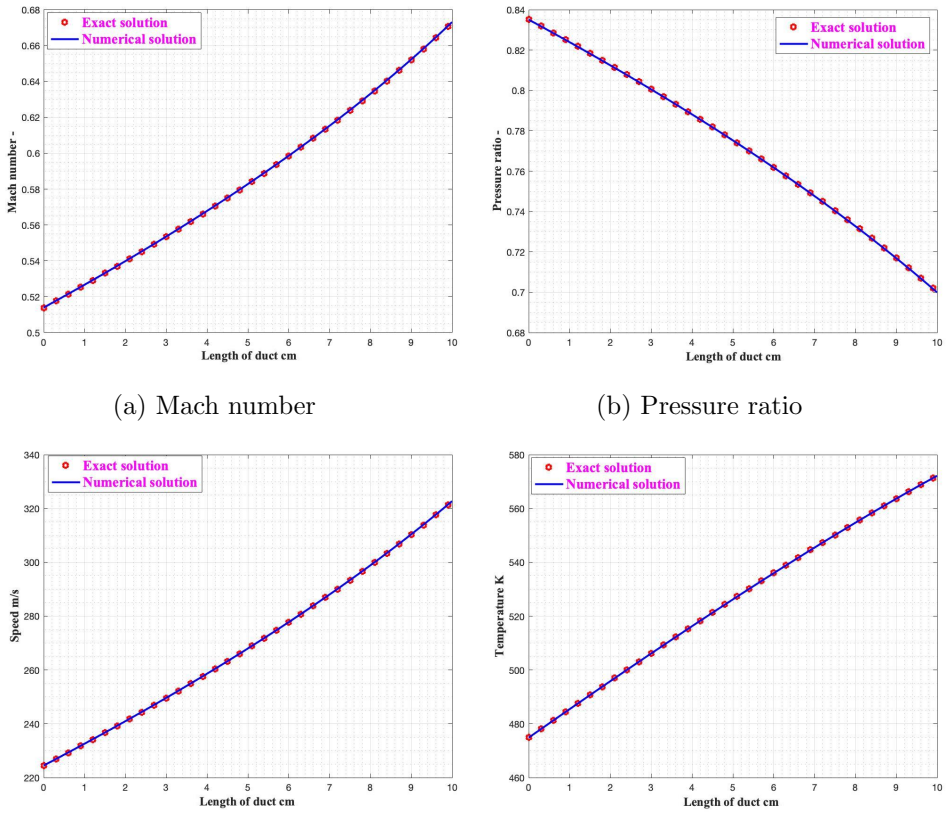

(a) Mach number

(b) Pressure ratio

(c) Speed

(d) Temperature

Figure 27: Subsonic Rayleigh's flow validation with an HR Godunov scheme.

composed by $N = 1000$ elements. The $q = 300000$ J/s/cm^2 and the f coefficient is null.

8.4.2 Supersonic Rayleigh flow

The results presented in figure (28), are obtained for a constant cross-section circular area duct with a diameter $D = 0.7$ cm, an inlet total pressure of $p^0 = 100000$ Pa, an inlet total temperature of $T^0 = 500$ K, an inlet $Mach = 2$ and an outlet pressure $p_2 = 70000$ Pa. The length is $L = 10$ cm. The grid is composed by $N = 1000$ elements. The $q = 300000\text{J/s/cm}^2$ and the f coefficient is null.

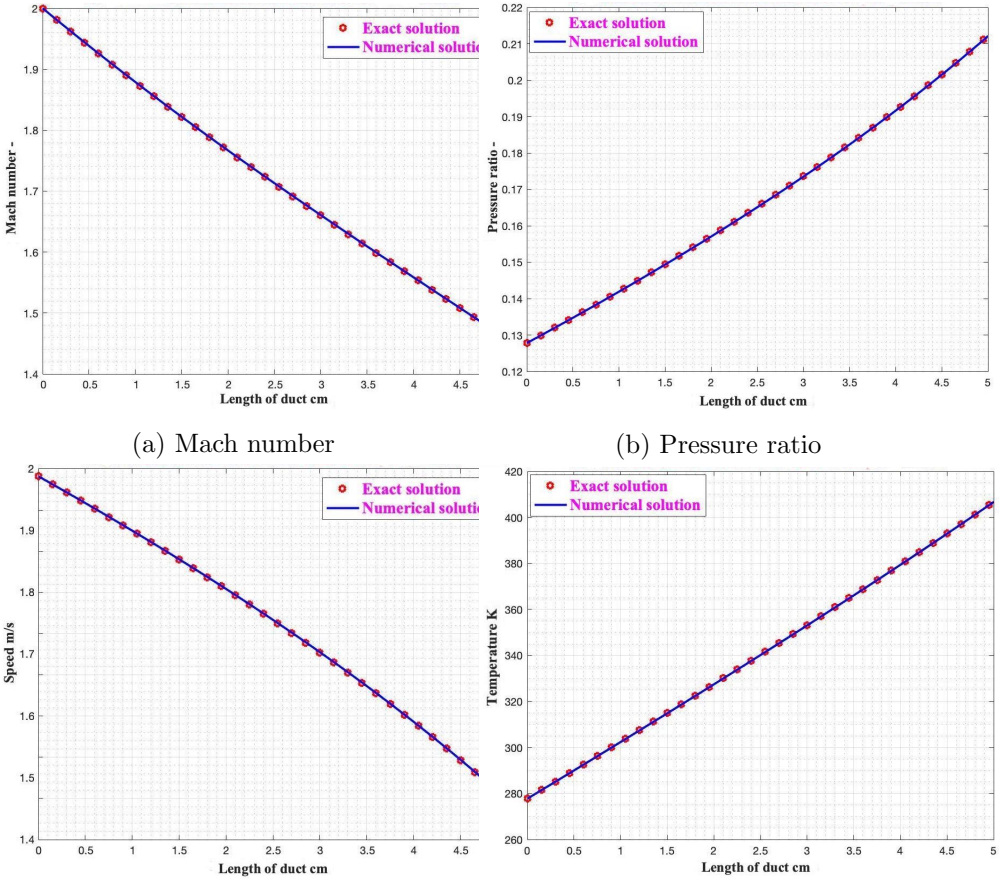

(a) Mach number

(b) Pressure ratio

(c) Speed

(d) Temperature

Figure 28: Supersonic Rayleigh flow's validation with an HR Godunov scheme.

8.4.3 Subsonic chocked Rayleigh flow

The results in figure (29), are obtained for a constant section circular duct with a diameter $D = 0.7$ cm, an inlet total pressure $p^0 = 100000$ Pa an inlet total temperature $T^0 = 500$ K and an outlet pres-

sure $p_2 = 30000$ Pa. The length is $L = 30$ cm. The grid is composed by $N = 1000$ elements. The $q = 300000$
J/s/cm^2 and the f coefficient is null.

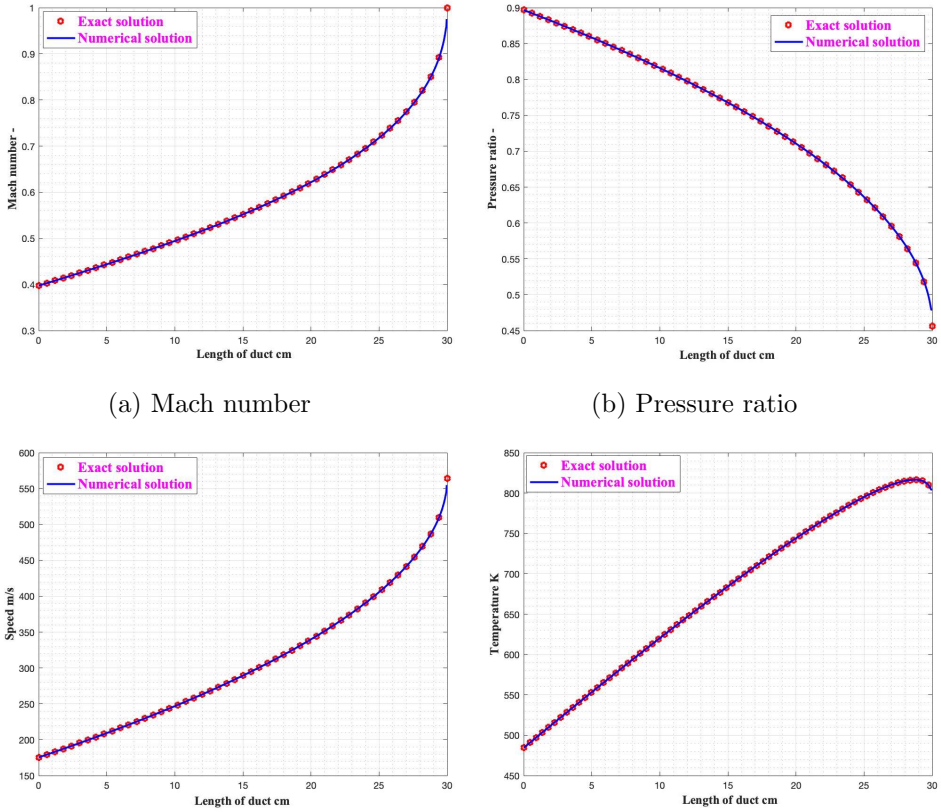

(a) Mach number

(b) Pressure ratio

(c) Speed

(d) Temperature

Figure 29: Subsonic chocked Rayleigh flow's validation with an HR Godunov scheme.

8.4.4 Supersonic Rayleigh's flow with a shock

The results in figure (30) are obtained for a constant section circular duct with a diameter with a diameter $D = 0.7$ cm, an inlet total pressure of $p^0 = 100000$ Pa, an inlet total temperature of $T^0 = 500$ K, an inlet Mach=2 and an outlet pressure $p_2 = 50000$ Pa. The length is $L = 12$ cm and the grid is composed by $N = 1000$ elements. The $q = 300000$
J/s/cm^2 and the f coefficient is null.

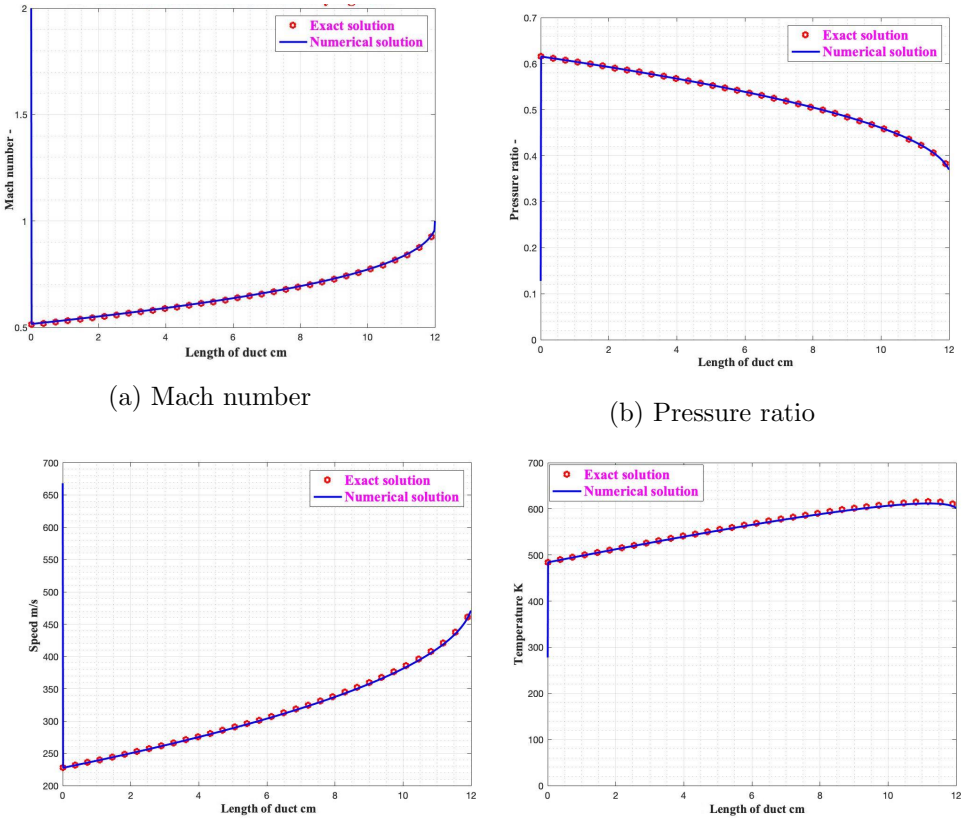

(a) Mach number

(b) Pressure ratio

(c) Speed

(d) Temperature

Figure 30: Supersonic shock Rayleigh flow's validation with an HR Godunov scheme.

8.4.5 Remarks

The numerical results are in good agreement with the analytical solutions. For the continuous *subsonic* and *supersonic* cases, no issues are present. The supersonic case needs a transmissive boundary to the right part to avoid a computational shock in the transition zone between subsonic and supersonic outlet. In the Rayleigh flow, in analogy with the Fanno flow we will have a limit condition for the flow after which the outlet properties will remain fixed. This condition and the relative star properties were found in (7.4) and we must fix them when the total temperature is higher than the limit total temperature that can be found easily from star properties. In the *supersonic shock case*, we can impose the star properties at the right boundary when the final total temperature is higher than the limit one. As we can see from the solutions, the system reacts creating a steady shock that must end

into the convergent divergent nozzle, making the evolution subsonic in the duct following the Second law of thermodynamic. Because of the non conservative boundary conditions at the inlet, the shock results blocked in the first cell. Unless this condition the whole evolution is correct. A convergent divergent nozzle can be inserted at the inlet of the duct to observe the phenomenon. In the *chocked subsonic case* we don't impose any star condition at the right boundary even if the Mach = 1 problems are still present. The reason has a computational nature because increasing the mesh size till $N = 1000$ points, the code becomes suddenly unstable imposing the star properties. Besides this consideration, if we make the code working with the classical BC in the right part we have a correct evolution except for the right last single value which gives a numerical wrong result. In this case the correct result without the presence of the analytical exit solution, is another prove of the effectiveness of the code.
The particular conditions for ducts with $L < L_*$ with an outlet pressure lower than the star pressure makes the code unstable for length lower than $L = 15$ cm and pressure ratios much lower than the pressure star ratio p_*/p_1^0. The problem in this case is linked to the post-expansion phenomena occurring in the outlet section and the non-conservative boundaries and can be solved adding a convergent nozzle at the inlet of the duct and so, using the Godunov scheme to solve the inlet of the duct.

8.5 One-dimensional diabatic flows with wall friction validation

We are ready now to apply our HR Godunov scheme on a one-dimensional diabatic flows with wall friction validation. This solution has been found form Ferrari [1] and is the most recent analytical solution for a 1D compressible flow .

8.5.1 Subsonic case

The study case is a subsonic flow in a duct with a length of $L = 30$ cm and a constant cross-section area of $D = 2.5$ cm. We consider an inlet total pressure of $p^0 = 100000$ Pa, an inlet total temperature of $T^0 = 600$ K and an inlet Mach=2 with an outlet pressure $p_2 = 80000$ Pa. We consider a $q = 600000$ J/s/cm^2 and a $f = 0.003$. The results are shown in figure (31).

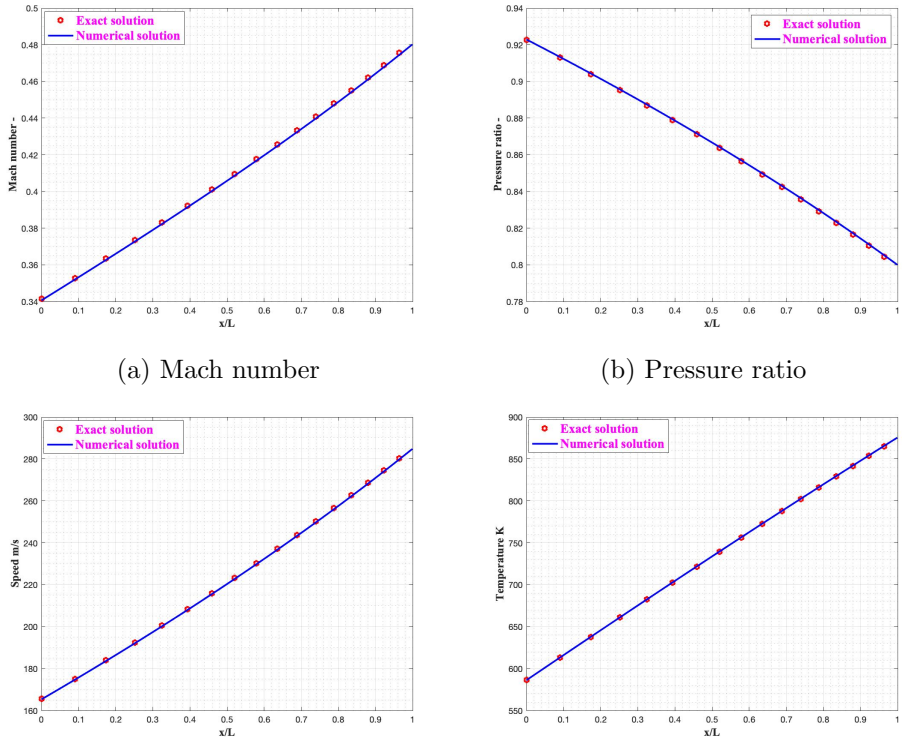

(a) Mach number

(b) Pressure ratio

(c) Speed

(d) Temperature

Figure 31: Validation of a subsonic diabatic flow with friction using an HR Godunov scheme

8.5.2 Supersonic case

The study case is a supersonic continuous flow in a duct with a length of $L = 60$ cm and a constant cross-section area of $D = 2.5$ cm. We consider an inlet total pressure of $p^0 = 300000$ Pa, an inlet total temperature of $T^0 = 800$ K and an inlet Mach=2 with an outlet pressure $p_2 = 30000$ Pa. We consider a $q = 100000$ J/s/cm^2 and a $f = 0.003$. The results are shown in figure (32).

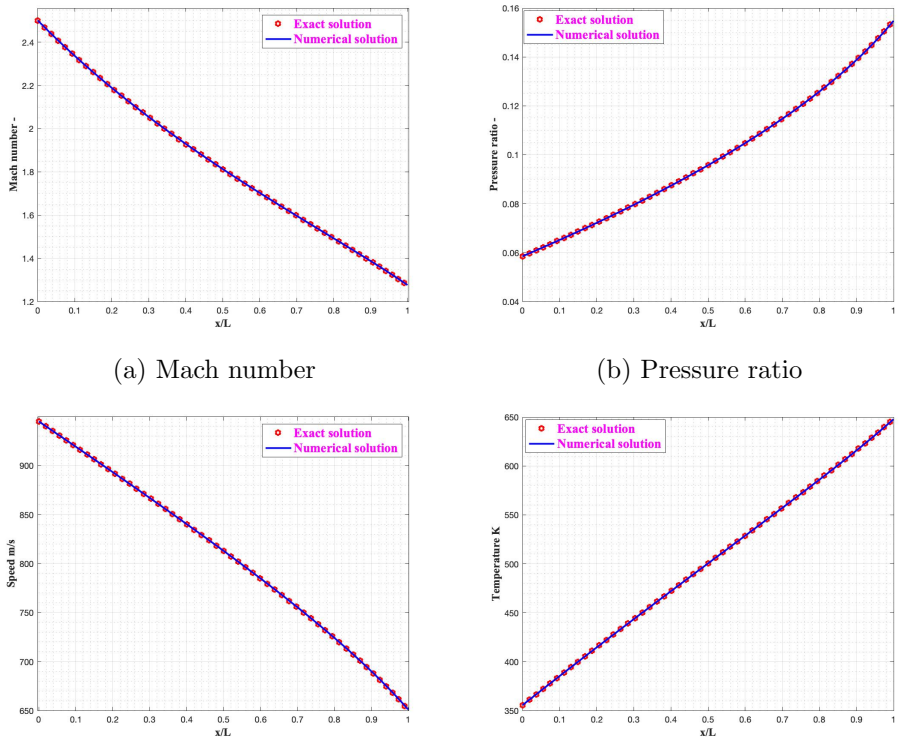

(a) Mach number

(b) Pressure ratio

(c) Speed

(d) Temperature

Figure 32: Validation of a supersonic continuous diabatic flow with friction using an HR Godunov scheme

8.5.3 Supersonic case with shock

The study case is a supersonic flow with a straight shock in a duct with a length of $L = 80$ cm and a constant cross-section area of $D = 2.5$ cm. We consider an inlet total pressure of $p^0 = 300000$ Pa, an inlet total temperature of $T^0 = 800$ K and an inlet Mach=2 with an outlet pressure $p_2 = 30000$ Pa. We consider a $q = 100000$ J/s/cm^2 and a $f = 0.003$. The results are shown in figure (33).

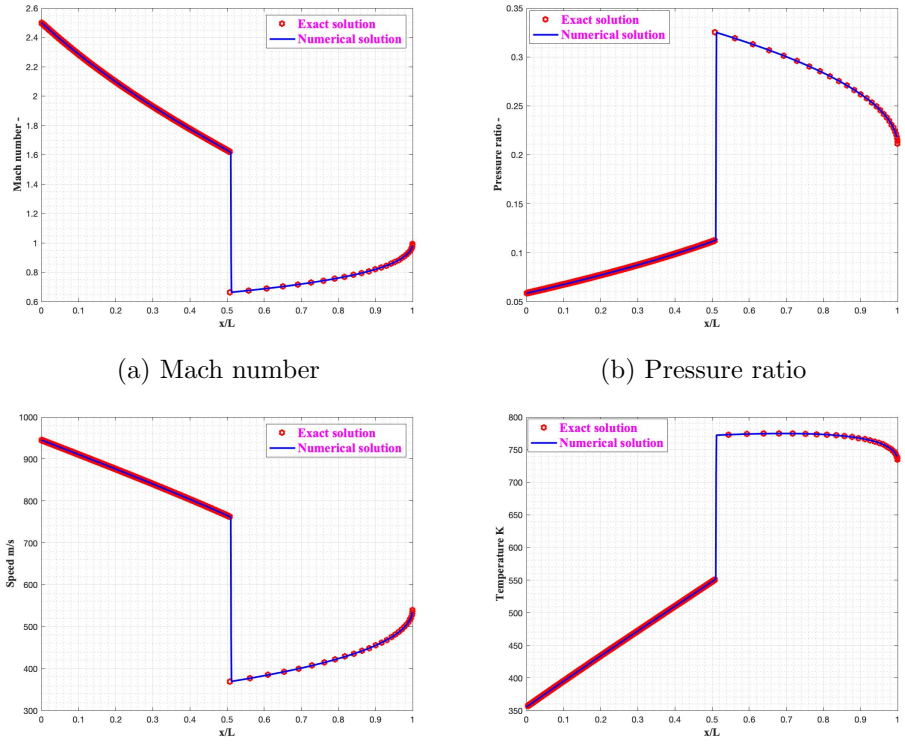

(a) Mach number

(b) Pressure ratio

(c) Speed

(d) Temperature

Figure 33: Validation of a supersonic diabatic flow with friction with a straight shock using an HR Godunov scheme

8.6 Comparison between First Order and High Resolution Godunov scheme

The aim of this part is to put in comparison the numerical solutions in case of First Order and high resolution Godunov scheme . After some numerical comparison we will analyze the pros and cons of each single method.

8.6.1 Convergent divergent nozzle

In this example we will compare the first order Godunov scheme and the high resolution Godunov scheme in the case of a convergent divergent nozzle with a geometry as fig.(2). We choose a total pressure $p^0 = 100000$ Pa and a total Temperature $= 500$
K at the inlet and an outlet pressure $p_2 = 70000$ Pa at the outlet with a length of 1 unit. The mesh size will be formed by $N = 200$ elements.

For this comparison we will use only the pressure as reference since

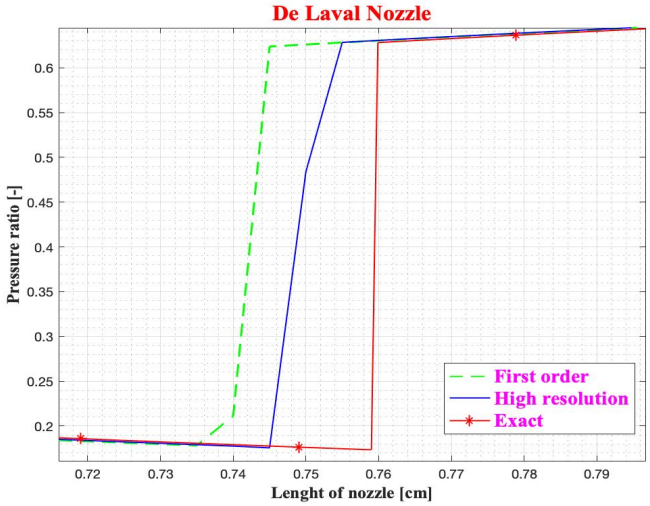

Figure 34: Shock position detail.

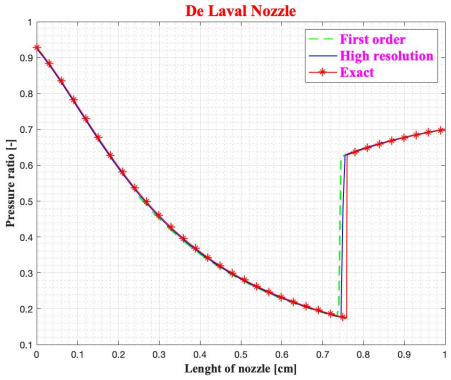

(a) Pressure ratio comparison between a first and an High resolution Godunov scheme.

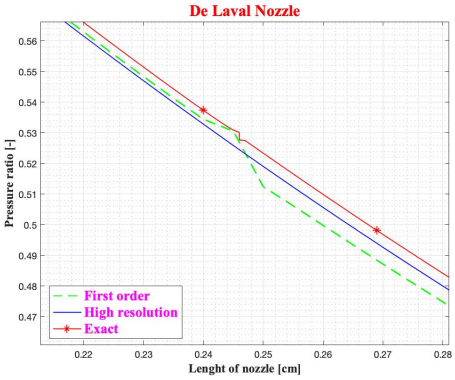

(b) Throat position detail.

all the other properties are already validated. The mesh used is a poor one in order to magnify the differences between the two methods. From the comparison in figure (fig.(35b)) we can appreciate a better result of the High resolution Godunov scheme especially in the section in which there's the throat area, where a numerical error is present even for the exact solution. Also in the zone of the shock discontinuity we can appreciate the best resolution of the HR Godunov scheme as shown in figure (34). This behaviour is due to the elimination of the first order's dissipation error. The time to compute the solution for the

HR Godunov is three time longer than the first order's one and it has a linear increasing trend as we increase the mesh size.

8.6.2 The Fanno's Flow case

We are going to analyze a supersonic Fanno's flow for a constant circular section's duct with a diameter $D = 0.7$ cm, an inlet total pressure of $p^0 = 100000$ Pa, an inlet total temperature of $T^0 = 500$ K and an inlet Mach=2. The outlet pressure $p_2 = 30000$ Pa ,the $f = 0.003$ with a length $L = 20$ cm and the q is null. The mesh size will be formed by $N = 500$ elements.

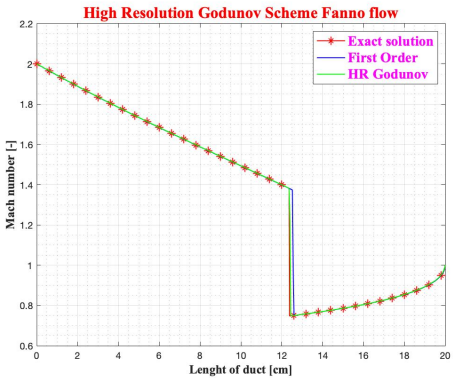

(a) Mach number comparison for first order and HR Godunov in Fanno flow.

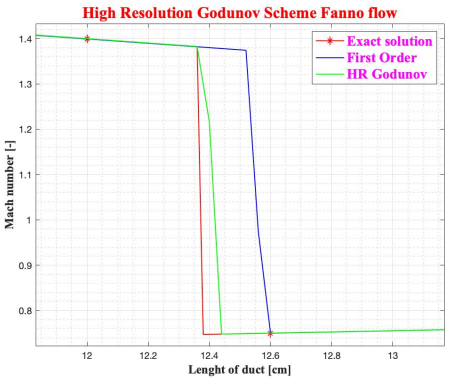

(b) Shock position detail.

In the Fanno's flow case comparison we can still appreciate the best resolution of the HR Godunov scheme as shown in figure (37a). The computational time is doubled than the first order's one.

8.6.3 The Rayleigh Flow case

We are going to analyze a supersonic Rayleigh's flow for a constant circular section's duct with a diameter $D = 0.7$ cm, a length $L = 5$ dm an inlet total pressure of $p^0 = 100000$ Pa, an inlet total temperature of $T^0 = 500$ K and an inlet Mach=2. The outlet pressure is $p_2 = 70000$ Pa, the $q = 300000$J/s/cm^2 and the f is null.
In the Rayleigh's flow case comparison we can observe something strange in respect with the different cases. The first order solution is more near to the exact one than the HR Godunov numerical result for the same mesh as shown in figure (37b). This can be explained because of the main issue of the high resolution schemes: the difficulty to reach the steady state condition. The structure of an HR numerical code is based on the linear variation of the piece-wise constant values time by time

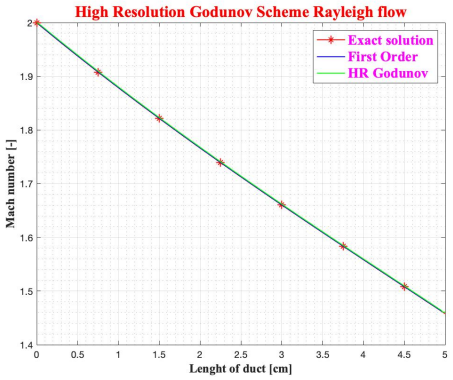

(a) Mach number comparison for first order and HR Godunov for Rayleigh flow.

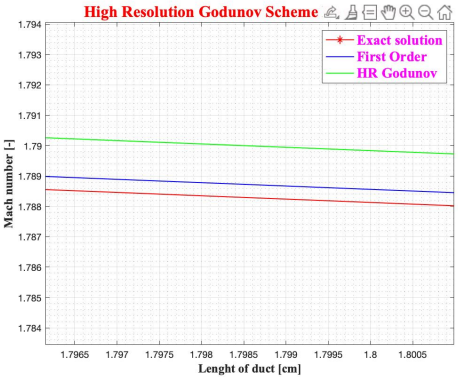

(b) Detail.

and so the variations from a time step to another are numerically created by the code.
This method allows us in reaching better numerical results but it also causes difficulties in reaching a stability state. In this particular case the resolution due to the steady condition of the first order code is higher than the numerical resolution performances of the HR Godunov.

8.6.4 Pros and cons of an High Resolution Godunov scheme

The results showed upside shows a general best performances of the HR Godunov scheme in respect with a first order Godunov scheme with the single exception for the supersonic continuous Rayleigh flow analyzed. The main difficulty for the HR Godunov scheme is to reach the steady state condition since, because of the linear variation inside the cell, the constant values are varied many times before a stable SS solution. In some case the resolution due to the convergence to a steady state of a first order's scheme, can be higher than the numerical resolution of the HR one.
From a qualitative point of view the pros , for an HR Godunov scheme, are much more than the cons since the resolution is better than the first order one for most of the cases analyzed.
Looking at the computational time, on the other hand, the HR Godunov require much more time than the first order one since it is a much more complex method. The computational time for an HR Godunov scheme time grows linearly with the mesh size. In case of further implementations of the code such as the 2D and 3D solutions the computational times could not justify the better resolution of the numerical

result.

8.7 Duct feeded by a De Laval nozzle

In this part we are going to analyze the behaviour of a geometry in which we have composed two simple parts to create a more realistic situations. In fact, if we want to obtain a supersonic flow, in reality, we must use a design nozzle to introduce the fluid into our duct. We will see all the possible patterns for the Fanno and the Rayleigh supersonic flows with a nozzle at the inlet. All the following cases are, reasonably, to be considered validated because all the single sub-parts have been already validated in the previous pages.In all the following cases we consider a De Laval nozzle without friction or heat exchange. Only as example here we report the validation of a Rayleigh's supersonic continuous case. The design De Laval used was the same seen in (8.2.3). The validation of this case is more easy since the Rayleigh's

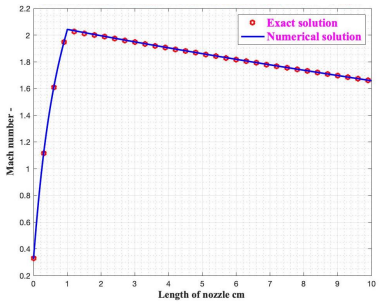

(a) Mach number

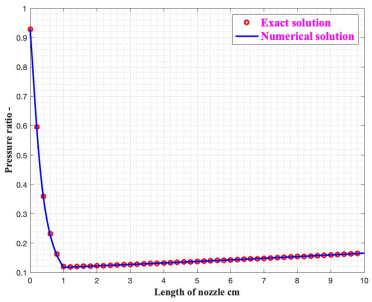

(b) Pressure ratio

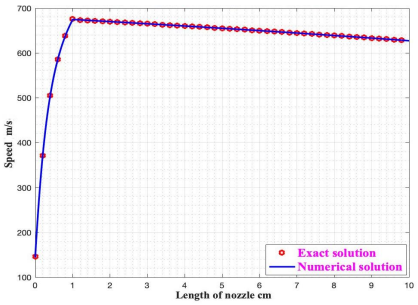

(c) Speed

Figure 39: Validation of a Rayleigh flow in a constant cross section duct feeded by a De Laval nozzle.

star properties of the supersonic flow must not be iterated time by

time since the inlet properties are constant. The exact solution has been found combining the two cases. In this case we are introducing into a $L = 1$ dm nozzle a subsonic flow with an inlet total pressure $p^0 = 100000$ Pa an inlet total temperature $T0 = 500$ K and an outlet pressure $p_2 = 30000$ Pa. The length of the duct is $L = 9$ dm with a constant circular section equivalent to the exit one of the nozzle with a $D = 1.9618$ cm The grid is composed by $N = 1000$ elements. The $q = 0$ and $f = 0$ for the nozzle. The The $q = 300000$ J/s/cm^2 and $f = 0$ for the duct. The results are presented in figure (39).

8.7.1 The supersonic Fanno flow with a De Laval nozzle at the inlet

The cases to be considered in this section are the continuous supersonic and the supersonic case with a straight shock inside the duct.

- *Supersonic Fanno's flow with a straight shock.* In the case we are introducing into a $L_n = 1$ dm nozzle a subsonic flow with an inlet total pressure $p^0 = 100000$ Pa an inlet total temperature $T^0 = 500$ K and an outlet pressure $p_2 = 30000$ Pa. The length of the duct is $L = 9$ dm with a constant circular section equivalent to the exit one of the nozzle with a $D = 1.9618$ cm The grid is composed by $N = 1000$ elements. The $q = 0$ and $f = 0$ for the nozzle. The $q = 0$ and $f = 0.03$ for the duct. For this particular situation the f coefficient has been magnified to capture the phenomenon in short length. The result are reported in figure (40).

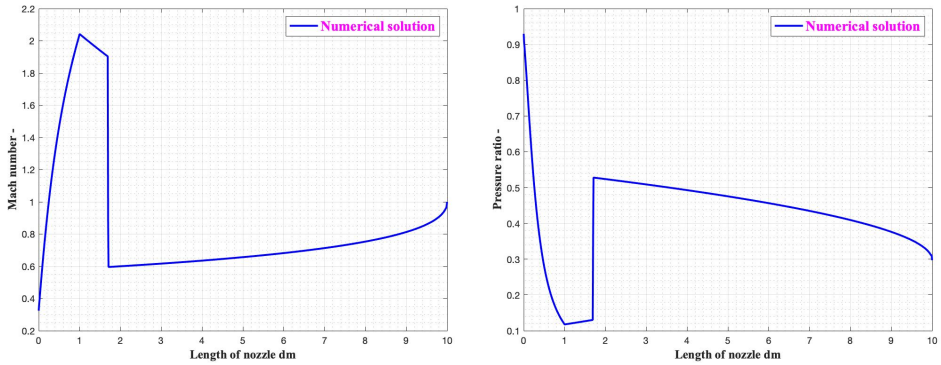

(a) Mach number

(b) Pressure ratio

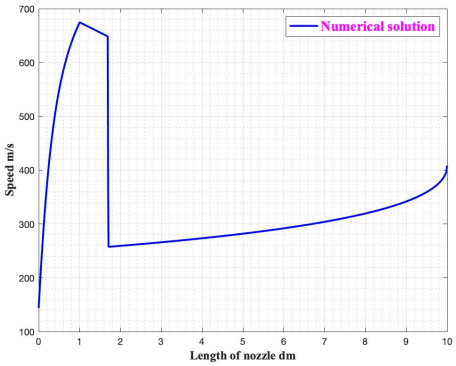

(c) Speed

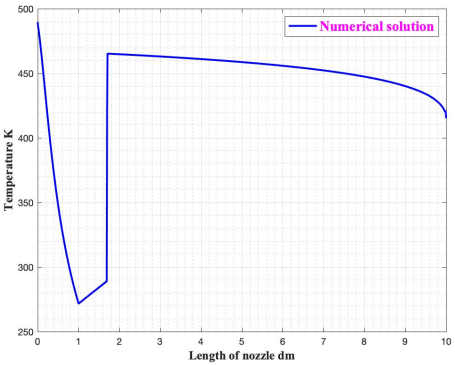

(d) Temperature

Figure 40: De Laval nozzle feeding a Fanno duct (straight shock in the duct)

- *Continuous supersonic case.* In this case we are introducing into a $L_n = 1$ dm nozzle a subsonic flow with an inlet total pressure $p^0 = 100000$ Pa an inlet total temperature $T^0 = 500$ K and an outlet pressure $p_2 = 30000$ Pa. The length of the duct is $L = 4$ dm with a constant circular section equivalent to the exit one of the nozzle with a $D = 1.9618$ cm The grid is composed by $N = 1000$ elements. The $q = 0$ and $f = 0$ for the nozzle. The $q = 0$ and $f = 0.003$ for the duct. The results are showed in figure (41).

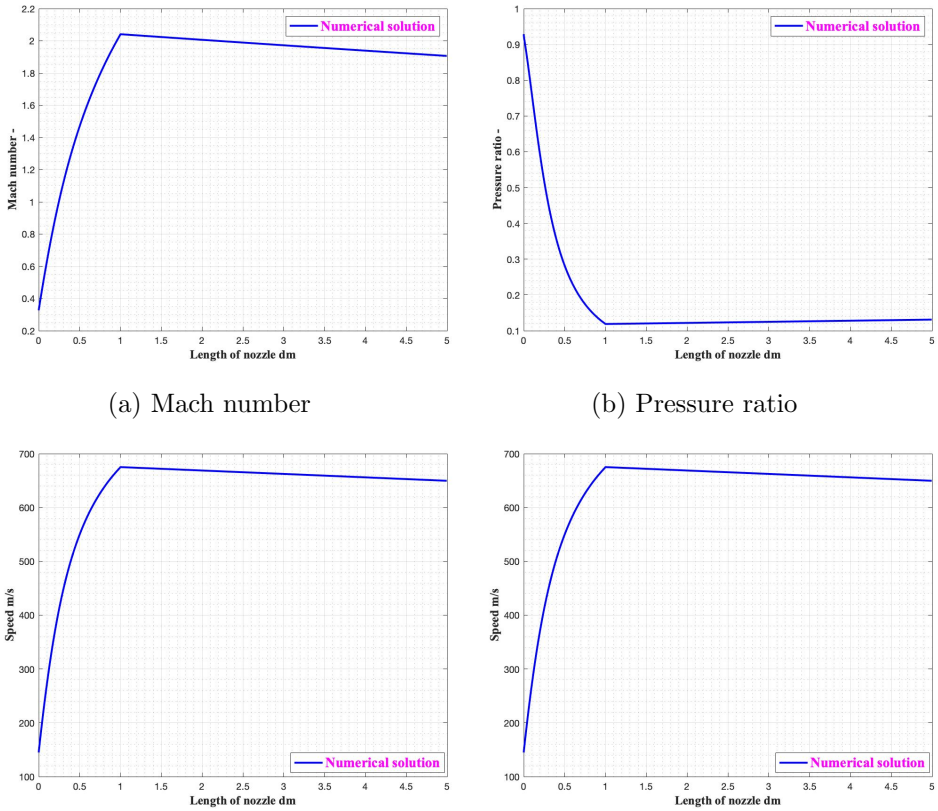

(a) Mach number

(b) Pressure ratio

(c) Speed

(d) Temperature

Figure 41: De Laval nozzle feeding a Fanno duct (continuous flow)

8.7.2 Remarks

The results obtained are very useful to understand how the inlet conditions vary as the configuration changes. The whole system is at constant total temperature. In the *Supersonic shock case* , if we increase the length of the duct more and more, after the $L*$ length we will see, as foregone from the theory, the straight shock going inside the nozzle. The *supersonic continuous case* confirm our data on the Fanno's flow simple duct case. The issues in this kind of configuration is linked to the great time required for a very good simulation. We are required of higher number of points to obtain better results, especially in the nozzle part with high computational times.

8.7.3 The supersonic Rayleigh flow with a design nozzle at the inlet

The cases considered in this part are: the continuous supersonic Rayleigh's flow and the supersonic Rayleigh's flow with a straight shock inside the nozzle.

- *Supersonic shock Rayleigh flow.* In the case we are introducing into a $L = 1$ dm nozzle a subsonic flow with an inlet total pressure $p^0 = 100000$ Pa an inlet total temperature $T^0 = 500$ K and an outlet pressure $p_2 = 50000$ Pa. The length of the duct is $L = 9$ dm with a constant circular section equivalent to the exit one of the nozzle with a $D = 1.9618$ cm The grid is composed by $N = 1000$ elements. The $q = 0$ and $f = 0$ for the nozzle. The $q = 300000\text{J/s/cm}^2$ and $f = 0$ for the duct. The results are shown in figure (42).

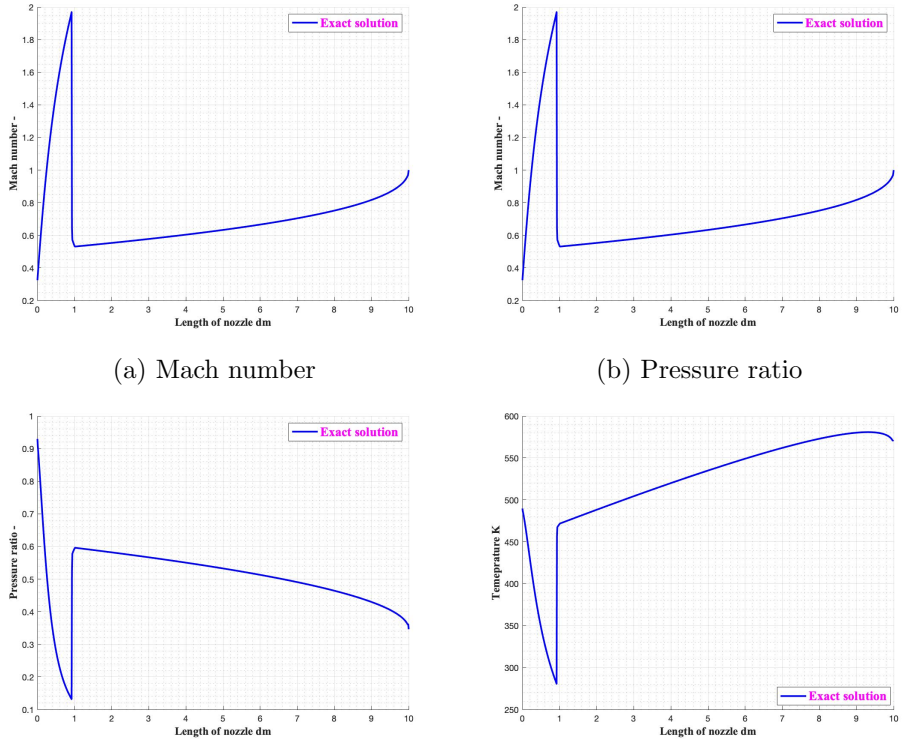

(a) Mach number

(b) Pressure ratio

(c) Speed

(d) Temperature

Figure 42: De Laval nozzle feeding a Rayleigh duct (straight shock at the inlet of the duct)

- *Continuous supersonic*. All the results about this case are reported in figure (39).

8.7.4 Remarks

From this configuration we can have a better evaluation of the physical phenomena foregone in the Rayleigh's theory. Considering the *supersonic shock case* we can clearly see that the only acceptable position of the shock in inside the nozzle. As we increase the heat flow inside the duct we move the shock position upside into the nozzle. The *continuous supersonic* case enforce our concepts already seen in Rayleigh theory. The issue, as for the analogous Fanno's case, is in applying a proper mesh size to obtain very clear results.

9 The complete numerical model

In this section we can finally introduce the numerical model for an unsteady one-dimensional De Laval nozzle with the presence of friction on the walls and heat exchange with the environment solved with an High Resolution Godunov scheme. The main structure of the code was presented in the chapter (7.1).
In the complete model we can add friction and heat exchange on a De Laval nozzle and evaluate the real impact of all these sources applied together. The effectiveness of this HR Godunov scheme stays in the possibility to solve this particular flow, that doesn't have an analytical solution, after the validation of simpler models.
We can solve also the cases with the only presence of friction and area variation by null q heat source term or the cases with only heat exchange and area variation by null f friction factor.
Another feature is the possibility to change the geometrical dimension and investigating different nozzle shapes.

9.1 De laval nozzle with friction

In this part we can investigate the presence of friction for a De Laval nozzle with an area section of :

$$A(x) = 2.5(x + 0.1) + \frac{0.3}{x + 0.1} \quad , \tag{193}$$

an inlet total pressure $p^0 = 100000$ Pa an inlet total temperature $T^0 = 500$ K and an outlet pressure $p_2 = 70000$ Pa. The length is $L = 1$ dm. The grid is composed by $N = 1000$ elements. The $f = 0.03$ and the q coefficient is null.
We have used a f coefficient ten times higher than the validation cases to magnify the effects of friction. The results show that the friction tends to position the straight shock more near to the inlet section in respect with the case of simple area variation. The results are shown in figure (43).

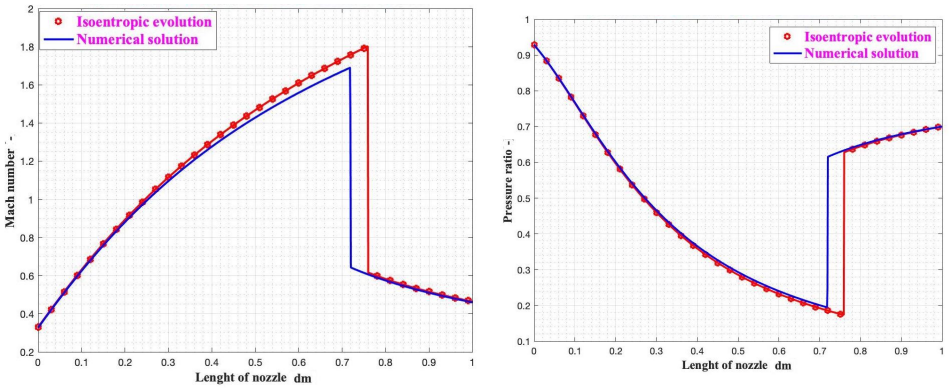

(a) Mach number

(b) Pressure ratio

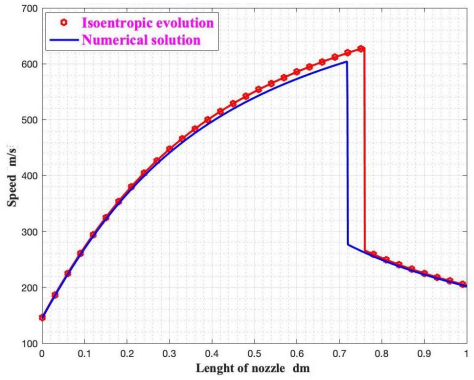

(c) Speed

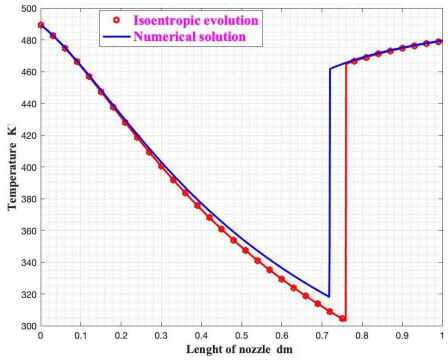

(d) Temperature

Figure 43: HR Godunov scheme for a De Laval nozzle with the presence of friction.

9.2 De laval nozzle with heat exchange

In this part we can investigate the presence of heat exchange for a De Laval nozzle with an area section of :

$$A(x) = 2.5(x + 0.1) + \frac{0.3}{x + 0.1} \quad , \tag{194}$$

an inlet total pressure $p^0 = 100000$ Pa an inlet total temperature $T^0 = 500$ K and an outlet pressure $p_2 = 70000$ Pa. The length is $L = 1$ dm. The grid is composed by $N = 1000$ elements. The $f = 0$ and the $q = 3000000$ J/s/cm^2 .
The presence of an heat source tends, as well as the case of friction, to shift the straight shock to the inlet of the nozzle as shown in figure (44). A peculiar change in the properties, in respect with the isoentropic evolution, is given by a great divergence of the T as we approach the outlet section. The results are showed in figure (44).

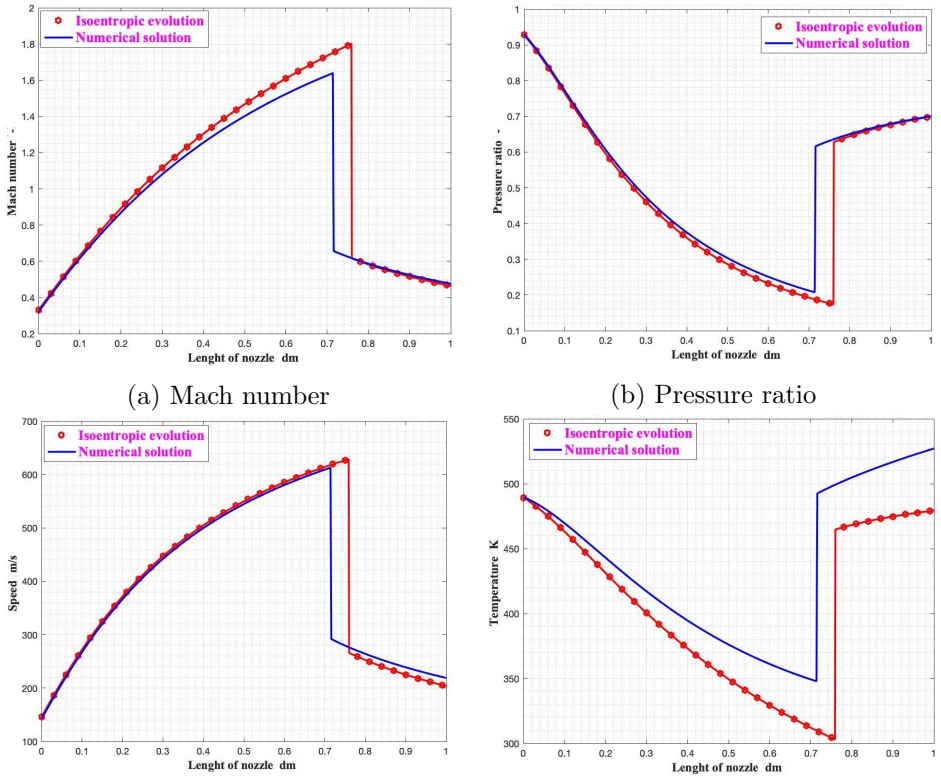

(a) Mach number

(b) Pressure ratio

(c) Speed

(d) Temperature

Figure 44: HR Godunov scheme for a De Laval nozzle with the presence of heat exchange.

9.3 De Laval nozzle with friction and heat exchange

In this part we can investigate the presence of friction for a De Laval nozzle with an area section of :

$$A(x) = 2.5(x + 0.1) + \frac{0.3}{x + 0.1} \quad , \tag{195}$$

an inlet total pressure $p^0 = 100000$ Pa an inlet total temperature $T^0 = 500$ K and an outlet pressure $p_2 = 70000$ Pa. The length is $L = 1$ cm. The grid is composed by $N = 1000$ elements. The $f = 0.03$ and the $q = 3000000$ J/s/cm^2 .
In this case we can observe that the simultaneous presence of friction an heat exchange tends to shift the straight shock toward the inlet more than the single cases analyzed before. The results are shown in figure (45).

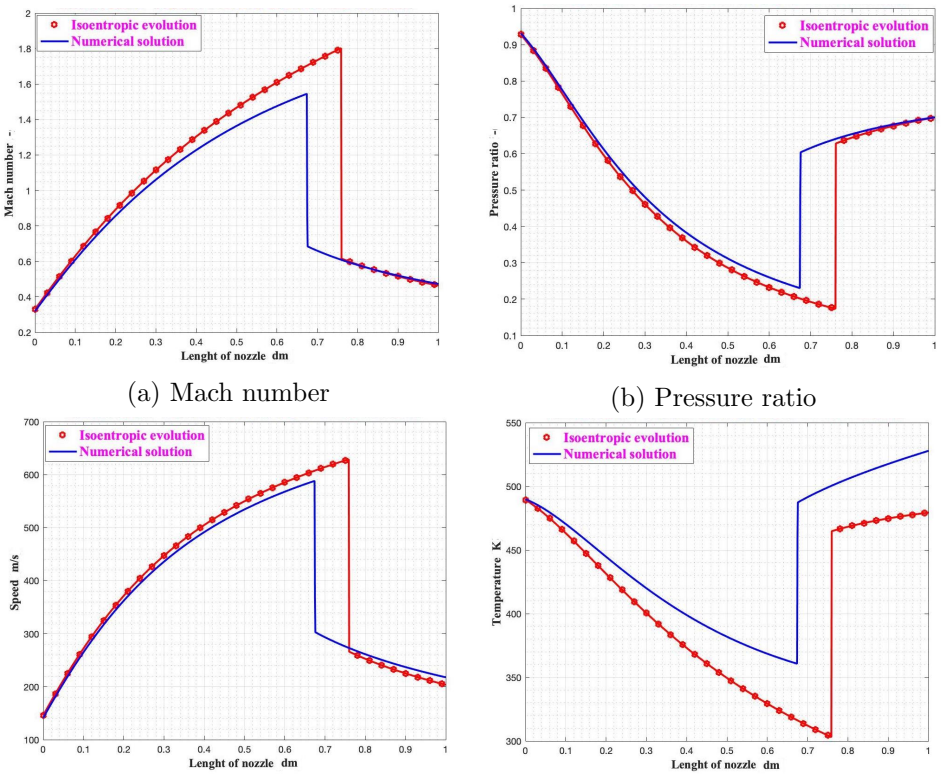

(a) Mach number

(b) Pressure ratio

(c) Speed

(d) Temperature

Figure 45: HR Godunov scheme for a De Laval nozzle with the presence of friction and heat exchange.

10 Further implementations

The work done till now in this thesis is the starting point to develop a more powerful code based on the same numerical model. The possible implementations can be resumed into four points:

- Application of conservative Boundary conditions.
- Correlation of friction and heat with more complex cases.
- Implementation of the HR Godunov with convergence method to easily steady state conditions.
- Covolume gasses, liquid and 2D model.

10.1 Application of conservative Boundary conditions

The main issue related to the HR Godunov scheme here presented, as well as for all the CFD codes, is represented by the boundary conditions

(BC). The development of the BC in this work has been done using the Method of characteristics which allowed us to have physical boundary conditions at inlet and outlet with very good results in most of the cases. The problem of this type of boundary conditions is that they are presented in a non conservative form and so they cannot respect the Rankine-Hugoniot jump condition for shocks at the boundaries. This can bring numerical discontinuities. The solution to this problem can be represented by implementing the boundary condition problem using conservative method such as Lax-Wendroff or with a Godunov scheme as proposed in [4] with a modified Riemann problem in BCs. The latter method should produce the best results.

10.2 Correlations of friction and heat in more complex cases

To use this code in practical and experimental cases more near to reality, we can enlarge the discussion on the heat flow and the friction factor. The heat flow in the model could be modeled with a convection heat exchange

$$Q = h(T_{env} - T_{in}) \ , \tag{196}$$

in which the T_{env} can be considered fixed and the T_{in} varying because of the x coordinate and the Q itself. It would require an iterative algorithm. However he most difficult thing in this case would be the introduction of the h convective coefficient that would be found also with another iteration on the Reynolds' number and on the Prandlt's number. Another issue in this case would be to find the exact solution using a non-constant heat flow for the Rayleigh's model for the validation. It is not immediate. The *friction factor* can be correlated with the materials involved in the model using a correlation analysis with experimental data. A typical setup could be the reproduction of a duct, with a pressure ratio imposed and the acquisition of all the properties of the fluid at the outlet. In this case with a curve fitting we can easily find the friction factor for the specific application.

10.3 Implementation of the HR Godunov with convergence method to easily steady state conditions.

The main issue of an HR Godunov scheme is in reaching the steady state conditions.
This issue could be solved building a convergence steady state condition when we are near the steady state. We must be careful to not convert our code in a first order one to reach the steady state.

10.4 Covolume gasses, liquid and 2D model.

We can try make our code working with the liquid. It is a non-explored field and the applications of this model could be very wide. The intermediate step to reach a Godunov scheme working with liquid should be the use of the conservative boundary condition to guarantee stability to our model and the use of fluids that gradually move away from the perfect gas model. As proposed by Toro in [6], the Covolume gasses are a more realistic fluids in which the perfect gas model is correlated with the local compression coefficients.
The 2D model can be a further implementation to catch the 2D phenomena not included in this work and occurring in our De Laval nozzle for critical conditions.

11 Conclusions

The numerical solution of a 1D compressible diabatic flow with wall friction has been found using an High resolution Godunov scheme with friction and heat exchange. The validated numerical code has been applied to a De Laval nozzle with a perfect gas, heat exchange and wall friction to analyze the numerical solutions. Since an analytical solution, in this case, is not disposable the application of a validated numerical method is the only way to have information about this model.
We have started from the physical description of a one-dimensional unsteady compressible flow with friction and heat exchange with the environment using a perfect gas as fluid. The single one-dimensional models of Fanno, Rayleigh and a flow with an area variation were all discussed in the first part. The Euler's homogeneous equations were introduced to model our study case starting form the integral formulation of the conservation laws. The mathematical properties of the hyperbolic non-liner system of the Euler equations was discussed and, also the source terms accounting for friction, heat exchange and area variation were considered. At this point the complete mathematical model was introduced as starting point for the Godunov scheme construction.
An overview about the conservative numerical methods and their stability, consistency and convergence was pointed out. The Godunov first order scheme and its construction was presented starting from the complete solution of the Riemann's problem for the Euler equations. The numerical model was created, with the physical parameters, the geometry and the application of the Riemann's problem to all the points inside the domain. The stability condition was explained and applied as well as the practical development of the boundary conditions with the Method of characteristics. The extension to an High resolution

Godunov scheme was the last point for building of our final numerical scheme. This passage was achieved evolving the Godunov's first order scheme to the second order and after by applying a slope limiter to avoid oscillations around the discontinuities. The REA algorithm summarized all this passages. Our HR Godunov scheme was completed and ready to be tested. The code has been validated by comparing the numerical outcomes with the results provided by the analytical solutions for the Fanno flow, the Rayleigh Flow and a flow across a nozzle. All the numerical solutions perfectly match the analytical flow properties trends. The validated numerical code has been used to assess the consistency of the new 1D exact solution pertaining a compressible flow experiencing heat exchange and wall friction in a constant cross-section pipe. It resulted that the analytical flow properties patterns are in perfect agreement with the numerical ones. A comparison between the performances between the first order and the HR Godunov scheme was presented. The results about the combination of a De Laval nozzle and a constant area Duct with friction or heat exchange were outlined. At the end the final numerical model was tested for different configurations and the results presented. The further possible developments for our numerical scheme were, at the end, presented for a future implementation of the HR Godunov scheme.

References

[1] Ferrari Alessandro. Analytical solutions for one dimensional diabatic flows with wall friction. 2021.

[2] Alessandro Ferrari. *Fondamenti di Termofluidodinamica per le macchine*. CittàStudi Edizioni, 2018.

[3] Alessandro Ferrari. *Advanced computational techniques for thermal and hydraulic machines*. Politecnico di Torino, 2020.

[4] Jaroslav Pelant Martin Kyncl. *THE BOUNDARY CONDITIONS FOR THE COMPRESSIBLE GAS FLOW*. Engineering MECHANICS, Vol. 21, 2014, No. 2, p. 121–127, 2014.

[5] Ascher H. Shapiro. *The Dynamics and Thermodynamics of Compressible Fluid Flow* . Ronald Press company, 1953.

[6] Eleuterio Toro. *Riemann Solvers and Numerical Methods for Fluid dynamic*. Springer, 2008.

Ringraziamenti

Vorrei in primo luogo ringraziare il professor Alessandro Ferrari ed il dottor Oscar Vento per avermi fatto appassionare e conoscere, dapprima con il corso di *Advanced computational techniques for thermal and hydraulic machines* e poi con questa tesi, il mondo della termofluidodinamica computazionale, materia grazie alla quale ho trovato le risposte a molte delle domande che mi hanno accompagnato durante tutti questi anni di università.

Vorrei ringraziare i miei genitori per essermi sempre stati vicini, in tutti i modi possibili ed immaginabili supportandomi nei momenti più difficili e permettendomi di conoscere, viaggiare e vivere degli splendidi anni universitari.
Un grazie a mia sorella, mia nonna, mio zio Carlo e mio zio Gianluca sempre disponibili per un consiglio o una parola gentile ed un grazie a mio nonno Salvatore, mia nonna Domenica e mio nonno Giuseppe che mi guardano da lassù.
Grazie a tutti i miei amici per aver reso questo percorso univesitario degno di essere vissuto e ricordato, per avermi compreso e per avermi sopportato a Torino come a Castrignano dei Greci. Grazie anche a chi solo con un consiglio, una parola o un sorriso è riuscito a farmi andare avanti, giorno dopo giorno, nel corso di questi bellissimi anni.

Ma che film la vita

Nomadi

Grazie a mia madre per avermi messo al mondo
A mio padre, semplice e profondo
Grazie agli amici per la loro comprensione
Ai giorni felici della mia generazione
Grazie alle ragazze, a tutte le ragazze

Grazie alla neve, bianca e abbondante
A quella nebbia, densa e avvolgente
Grazie al tuono, pioggia e temporali
Al Sole caldo che guarisce tutti mali
Grazie alle stagioni, a tutte le stagioni

Ma che film la vita,
Tutta una tirata
Storia infinita a ritmo serrato
Da stare senza fiato

Ma che film la vita,
Tutta una sorpresa
Attore, spettatore tra gioia e dolore
Tra il buio ed il colore

Grazie alle mani che mi hanno aiutato
A queste gambe che mi hanno portato
Grazie alla voce che canta i miei pensieri
Al cuore capace di nuovi desideri
Grazie alle emozioni, a tutte le emozioni

Ma che film la vita,
Tutta una tirata
Storia infinita a ritmo serrato
Da stare senza fiato

Ma che film la vita,
Tutta una sorpresa
Attore, spettatore tra gioia e dolore
Tra il buio ed il colore